UNDERGROUND MINE PILLAR DESIGN UTILIZING ROCK MASS

PROPERTIES, MARBLE PEAK, PIMA COUNTY, ARIZONA

by

David Emery Nicholas

———————————————

A Thesis Submitted to the Faculty of the

DEPARTMENT OF MINING AND GEOLOGICAL ENGINEERING

In Partial Fulfillment of the Requirements
For the Degree of

MASTER OF SCIENCE
WITH A MAJOR IN GEOLOGICAL ENGINEERING

In the Graduate College

THE UNIVERSITY OF ARIZONA

1 9 7 6

ACKNOWLEDGMENTS

TABLE OF CONTENTS

TABLE OF CONTENTS--<u>Continued</u>

TABLE OF CONTENTS--<u>Continued</u>

LIST OF ILLUSTRATIONS

LIST OF ILLUSTRATIONS--Continued

LIST OF ILLUSTRATIONS--<u>Continued</u>

LIST OF TABLES

x

LIST OF TABLES--<u>Continued</u>

ABSTRACT

Rock mass properties and the in situ stress field were used to compare different stope-and-pillar design methods at the Continental Copper, Inc. Control Property, located in the north-central portion of the Santa Catalina Mountains, Pima County, Arizona. Copper mineralization occurs in a sequence of hydrothermally altered limestones.

Rock mass properties were estimated by testing core samples and by measuring the engineering characteristics of the structural features. A model was developed that infers that a step failure path will have 20 percent intact rock. Estimated rock mass strength is 620 psi $+ \sigma_N \tan 37^\circ$. The in situ stress field was estimated by two indirect methods, residual stress field and correlation with geology, which predict similar orientations for the in situ stress field.

A stope-and-pillar design contains two major elements: roof stability and pillar stability. The maximum roof width was determined by calculating the bending stress at the center of the uniformly loaded, fixed-end roof beam and comparing it with the in situ stress acting in the same direction. A number of methods to calculate the load-carrying capacity of a pillar were analyzed to determine which method takes into account the way that a pillar carries the load with respect to its geometry, the rock mass strength, and the in situ stress field.

CHAPTER 1

INTRODUCTION

The design of underground openings is becoming more critical as the grade of mined deposits becomes lower, initial investments increase, ore depth increases, additional safety regulations come into law, and increased ore recovery is required for conservation of minerals. The stability of these openings is dependent upon the strength of the rock mass and the in situ stress field.

Rock mass comprises the rock substance (solid blocks of rock) and the structural features (faults, joints, bedding, etc.). In most cases, it is not possible to test the rock mass because the volume of material needed would exceed the capacity and capability of any testing equipment presently available. In addition, the cost in all probability would exceed the value of information obtained. Therefore, the two segments of the rock mass, rock substance and structural features, generally must be tested independently and the results combined to estimate the strength of the rock mass itself. Rock substance properties measured to evaluate the strength of the rock mass are compression strength, tensile strength, stiffness (Young's modulus), Poisson's ratio, internal angle of friction, intact rock cohesion, rock-on-rock friction angle, and rock-on-rock cohesion. The major characteristics of the structural features measured to evaluate the rock mass strength are structure type, orientation, roughness, length, spacing, and filling.

1

At the present time, there is no generally accepted method of combining the rock substance properties with the characteristics of the structural features to calculate the strength of the rock mass.

The stress field is defined in terms of its principal orientations and their magnitudes. Methods exist that "directly" measure the in situ stress in competent, relatively massive rocks. These methods are intricate and costly to employ and were therefore not used in this study. The pre-mine stress field can also be evaluated by measuring the residual (locked-in) stresses and correlating them with structural features.

Because there is no unique value for rock mass strength and in situ stress field, it is important to know their variations and to account for these variations in the design of underground openings. The design method that best fits the condition or includes as many variables as possible should be chosen. The purpose of this thesis is to evaluate the rock mass strength and in situ stress field and use these values to compare a number of pillar design methods. Because of the broad nature of this study, some aspects have not been covered in great detail. All data were collected at the Control Property of Continental Copper, Inc., near Tucson, Arizona, where a stoping system employing pillars is being considered.

CHAPTER 2

GEOLOGIC SETTING

The Control Property is located in the west-central part of T. 11 S., R. 16 E., in the north-central portion of the Santa Catalina Mountains (Fig. 1). The Mount Lemmon road connecting Oracle, Arizona, with Summerhaven is the main access to the area.

The area is mountainous, with an average elevation of 6,500 feet and slope angles ranging between 11 and 27 degrees. The highest point in the area is Marble Peak at 7,670 feet. Rainfall averages 21 inches per year, which sustains vegetation ranging from scrub oak to ponderosa pine.

General Geology

The following brief discussion of the geologic history of the Santa Catalina Mountains is taken from work by Wallace (1954), Peirce (1958), DuBois (1959), Hanson (1966), and Braun (1969). For the discussion below, refer to the geology map of the Santa Catalina Mountains (Fig. 2) and of Marble Peak (Fig. 3).

During the Precambrian, sediments were deposited and the granite was emplaced. Peirce (1958) interprets the granite to have been formed from the Pinal Schist. After formation of the granite, a period of erosion occurred followed by a depositional period. The Scanlan Conglomerate, Pioneer Shale, Barnes Conglomerate, Dripping Spring quartzite, and Mescal Limestone (all of the Apache Group) were conformably

3
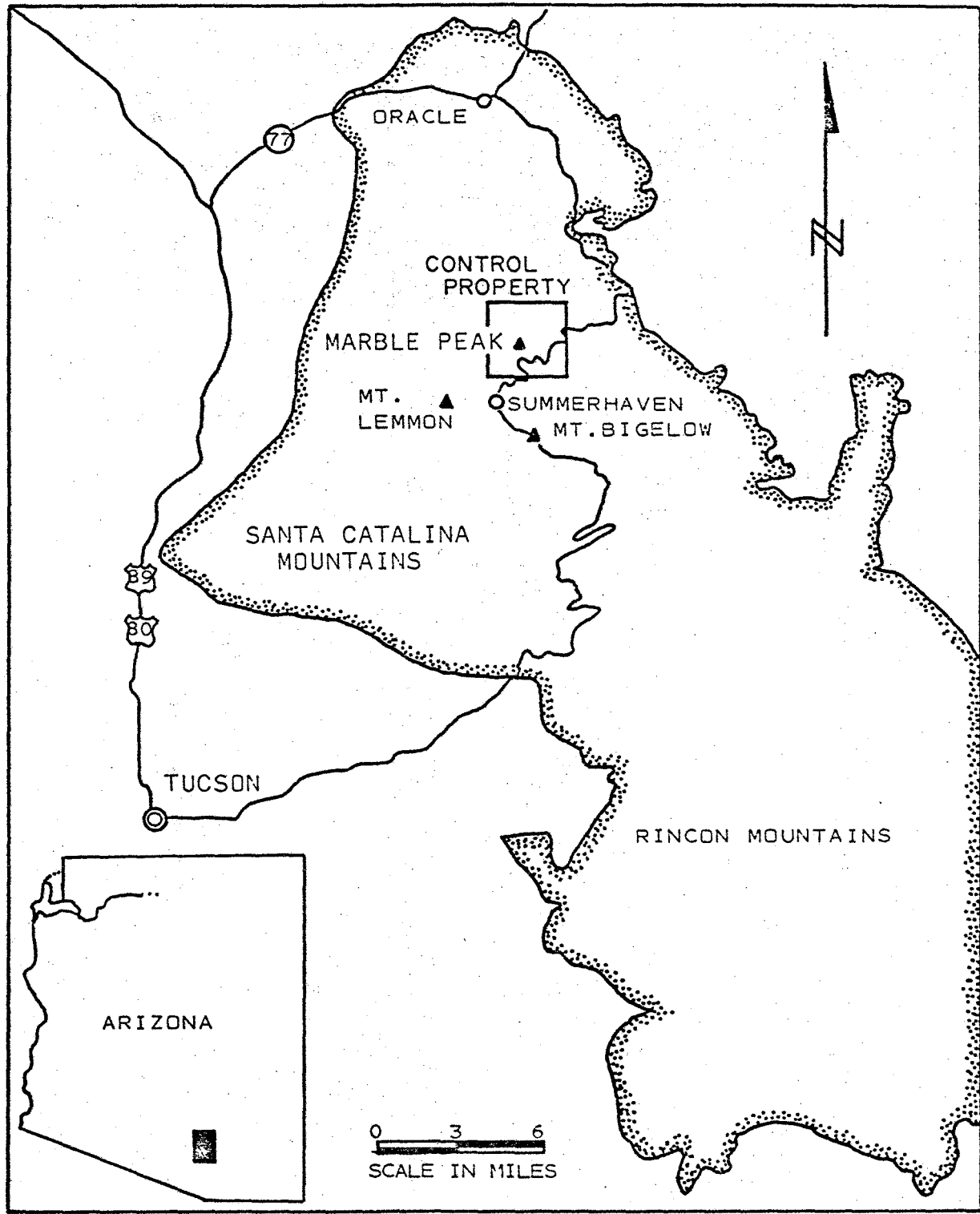
Figure 1. Location map of Control Property

Figure 2. General geology of the Santa Catalina Mountains—
After Wilson, Moore, and Cooper (1969)

Explanation

Qs	Quaternary sediments; chiefly alluvial basin deposits
Ts	Tertiary sedimentary rocks
Tms	Tertiary metasediments
TKgn	Tertiary or Cretaceous gneiss
Ks	Cretaceous sedimentary rocks
Kv	Cretaceous volcanics
dk	Precambrian and post-Cambrian dikes
pЄin	Precambrian intrusive rocks
pЄms	Precambrian metasediments

—┼— Anticline

〜 Faults

——— Contacts
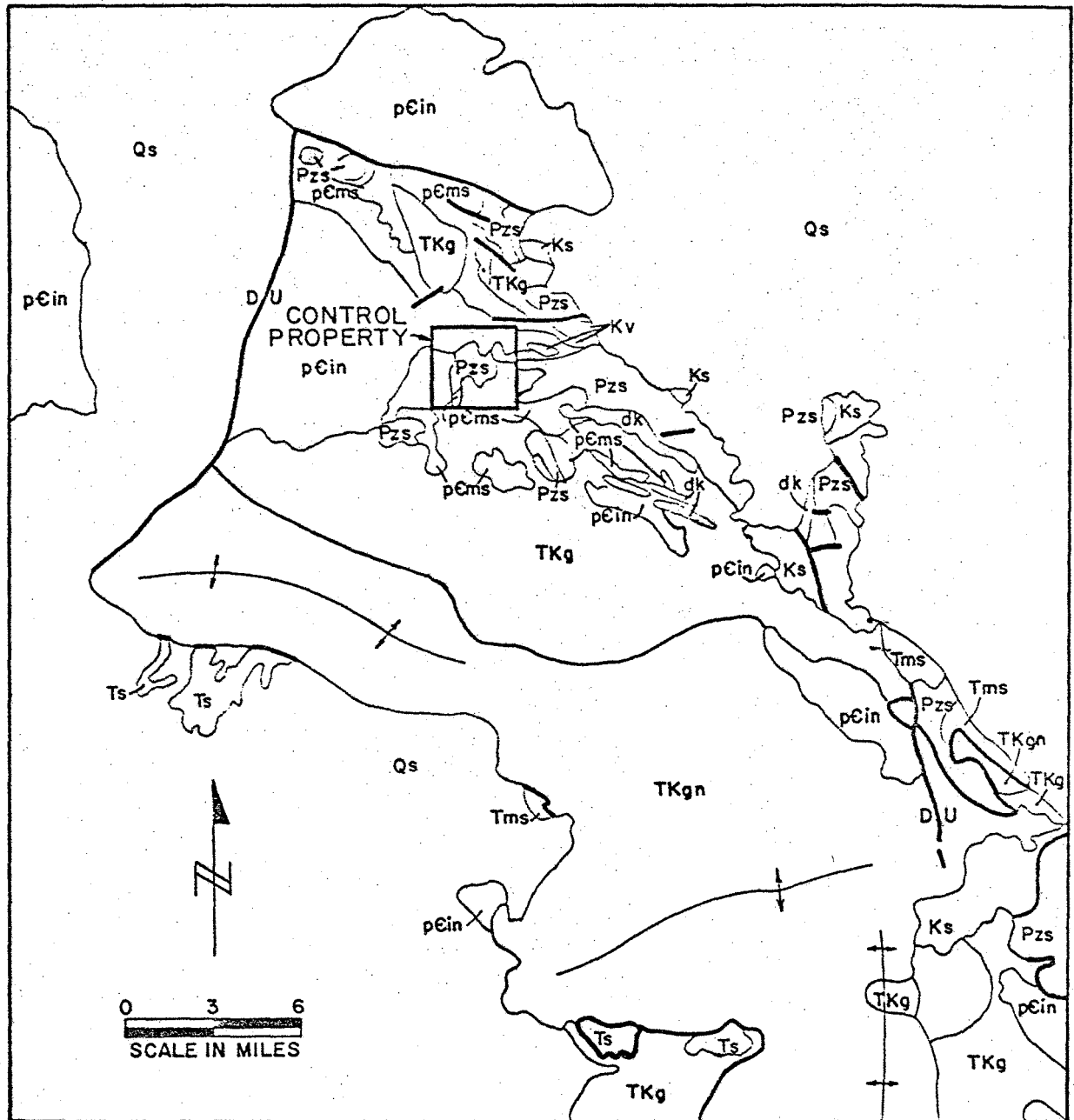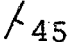
Figure 2. General geology of the Santa Catalina Mountains—
After Wilson, Moore, and Cooper (1969)

Figure 3. General geology of the Marble Peak area—After Creasey and Theodore (1975)

Explanation

TKgd	Cretaceous or Tertiary quartz diorite
Pn	Pennsylvanian Naco Limestone
Me	Mississippian Escabrosa Limestone
Dm	Devonian Martin Limestone
€a	Cambrian Abrigo Formation
€b	Cambrian Bolsa Quartzite
Ydb	Precambrian diabase; Apache Group
Ymd	Precambrian Mescal Limestone and Dripping Spring Quartzite
Yp	Precambrian Pioneer Formation
Ya	Precambrian undifferentiated Apache Group
Yo	Precambrian Oracle granite

～ Contacts   ╱45   Bedding Orientation

╫ Syncline

～ Faults
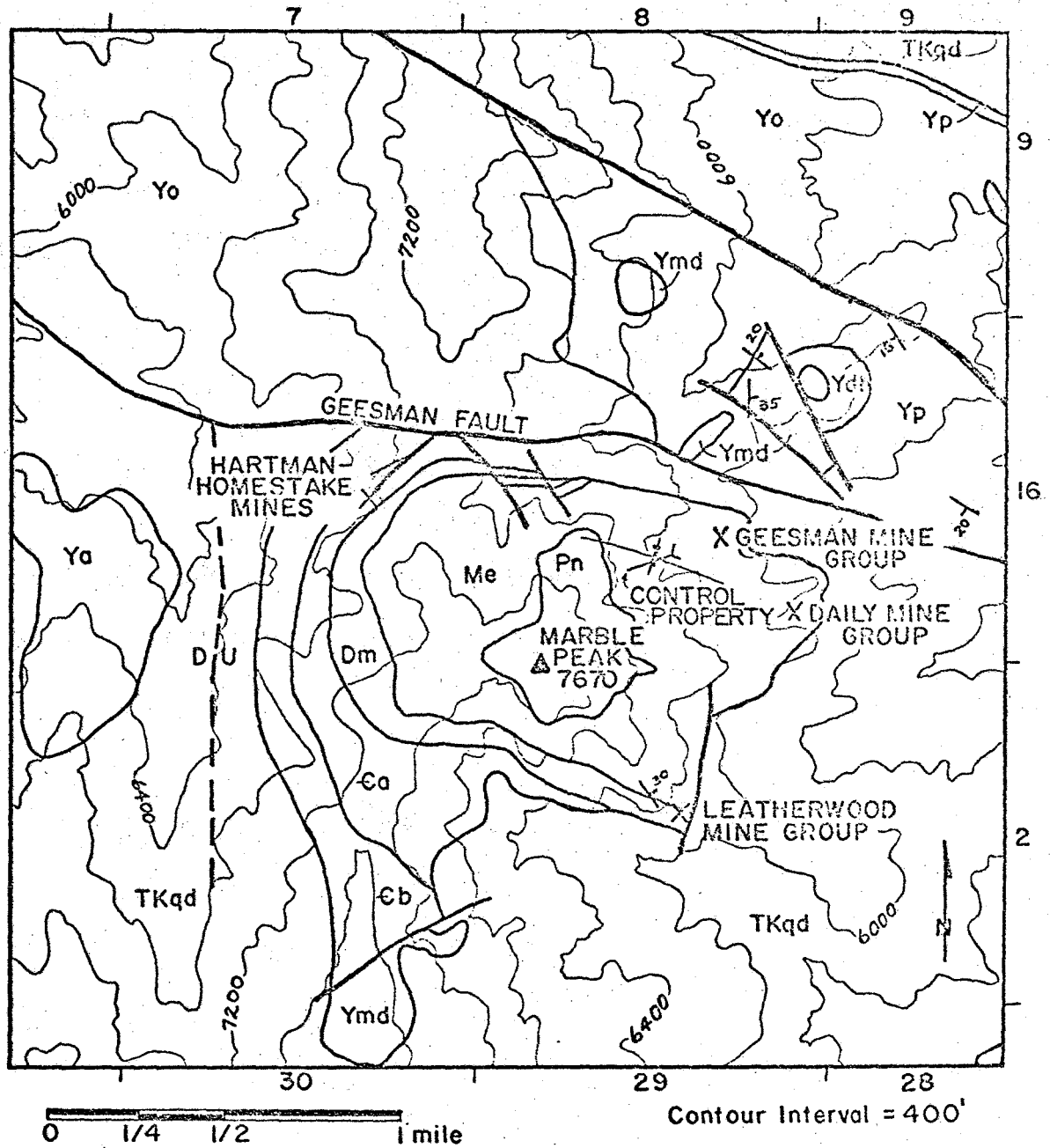
Figure 3. General geology of the Marble Peak area—After
Creasey and Theodore (1975)

deposited during this period. Only small probably remnants of the Mescal Limestone exist in the Marble Peak area (Wallace, 1954). The Apache Group was then cut by diabase sills and dikes, also believed to be of Precambrian age.

Unconformably overlying the Mescal Limestone is a series of Paleozoic sediments. The definable units are the Cambrian Bolsa Quartzite and Abrigo Limestone, the Devonian Martin Limestone, the Mississippian Escabrosa Limestone, and the Pennsylvanian Horquilla Limestone. In the Marble Peak area, these units are capped by 100-foot-thick quartzite unit, which is part of the Naco Group (Horquilla Limestone). It is believed that deposition stopped or that a period of erosion occurred between the Cambrian and Devonian. Peirce (1958) proposes that metamorphism occurred during the Laramide orogeny. This metamorphism was caused by both heating at depth and a north-south compressional force. The Precambrian granite was mobilized and portions of the overlying sediments were recrystallized. The Leatherwood Quartz Diorite intruded the Paleozoic sediments during Laramide time and was closely followed by intrusion of the Catalina granite. Braun reports the age of the Leatherwood Quartz Diorite as 26.6 ± 0.9 m.y., which was determined by K-Ar dating of a biotite crystal. Pegmatite dikes were emplaced during or after the intrusion of the Catalina granite.

Dating of the faulting is difficult. Sometime after the emplacement of the Catalina granite, a major east-west fault system was produced. The Geesman fault is part of this system and forms one of the major structures in the area, with a vertical displacement of 3,000 feet (Peirce, 1958).

Geology of Study Area

The mineralization in the Paleozoic rocks was possibly formed during the Laramide metamorphism and intrusion of the igneous material. Deposited in fractures and disseminated in the rock, the mineralized zones have a tabular shape which generally parallels the bedding. Located in the upper 65 feet of the Abrigo, Martin, and Escabrosa units, these tabular bodies range in thickness from 10 to 70 feet and have a strike length from 100 to 1,000 feet with a dip length of 300 to 900 feet.

This study deals with one of these tabular bodies defined as the ABC mineralized bed. The ABC zone is located mainly in the upper Abrigo and crosses into intense alteration zones of the Martin Limestone. The main gangue minerals are diopside, epidote, and garnet with minor amounts of magnetite and quartz. The original upper Abrigo Limestone was a limestone with shaley interbeds. The altered but unmineralized upper Abrigo has undergone only partial replacement, while in the mineralized zone there is little of the original limestone remaining. The basal 10 feet of unmineralized Martin Limestone is a massive clear limestone, which is also locally replaced. Throughout the remaining portion of this paper, these rock units will be referred to as:

ABC mineralized zone = ABC zone

Unmineralized upper Abrigo Limestone = upper Abrigo

Basal 10 feet unmineralized Martin Limestone = Martin.

Mining History

Previous mining in the area occurred along the contact between the Leatherwood Quartz Diorite and Paleozoic sediments, where copper

sulfide outcrop was visible. Mining was limited to five specific properties: Leatherwood, Hartman-Homestake, Stratton, Daily, and Geesman (Fig. 3). Production started in the early 1900's and continued intermittently through 1970. Copper was the main ore mined, with grades ranging between 2.5 and 3.5 percent. Minor amounts of silver, gold, and zinc were also produced. Braun (1969) reports that 92,400 tons of 3.25% Cu was mined out of the Geesman claims from 1906 to 1946 and 20,000 tons of 2.5% Cu was mined from the Daily mine between 1937 to 1940. The newly defined mineralization in the Paleozoic rocks was discovered through geophysics (magnetics), detailed geologic mapping, and extensive diamond drilling.

CHAPTER 3

STRUCTURE ANALYSIS

The structure analysis will be discussed in two sections: major structures and rock fabric. Major structures are those that are continuous and have a trace length in the same order as that of the mineralized zone. The rock fabric are those structures that are discontinuous but have a high frequency of occurrence.

Major Structure

Data Collection

Most data used to evaluate the major structures were obtained from surface and underground geology maps of Continental Copper, Inc. (1974a, 1974b). Data were also obtained from Peirce (1958) and Braun (1969). The major structure data were plotted and contoured on a lower hemisphere equal-area Schmidt net.

The major structures analyzed were bedding, faults, dikes, and folds. To determine if the structural system was continuous through the Paleozoic sedimentary rocks, major structures were analyzed by rock type and by location, that is, surface data versus underground data.

Faults

The Geesman fault (Fig. 3) is the major fault in the area and strikes N. 70° W. and dips 75° SW. Cutting nearly through the ABC zone are a series of faults, striking generally N. 30° W. and dipping steeply.

The Schmidt contour plots of the faults are shown in Figure 4 by rock types and location. The modal orientation of the fault sets is given in Table 1. The surface data from the Horquilla, Escabrosa, and Martin all show the following fault systems:

General Strike	General Dip	Set Name
N. 30° W.	40° NE.	Bedding
N. 55° E.	45° NW.	Northeast Flat
N-S	90°	North-South
E-W	85° SW.	East-West
N. 50° W.	75° SW.	Northeast
N. 40° E.	85° SE.	Northeast

The Abrigo surface data only show the Northeast and East-West fault sets; however, there were only eight faults observed for the Abrigo surface data.

The most obvious difference between the underground data and the surface data is in the presence of an underground system striking northeast and dipping 35° to 55° NW. This can be explained because the set is "flat" and not identifiable. The Escabrosa underground data do not show the strong North-South or East-West sets that the surface data shows. This difference is probably due to lack of underground data. The Martin underground data suggest the existence of the East-West and Northwest sets, but the limited number of observations prevent any conclusions. The Abrigo underground data show the North-South and Northwest sets and also indicate a Northeast set.
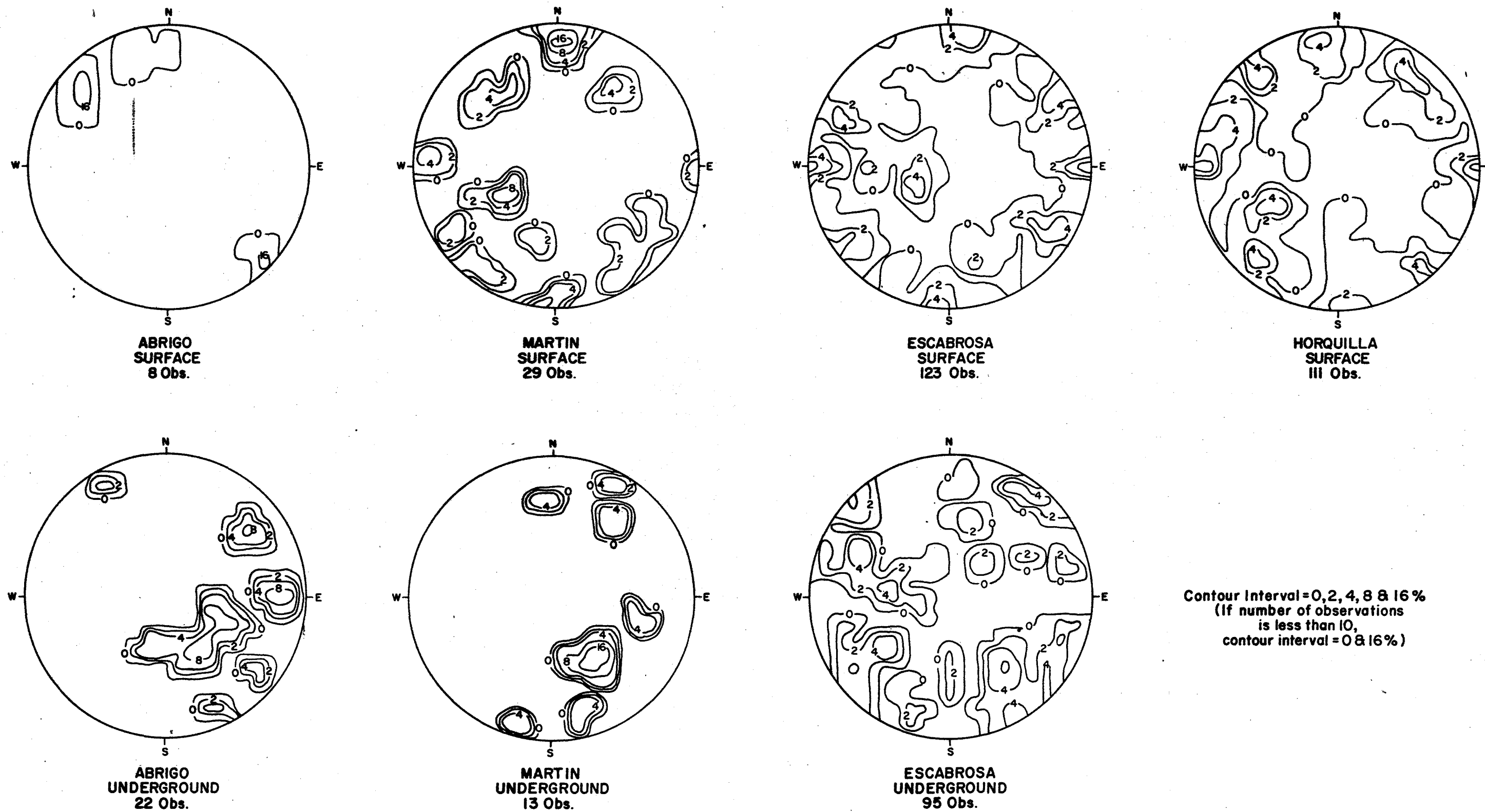
Figure 4. Schmidt polar plots of faults

Table 1. Modal orientations of significant fault systems

Percentages of points making up sets are given under orientations. Data are from Continental Copper, Inc.'s (1974a, 1974b) geology maps.

Set Name	Horquilla Surface (111 obs)	Escabrosa Surface (123 obs)	Escabrosa Underground (95 obs)	Martin Surface (29 obs)	Martin Underground (13 obs)	Abrigo Surface (8 obs)	Abrigo Underground (22 obs)
Bedding	N 30 W 45 NE (6.2%)	N 28 W 24 NE (7.3%)	N 8 E 38 SE (9.3%)	N 30 W 35 NE (10.4%)			
Northeast Flat			N 52 E 53 NW (14.0%)		N 56 E 44 NW (50.0%)		N 60 E 38 NW (56.0%)
North-South	N-S 85 E (21.6%)	N-S 90 (12.2%)		N 10 E 85 SE (6.9%)			N-S 74 W (20.8%)
East-West	N 82 E 80 SE (25.7%)	N 78 W 81 SW (14.6%)		N 88 W 80 SW (27.6%)			
Northwest	N 55 W 75 SW (22.6%)	N 32 W 85 SW (15.4%)	N 58 W 85 SW (23.2%)	N 56 W 60 SW (10.3%)			N 40 W 66 SW (12.5%)
Northeast	N 50 E 85 SE (12.4%)	N 30 E 82 NW (25.2%)	N 26 E 60 SE (30.2%)	N 55 E 55 SE (10.3%)		N 42 E 80 SE (37.5%)	
Other			N 30 W 50 NE (7.0%)				

Bedding

The bedding strikes generally north–south to N. 15° W. and dips between 25° to 45° E. Figure 5 shows the Schmidt contour plots of the bedding data. The contour plot of the Horquilla (Fig. 5) best displays the variation of the bedding orientation. This variability may be due to folding; however, there is no apparent fold axis shown by the bedding. The modal orientations are listed in Table 2.

Folds

Continental Copper, Inc.'s (1974a) surface geology map shows a major syncline in the area with a flat plunge generally bearing 105 degrees. This fold approximately parallels the Geesman fault (Fig. 3).

Drag folds exist in the area. Braun (1969) shows two folds bearing generally north and plunging 5 degrees and one fold bearing 231 degrees and plunging 35 degrees. Peirce (1958) mapped a series of drag folds in the Bear Wallow area that bear generally 90 degrees and plunge 15 degrees.

Dikes

Dikes in the area generally follow the faults. Figure 6 shows the Schmidt contour plot of the dikes and Table 3 lists the modal orientations. The dikes appear to follow all major faults sets except the Bedding and Northeast sets; however, because of the limited number of observations, no definite conclusions can be reached about preferred dike orientations.
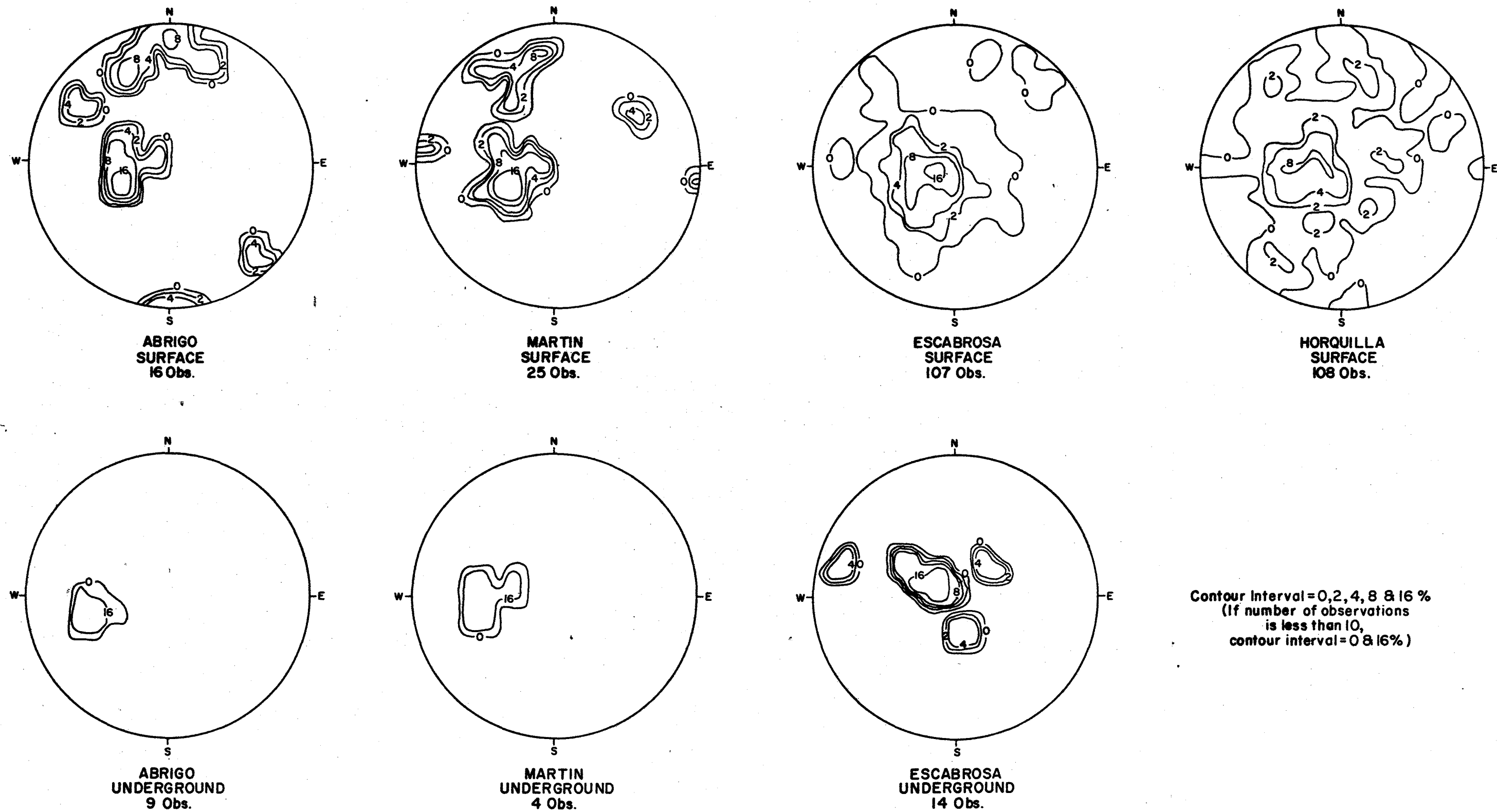
Figure 5. Schmidt polar plots of bedding

Table 2. Modal orientations of bedding

Percentages of points making up sets are given under orientations.
Data are from Continental Copper, Inc.'s (1974a, 1974b) geology maps.

Rock Type	Predominant Orientation	Other Orientations		
Horquilla				
Surface (108 obs)	N-S 30 E (43.5%)	N 50 E 70 SE (3.7%)	N 72 W 54 SW (5.6%)	N 78 W 38 NE (5.6%)
Escabrosa				
Surface (107 obs)	N-S 10 E (49.5%)			
Underground (14 obs)	N 40 E 14 SE (66.7%)			
Martin				
Surface (25 obs)	N 30 W 35 NE (52.0%)	N 80 E 70 SE (8.0%)		
Underground (4 obs)	N 5 W 50 NE (100.0%)			
Abrigo				
Surface (16 obs)	N-S 35 E (54.6%)	E-W 80 S (36.4%)		
Underground (9 obs)	N 10 W 45 NE (100.0%)			

ABRIGO
UNDERGROUND
I Obs.

ESCABROSA
SURFACE
13 Obs.

MARTIN
SURFACE
14 Obs.

HORQUILLA
SURFACE
I Obs.

ESCABROSA
UNDERGROUND
7 Obs.

Contour Interval=0,2,4,8 & 16 %
(If number of observations
is less than 10,
contour interval = 0 & 16 %)
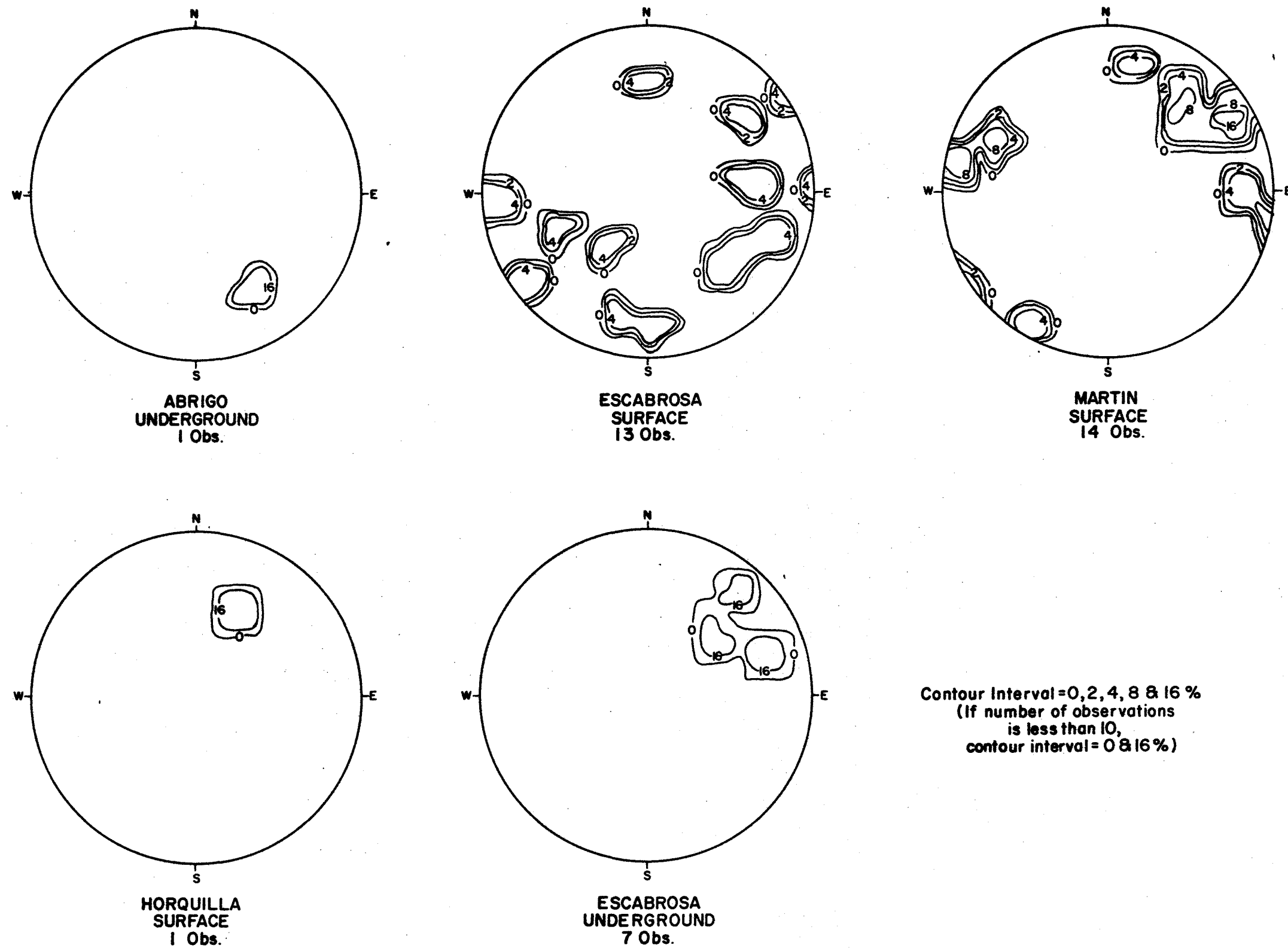
Figure 6. Schmidt polar plots of dikes

Table 3. Modal orientations of significant dike systems

Percentages of points making up sets are given under orientations. Data are from Continental Copper, Inc.'s (1974a, 1974b) geology maps.

Set Name	Horquilla Surface (14 obs)	Escabrosa Surface (13 obs)	Escabrosa Underground (7 obs)	Martin Surface (1 obs)	Martin Underground (0 obs)	Abrigo Surface (1 obs)	Abrigo Underground (1 obs)
Bedding							
Northeast Flat		N 30 E 55 NW (7.7%)				N 62 E 56 NW (100%)	N 56 E 55 NW (100%)
North–South	N 10 E 90 (21.4%)	N 5 W 90 (7.7%)					
East–West	N 80 W 70 SW (7.1%)	E-W 75 N (7.7%)					
Northwest	N 35 W 80 SW (50.0%)	N 40 W 90 (7.7%)	N 48 W 48 SW (100%)	N 70 W 50 SW (100%)			
Northeast							
Other							

Rock Fabric

Data Collection

The rock fabric data was compiled from Continental Copper Inc.'s (1974a, 1974b) surface geology map and underground geology map and collected by detail line mapping on the 6400-foot level (Fig. 7). The method of detail line data collection is discussed in Appendix A.

Joint Set Data

The data collected from the geology maps were segregated by rock type and by location (surface versus underground) to evaluate structural continuity in the Paleozoic units. The contoured Schmidt plots of the joint sets are shown in Figure 8. Table 4 lists the modal orientation for each Schmidt plot.

The surface data from the Horquilla, Escabrosa, and Martin all show steeply dipping joint sets with the following orientations: north-south, east-west, northeast, and northwest. The Abrigo surface data show only the North-South and Northeast sets. This is probably due to the limited number of observations.

The Escabrosa underground data reveal the Northeast and Northwest sets. The North-South set may be present but slightly rotated to the east. The East-West set is absent. No conclusions can be made from the underground Martin data because of the limited number of observations. The underground Abrigo data show all of the steeply dipping fracture sets plus a Northeast Flat fracture set dipping 45° NW.
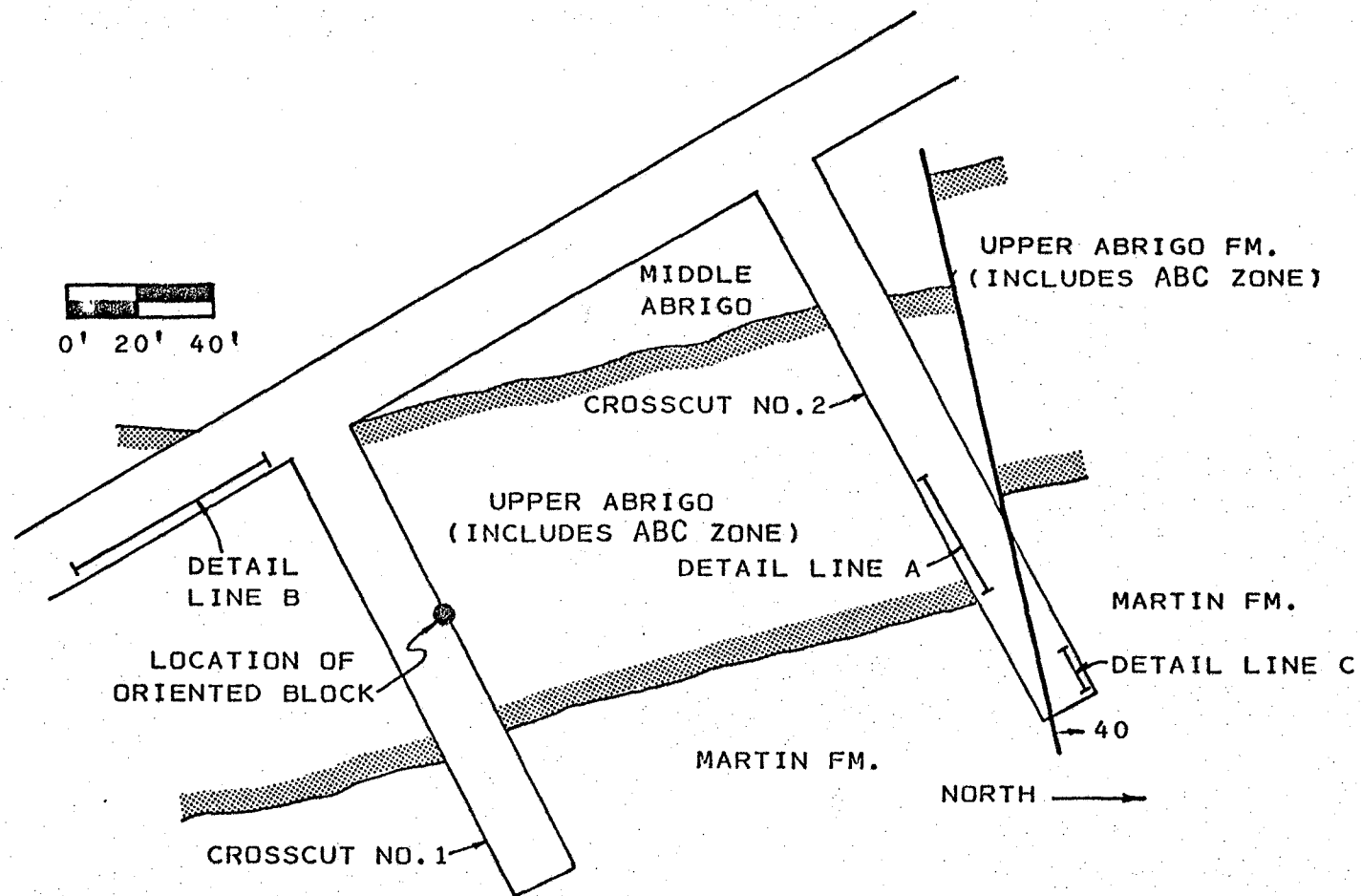
Figure 7. Location of detail lines A, B, and C and oriented block for residual stress analysis
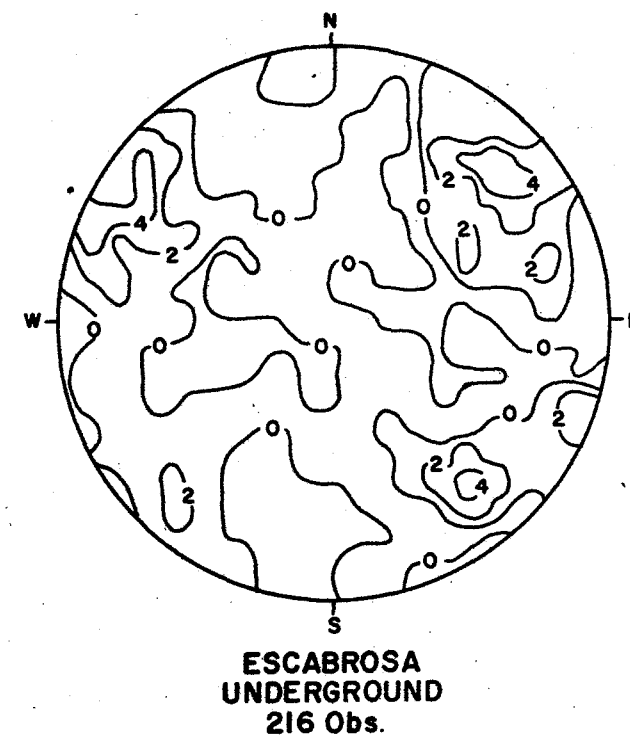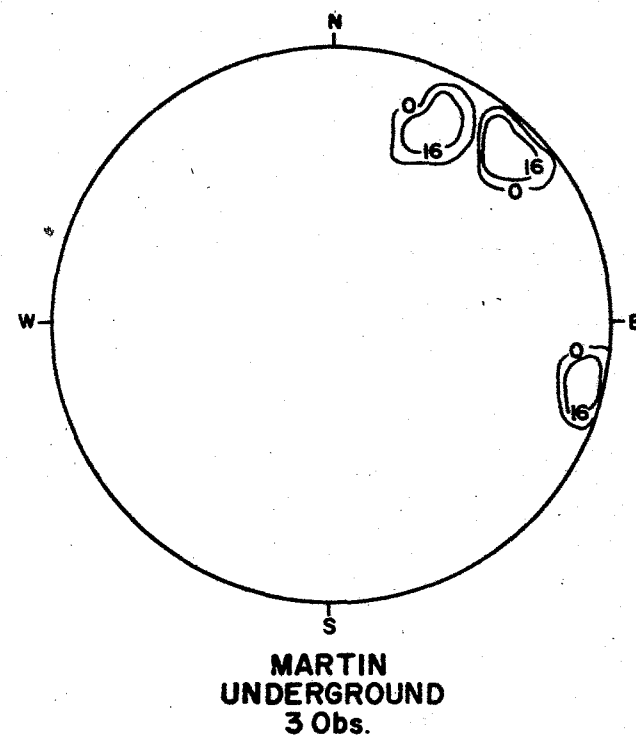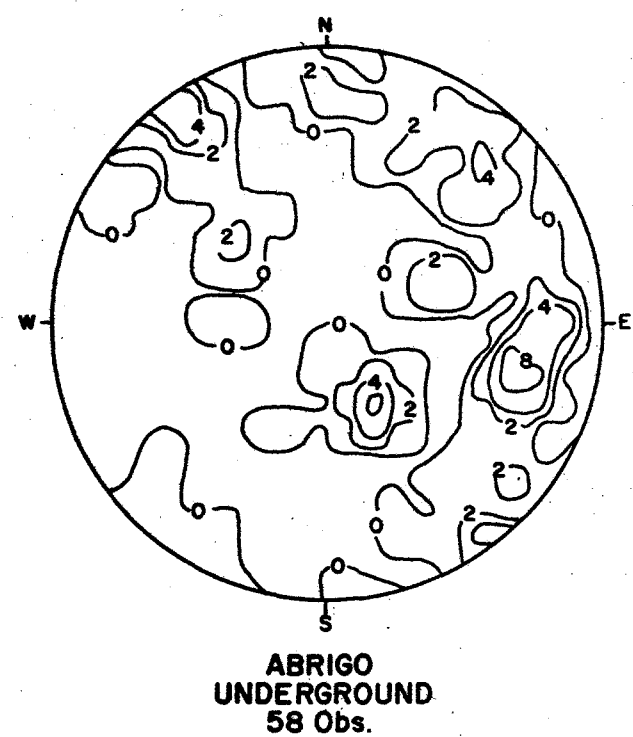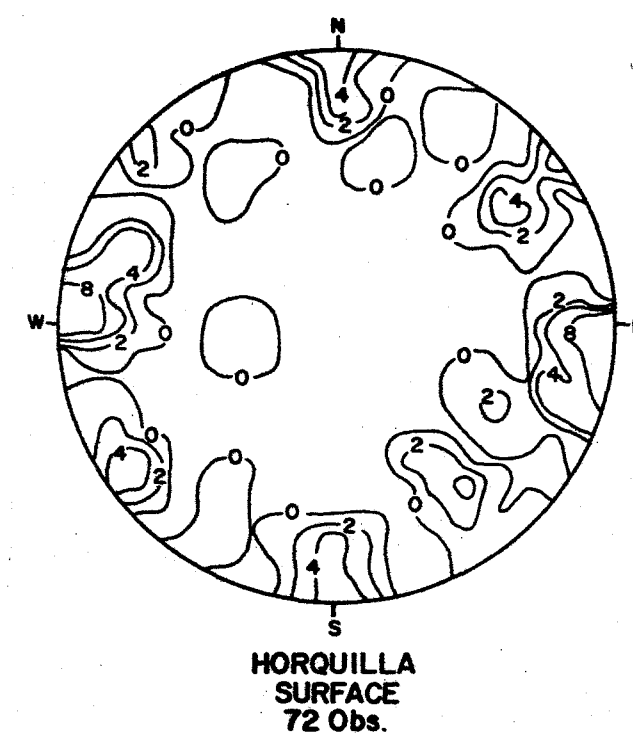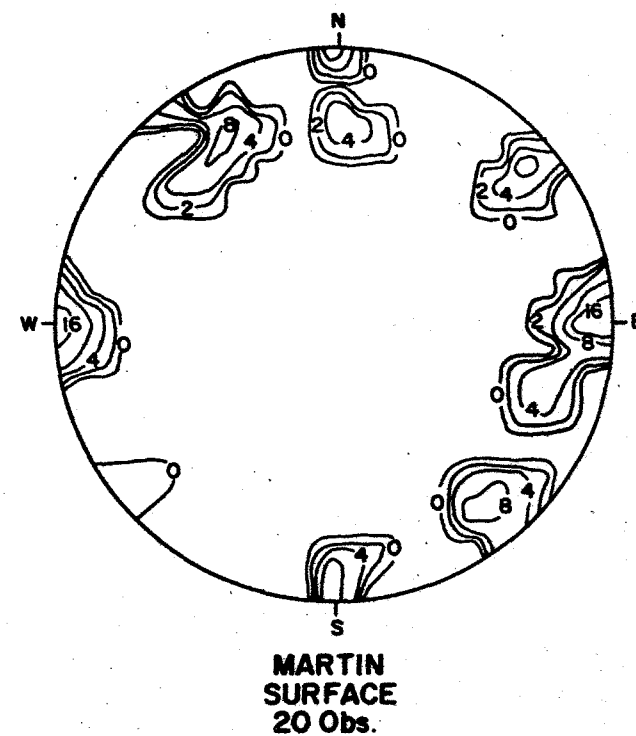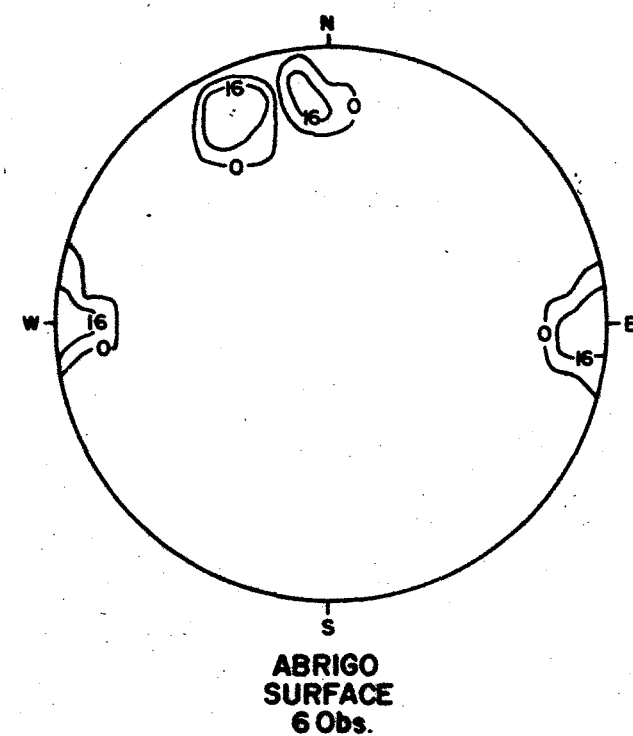
Figure 8.   Schmidt polar plots of joints

Table 4. Modal orientations of significant joint sets

Percentages of points making up sets are given under orientations. Data are from Continental Copper, Inc.'s (1974a, 1974b) geology maps.

Set Name	Horquilla Surface (72 obs)	Escabrosa Surface (236 obs)	Escabrosa Underground (216 obs)	Martin Surface (20 obs)	Martin Underground (3 obs)	Abrigo Surface (6 obs)	Abrigo Underground (58 obs)
Bedding							
Northeast Flat							N 55 E 30 NW (12.1%)
North-South	N-S 85 E (29.2%)	N-S 90 (33.1%)	N 18 E 85 NW (6.6%)	N-S 90 (26.7%)	N 15 E 80 NW (33.3%)	N-S 90 (33.3%)	N 15 E 60 NW (18.0%)
East-West	E-W 90 (20.8%)	E-W 80 N (11.6%)		E-W 90 (13.3%)		N 70 E 75 SE (66.7%)	N 85 W 70 SW (5.2%)
Northwest	N 35 W 80 NE (12.5%)	N 32 W 85 SW (13.1%)	N 43 W 75 SW (28.3%)	N 40 W 80 SW (6.7%)	N 55 W 80 SW (66.7%)		N 45 W 75 SW (17.2%)
Northeast	N 50 E 65 NW (11.1%)	N 28 E 80 SE (28.8%)	N 50 E 65 NW (45.3%)	N 50 E 80 NW (40.0%)			N 56 E 85 SE (17.2%)
Other							

Detail Line Data

The contoured and point Schmidt plots of the three detail lines (Fig. 9) reveal a maximum of seven joint sets of which five are common to all three lines. These joint sets are defined based on design considerations. Within one design joint set there may be more than one geologic joint set; however, to design for each geologic set is not realistic. The mean vector orientations and the characteristics of each fracture set for each line are given in Table 5. Although each line has its own fracture-set characteristics, the lines have been combined for the following reasons:

1. The rock properties of the ABC zone and Martin appear to be from the same population.

2. All structure data indicate that the upper Abrigo, Martin, and Escabrosa formations have the same major structure orientations.

3. The difference in fracture-set characteristics for a fracture set found in each line is not unrealistic.

4. It is not realistic at this point to suggest a design for each rock unit because of the limited data available.

The combined Schmidt contour and point plots are shown in Figure 9. The fracture characteristics of each joint set for the combined lines are given in Table 6. Because the mean values for the fracture-set characteristics (length, spacing, roughness, and dip) do not illustrate the distribution of these characteristics, curves were fitted to the data. The dip values best fit a normal distribution, while the length, spacing, and roughness fit a negative exponential. The normal distribution is

PERCENT PLOTS

DETAIL LINE A	DETAIL LINE B	DETAIL LINE C	COMBINED DETAIL LINES
ABRIGO (ABC ZONE)	ABRIGO (ABC ZONE)	MARTIN	A & B & C
100 obs.	98 obs.	58 obs.	256 obs.

POINT PLOTS

Contour Interval = 0, 2, 4 & 8 %
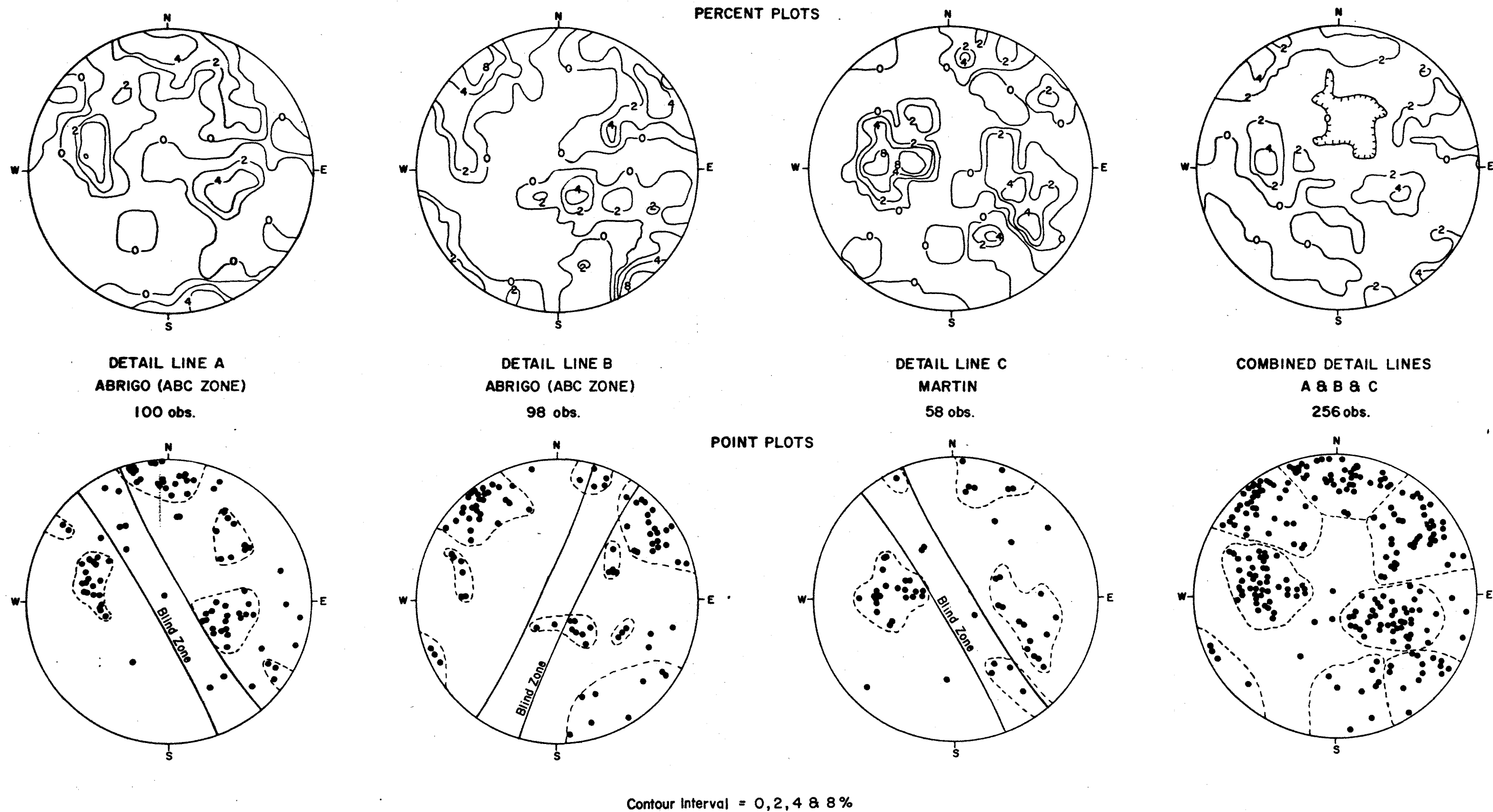
Figure 9. Schmidt polar plots of detail lines

Table 5. Fracture set characteristics for detail lines A, B, and C

Set Name	Observations (%)	Mean Vector		Roughness (mean)	Filling (%) [a]								Length (feet)			Spacing (feet)		
		Strike	Dip		N	CL	Q	C	M	E	Fe	G	Mean	Mode	Max.	Mean	Mode	Min.
Detail Line A																		
Bedding	21	N13E	47SE	2.8	57	19	10	14	5	10	0	0	5.7	10.0	13.0	0.9	0.4 .3	0.1
Northeast Flat	21	N16E	35NW	6.5	60	25	20	25	20	5	0	0	4.2	2.0	15.0	.6	.4	<.1
East-West	24	N86E	81SE	2.6	25	4	8	8	17	63	0	0	1.9	1.0	5.0	.6	.1	<.1
Northwest	6	N44W	56SW	2.6	80	0	0	0	0	20	0	0	2.2	1.0	6.0	2.4	.2 .6	.1
Northeast	9	N30E	81NW	1.9	33	0	0	56	11	0	0	0	1.1	1.0	2.5	2.7	.2 .6	.2
Detail Line B																		
Northeast	41	N53E	84SE	4.8	60	5	3	28	5	8	3	0	3.0	1.0	12.0	1.0	0.5	0.1
Northwest	26	N36W	79SW	4.8	52	4	12	36	4	20	0	12	4.2	1.0	11.0	.5	.2	.1
Northeast Flat	9	N63E	18NW	5.3	78	0	0	0	0	11	0	11	3.7		10.0	1.0	.7	.1
Bedding	6	N11E	60SE	4.3	67	0	0	0	17	17	17	17	4.8		10.0	4.3	.2	.2
East-West	5	N73W	82SW	1.4	80	0	0	20	0	0	0	0	2.8		5.0	.7		.2
Northeast 45	3	N25E	43NW	10.7	67	0	0	0	33	0	0	33	5.7	1.0	15.0	4.0		.2
Detail Line C																		
Bedding	38	N5E	37SE	7.6	50	18	0	36	5	0	0	0	3.8	1.0 1.5 4.5	12	0.7	0.2 .6	0.1
Northeast 45	26	N19E	46NW	7.7	60	13	0	40	0	0	0	0	2.8	.5	15	.1	.1	.1
East-West	12	N67W	78SW	4.1	71	0	0	29	0	0	0	0	2.1	2.0	4.5	1.5		.1
Northeast	9	N56E	62NW	6.2	40	60	60	40	0	40	0	0	2.4	.5	7.0	.5	.1	.1

a. N = none; CL = chlorite; Q = quartz; C = calcite; M = mineralized; E = epidote; Fe = iron oxide; G = garnets.

Table 6. Fracture set characteristics for combined detail lines

Set Name	Observations (%)	Mean Vector		Roughness (mean)	Filling (%) [a]								Length (feet)			Spacing (feet)		
		Strike	Dip		N	CL	Q	C	M	E	Fe	G	Mean	Mode	Max.	Mean	Mode	Min.
Bedding	14	N11E	46SE	4.5	55	16	4	24	6	6	2	2	4.7	1.0 4.0	13.0	1.2	0.4	0.1
Northeast Flat	17	N25E	33NW	6.0	68	20	17	22	15	5	0	5	3.6	1.0	15.0	.9	.1	<.1
Northeast	26	N50E	83SE	4.3	64	7	2	29	3	2	0	0	2.9	1.0	15.0	1.0	.1 .2	.1
Northwest	21	N38W	67SW	4.0	54	2	7	35	4	10	0	0	2.9	1.0	11.0	1.3	.1	.1
East-West	18	N87W	85SW	2.8	36	9	4	11	13	43	2	0	2.2	1.0	12.0	1.3	.1	<.1

a. N = none; CL = chlorite; Q = quartz; C = calcite; M = mineralized; E = epidote; Fe = iron oxide; G = garnets.

defined by the mean and standard deviation, and the exponential is of the form $Y = Ae^{-BX}$. The cumulative exponential curves are forced through 100% at the X value equal to zero resulting in an equation of the following form:

$$Y = 100\, e^{-BX}. \tag{1}$$

The distributions of the set characteristics for each fracture set are given in Figures 10 through 14. Because Table 6 contains an abundance of information, only the main conclusions are discussed below.

The Bedding and Northeast Flat fracture sets have potentially the lowest shear strength present. Both sets have minimal amount of filling and they are the most continuous, thereby having the lowest shear strength. The East-West set has the highest shear strength because over 50 percent of the fractures are filled with epidote and it is the most discontinuous set. The Northeast and Northwest fracture sets have shear strengths between those of the above two joint sets. These two sets are less than 50 percent filled, with the Northeast having the closest spacing of all sets.

Structural Continuity

It is apparent from this analysis that there are six major joint sets in the Paleozoic section on Marble Peak. Certain sets are missing for each condition, i.e., rock types, location; however, this may be attributed to lack of data or local variations. One example of this is the missing North-South set in the detail line data that exists in the surface data. One case that cannot be explained without further work is the Northeast Flat set. This set obviously exists in the underground data
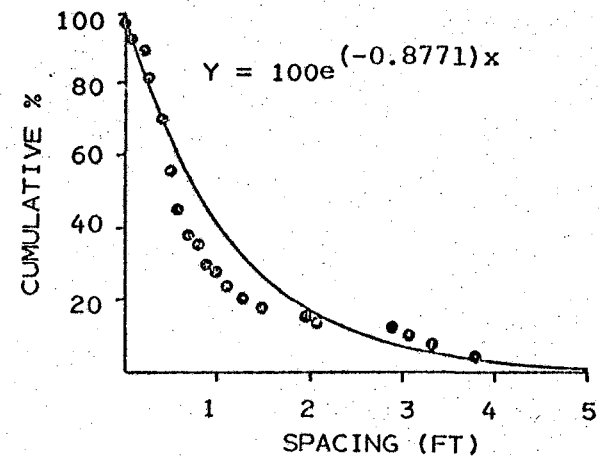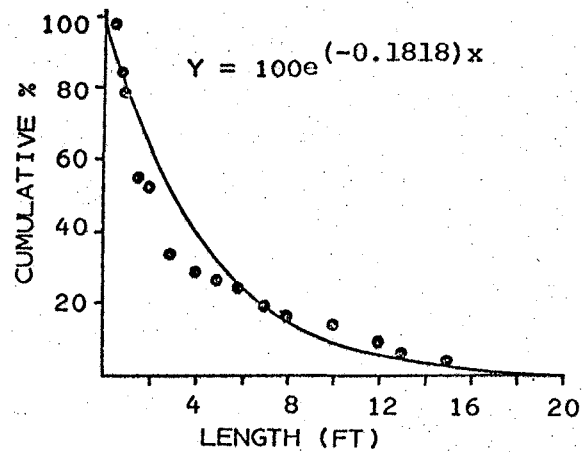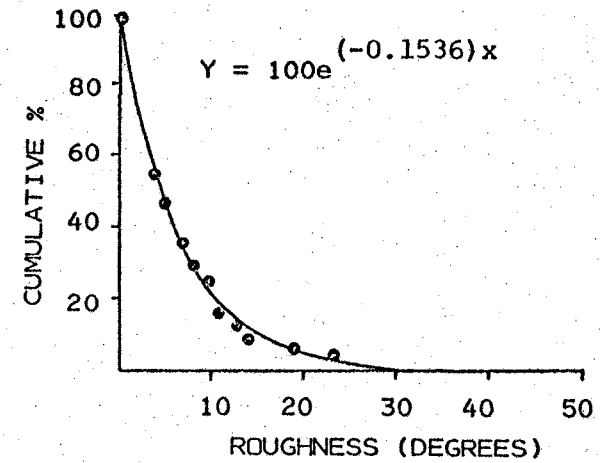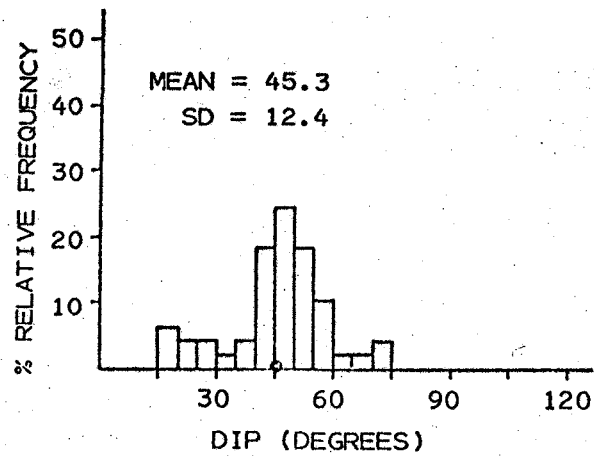
Figure 10. Distributions of dip, roughness, length, and spacing for the Bedding fracture set
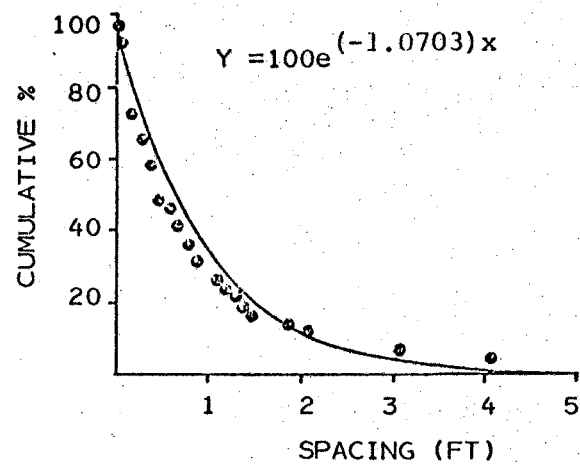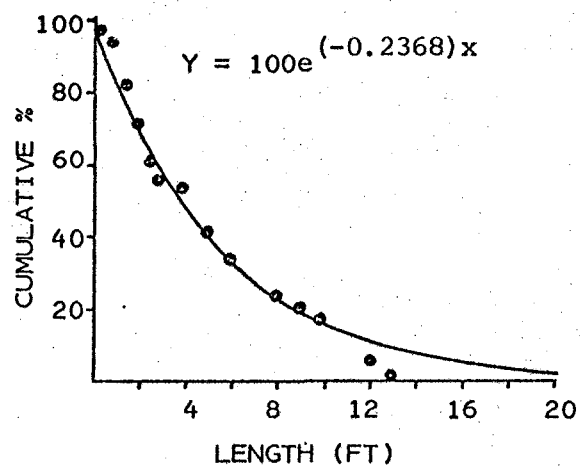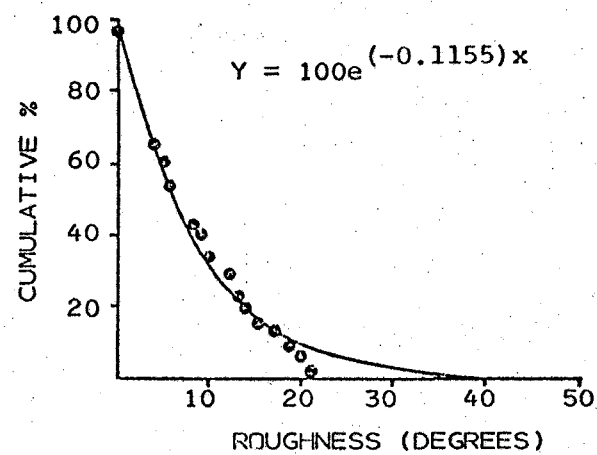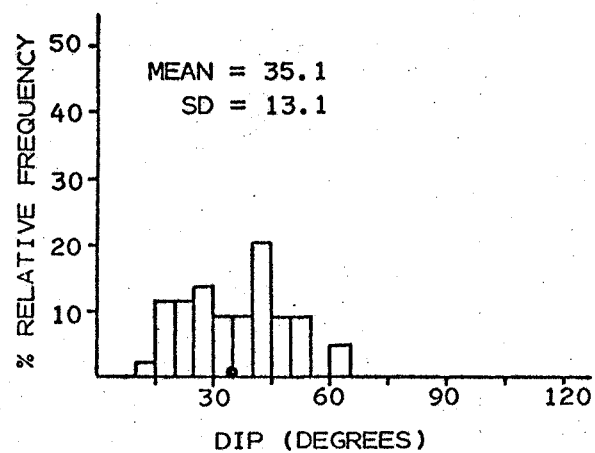
Figure 11. Distributions of dip, roughness, length, and spacing for the Northeast Flat fracture set
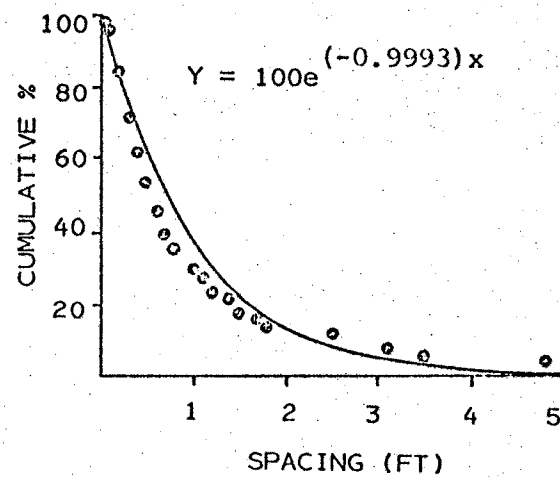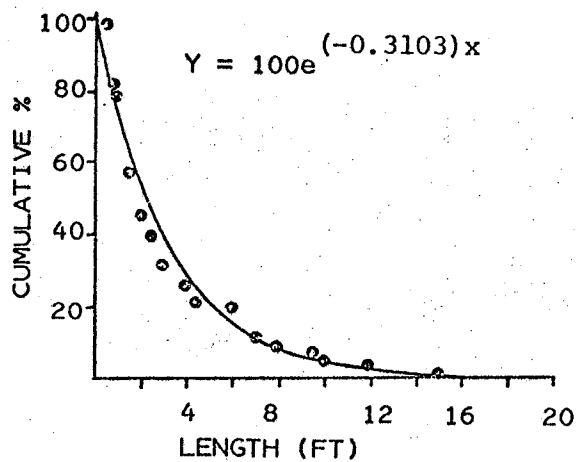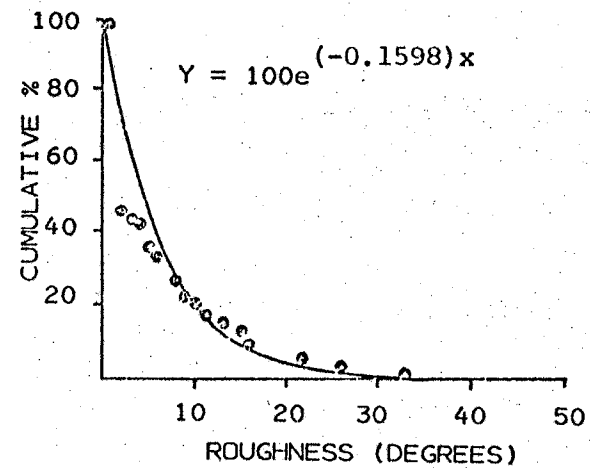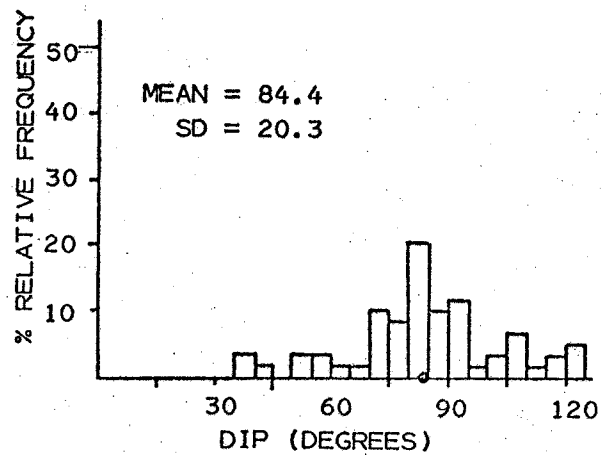
Figure 12. Distributions of dip, roughness, length, and spacing for the Northeast fracture set

% RELATIVE FREQUENCY

MEAN = 66.6
SD = 18.7

DIP (DEGREES)

$$Y = 100e^{(-0.1744)x}$$

ROUGHNESS (DEGREES)

$$Y = 100e^{(-0.3039)x}$$

LENGTH (FEET)

$$Y = 100e^{(-0.7023)x}$$
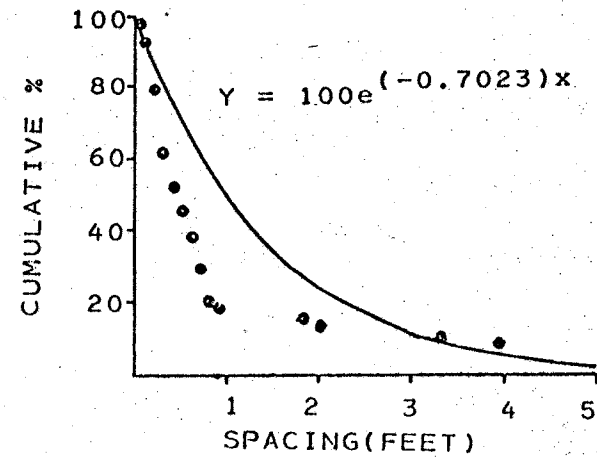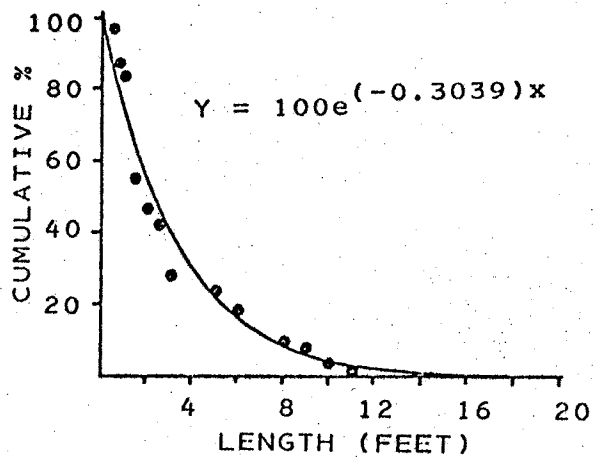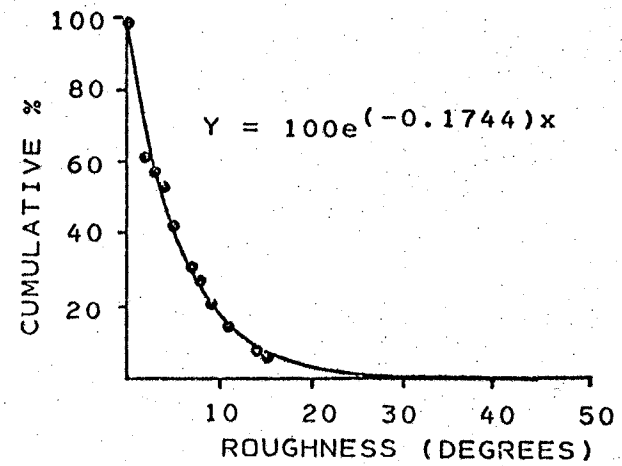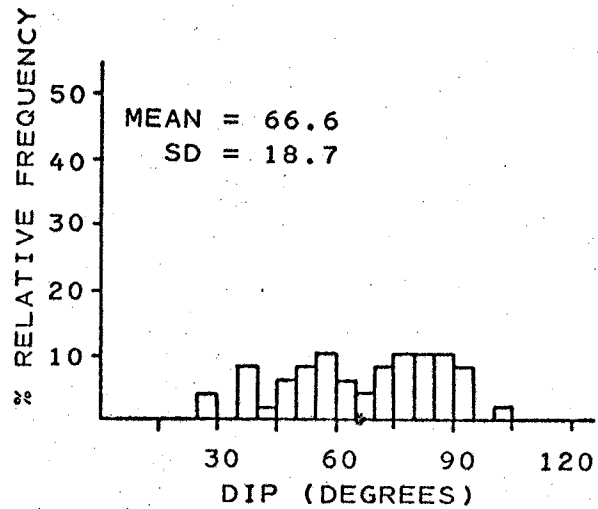
SPACING (FEET)

Figure 13. Distributions of dip, roughness, length, and spacing for the Northwest fracture set
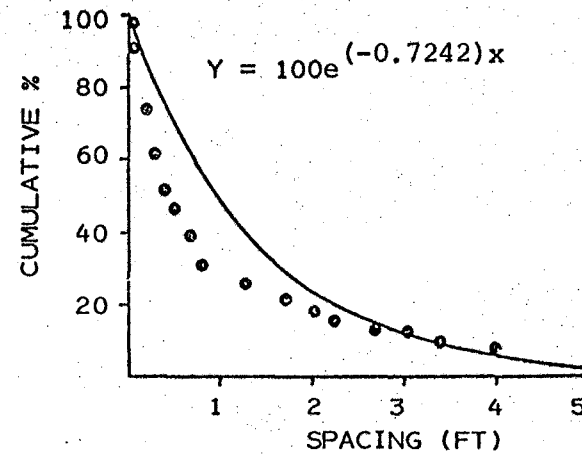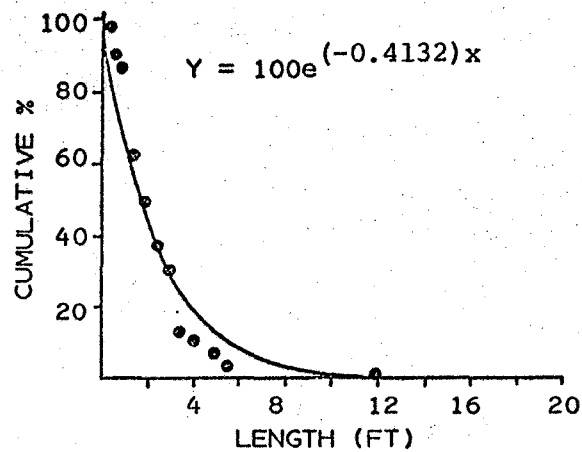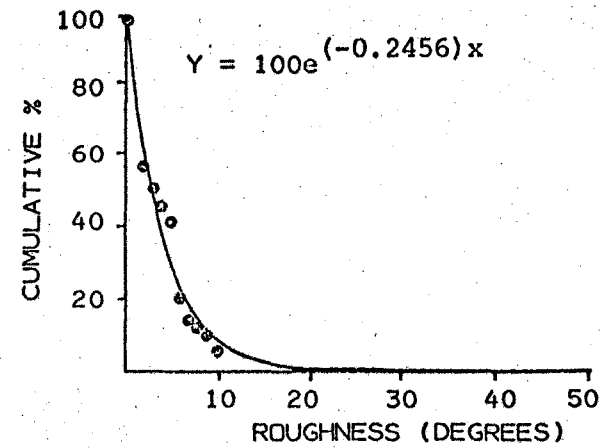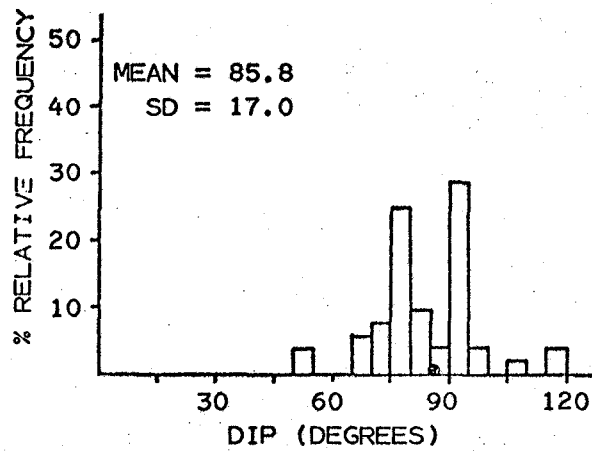
Figure 14. Distributions of dip, roughness, length, and spacing for the East-West fracture set

but is lacking in the surface data. Recent work by Fritts (1974a) has shown a thrust fault system exists just above the mineralization. Because the Northeast Flat set was observed in the ABC zone, it will be included as part of the structural system.

CHAPTER 4

ROCK SUBSTANCE PROPERTIES

Rock substance and fracture strength properties were obtained from uniaxial compression, triaxial compression, Brazilian disc tension, and direct shear tests. Laboratory procedures for these methods have been discussed by Hawkes and Mellor (1970, 1971), Handros (1959), Donath (1966), and Coulson (1970). The rock substance properties that were measured or calculated in the testing program included compression strength, tensile strength, stiffness (Young's modulus), Poisson's ratio, internal angle of friction, intact rock cohesion, rock-on-rock friction angle, and rock-on-rock cohesion. Appendix B outlines the procedure for calculating the rock substance values and explains the laboratory methods used for this study.

Sample Collection

NX core specimens of the ABC zone, upper Abrigo, and Martin were collected from seven drill holes in the area of the ABC zone. Because most of the drill core from the mineralized zone was split for assaying, block samples were collected from two crosscuts on the 6400-foot level. These block samples were cored in laboratory.

Table C-1 (Appendix C) lists the specimen number, diamond drill hole number, depth below collar, rock type, and height-to-diameter ratio for the uniaxial compression tests. Tables C-2 and C-3 (Appendix

34

C) list the same information for the Brazilian disc tension, triaxial compression, and direct shear tests.

Uniaxial Compression Strength

A list of specimens tested, the angle between bedding and the vertical axis of the core, failure mode, failure control, and ultimate uniaxial compression strength for the three rock units is given in Table 7. Failure mode was divided into three categories: violent (V), indicating the specimen exploded; moderate (M), mean the specimen broke into many pieces; and passive (P), meaning the specimen broke into two or three pieces. Failure control is classified as (1) structural control (SC), with failure occurring on an existing plane, and (2) no structural control (NSC).

Plots of the vertical stress versus longitudinal strain and lateral versus longitudinal strain were recorded during the compression test. From these graphs, the ultimate strength, stiffness (Young's modulus) with its stress range, and Poisson's ratio with its stress range can be calculated (Table C-4, Appendix C). The mean standard deviation and 95% confidence interval for the uniaxial test are given in Table 8. Rock stiffness and Poisson's ratio were selected at 50% of failure.

In calculating the mean ultimate strengths, specimen D-6 was excluded from the Martin unit because of its anomalous value (greater than 2 times the standard deviation). Specimen D-6 could be included in the mean calculation, if strengths of the core that was already broken in the core box could be included. Its exclusion results in a more realistic estimate of the mean. Due to testing error, rock stiffness was not

Table 7. Bedding angle, failure mode, failure control, and ultimate strength for uniaxial compression test

Specimen No.	Angle of Bedding to Core	Failure Mode [a]	Failure Control [b]	Ultimate Uniaxial Strength (psi)
ABC Zone				
A-1	none present	V	NSC	28,000
B-2	42°	V	SC	20,500
B-3	15	V	SC	33,500
B-4	55	V	SC	17,300
B-5	35	V	SC	33,100
B-6	25	V	SC	20,400
Unmineralized Upper Abrigo Unit				
C-1	70	M	SC	15,000
C-2	65	M	SC	16,100
C-3	25	M	SC	24,500
C-4	55	M	SC	15,000
C-5	60	M	SC	13,000
C-6	50	M	SC	14,500
Unmineralized Martin Unit				
D-1	65	M	SC	10,500
D-2	60	M	NSC	13,500
D-3	60	V	SC	26,600
D-4	60	M	SC	16,700
D-5	30	M	SC	20,500
D-6	55	V	NSC	39,000

a. V = violent; M = moderate; P = passive.

b. SC = structural control; NSC = no structural control.

Table 8. Mean, standard deviation, and 95% confidence interval for ultimate strength, stiffness, and Poisson's ratio

$\overline{X}$ = mean; SD = standard deviation; CI = confidence interval.

Rock Unit	Ultimate Strength (psi)			Stiffness (psi)			Poisson's Ratio		
	$\overline{X}$	SD	95% CI	$\overline{X}$	SD	95% CI	$\overline{X}$	SD	95% CI
ABC Zone	25,500	7,000	± 7,400	14.0×10^6	3.0×10^6	$\pm 3.2 \times 10^6$	0.27	0.17	± 0.18
Upper Abrigo	16,400	4,100	± 4,300	10.6	2.9	± 3.6	.26	.12	± .31
Martin	17,600	6,300	± 7,800	11.0	6.2	± 6.4	.28	.13	± .17

calculated for specimen C-2 and Poisson's ratio was not calculated for specimens C-1, C-2, and C-6.

The ABC mineralized zone is the strongest and stiffest unit tested. The Martin is slightly stronger than the upper Abrigo. This difference occurs because the Martin is a massive limestone while the upper Abrigo is a limestone containing shaley interbeds.

Tensile Strength

Tensile failure during a Brazilian disk tension test is caused by an applied compressive stress that induces a tensile stress. This mode of tensile failure is probably the same as the mode of underground tensile failures. Work by Hardy and Jayaraman (1970) indicates that the "true" tensile strength is 0.6 to 0.93 of the Brazilian tensile strength. Vouille (1964) found the "true" tensile strength to be 0.5 of the Brazilian tensile strength. However, because the disk tension test simulates the most probable mode of tensile failure, the Brazilian disk tensile strength will be used as the rock-substance tensile strength.

Tables 9 and 10 give the results for the Brazilian tests for the three units. Generally, tensile strength is 0.10 to 0.20 of the uniaxial compressive strength, and tensile strengths of the ABC zone, the upper Abrigo and the Martin fall within this range. No relationship between tensile strengths and failure control is shown.

Statistical Analysis of Population Similarity

To determine if the rock types are similar, a statistical analysis was made. The two statistical tests used to evaluate sample similarity were the Student's t test, which compares population means, and the

Table 9. Angle of loading to bedding, angle of loading to major fractures, failure control, and tensile strength for Brazilian disk tension test

Specimen No.	Angle, Loading to Bedding	Angle, Loading to Major Fractures	Failure Control[a]	Disk Tension Strength, psi
ABC Zone				
M-1		90°	NSC	2,640
M-2		0	SC	710
M-3		0	NSC	480
M-4	0°	0	NSC	2,200
M-5	90	0	SC	1,720
M-6		90	SC	1,150
M-7	0	0	NSC	2,060
M-8		0	SC	780
M-9	90	0	NSC	1,440
M-10		0	SC	760
Unmineralized Upper Abrigo				
N-1		0	SC	410
N-2	90	0	SC	1,060
N-3	45	90	SC	550
N-4	0		SC	1,810
N-5	90	90	NSC	1,360
N-6	0	90	SC	1,110
N-7	30	0	SC	660
N-8		90	NSC	2,280
N-9		0	SC	2,460
N-10		0	SC	2,030
Unmineralized Martin				
O-1	0		NSC	1,040
O-2	90		NSC	1,430
O-3		90	SC	1,900
O-4		0	SC	2,290
O-5		0	NSC	2,140
O-6		90	NSC	2,090

a. SC = structural control; NSC = no structural control.

Table 10. Mean, standard deviation, and 95% confidence interval for Brazilian disk tension strength

Rock Unit	n	$\overline{X}$	s	95% Confidence Interval
ABC Zone	10	1,390 psi	740	± 530 psi
Upper Abrigo	10	1,370	740	± 530
Martin	6	1,820	480	± 510

F test, which compares the shape of the sample distribution curves. In a strict statistical analysis two rock units can be considered from the same population if all t and F tests are passed. Table 11 shows the results of the t and F tests.

Within the 95% confidence level, it can be inferred that the ABC zone and upper Abrigo and the upper Abrigo and Martin are from the same population of rock properties. The ABC zone and Martin could also be inferred to be from the same population except their tensile strengths do not pass the t test. Cochran et al. (1954, p. 19) states "the step from sampled population to target population is based on subject-matter knowledge and skill, general information and intuition but not on statistical methodology." Therefore, based on engineering judgment and subject matter knowledge, the combined physical properties of all three units will be used in the design analysis. The reasons for combining these units are:

1. Only one test failed and it was by a small margin.

2. The separation of the ABC zone and the upper Abrigo in the design is not reasonable at this time.

Table 11. Statistical analysis to evaluate population similarities of rock units

The first number is the calculated t or F value; the second number is table t or F value.

Property	ABC Zone + Upper Abrigo		ABC Zone + Martin		Upper Abrigo + Martin	
	t test	F test	t test	F test	t test	F test
Compressive Strength	Pass (0.06-2.23)	Pass (1.00-7.15)	Pass (1.95-2.36)	Pass (1.25-9.36)	Pass (0.39-2.36)	Pass (2.32-9.36)
Stiffness	Pass (1.90-2.26)	Pass (1.07-7.39)	Pass (1.05-2.26)	Pass (0.23-7.39)	Pass (0.13-2.31)	Pass (0.22-9.60)
Poisson's Ratio	Pass (0.09-2.36)	Pass (2.01-39.3)	Pass (0.11-2.26)	Pass (1.71-7.39)	Pass (0.22-2.45)	Pass (0.85-39.2)
Tensile Strength	Pass (1.68-2.10)	Pass (0.89-4.03)	Fail (3.04-2.14)	Pass (2.13-4.48)	Pass (1.32-2.14)	Pass (2.38-4.48)

The rock properties for the combined ABC zone, upper Abrigo, and Martin rock units are listed in Table 12.

Table 12. Mean and standard deviation of combined rock properties

	Compressive Strength	Stiffness	Poisson's Ratio	Tensile Strength
Mean	19,920	10.84×10^6 psi	0.27	1,480 psi
Standard Deviation	6,970	4.57	0.12	690

Intact Rock Shear Strength

Table 13 lists the specimen numbers, angle between bedding and vertical axis of core, failure control, confining stress, and failure stress. Only specimens in the ABC zone and upper Abrigo were tested triaxially. Specimens were not tested beyond a confining stress of 2,000 psi because of limitations in the testing equipment.

Assuming a Mohr-Coulomb failure envelope, the accepted method of calculating the internal angle of friction and the cohesion is to construct a Mohr circle for each test and to connect the common tangents of these circles. Because the rock is such a variable material, the Mohr circles are difficult to connect (Fig. 15). An alternate method of calculating the internal friction angle is plotting the failure stress against confining stress and calculating the best fit straight line for the points (Fig. 16). The internal angle of friction ($\emptyset$) and cohesion (c) are then found by using the slope of the line m in the following formulas

Table 13. Angle of bedding to vertical axis of core, failure control, confining stress, and failure stress for triaxial compression test

Specimen No.	Bedding Angle	Failure Control	Confining Stress	Failure Stress
ABC Zone				
A-2		NSC	500 psi	29,100 psi
T-3	40°	SC	500	30,600
T-2	40	SC	1,000	21,000
T-4	40	NSC	1,000	34,000
B-7	25	NSC	1,000	37,600
T-1	40	SC	1,500	38,600
B-2	42	SC	1,500	31,000
T-5	25	SC	2,000	40,600
Upper Abrigo				
C-7	55	SC	2,000	13,000
C-8	65	SC	1,000	31,000
C-9	35	SC	2,000	15,800
C-10	35	SC	500	21,500
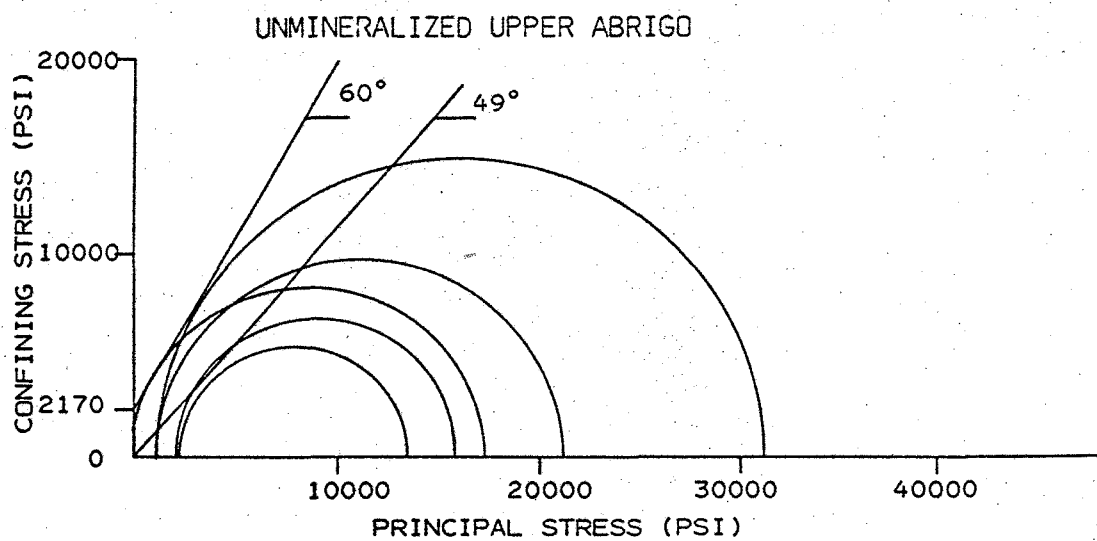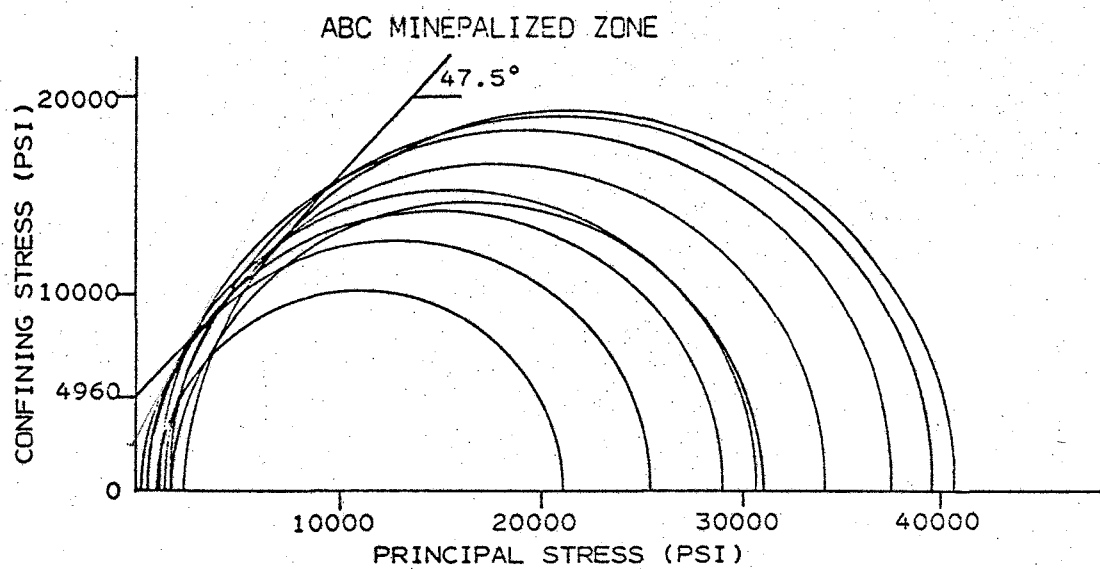
Figure 15. Mohr circles for ABC zone and upper Abrigo
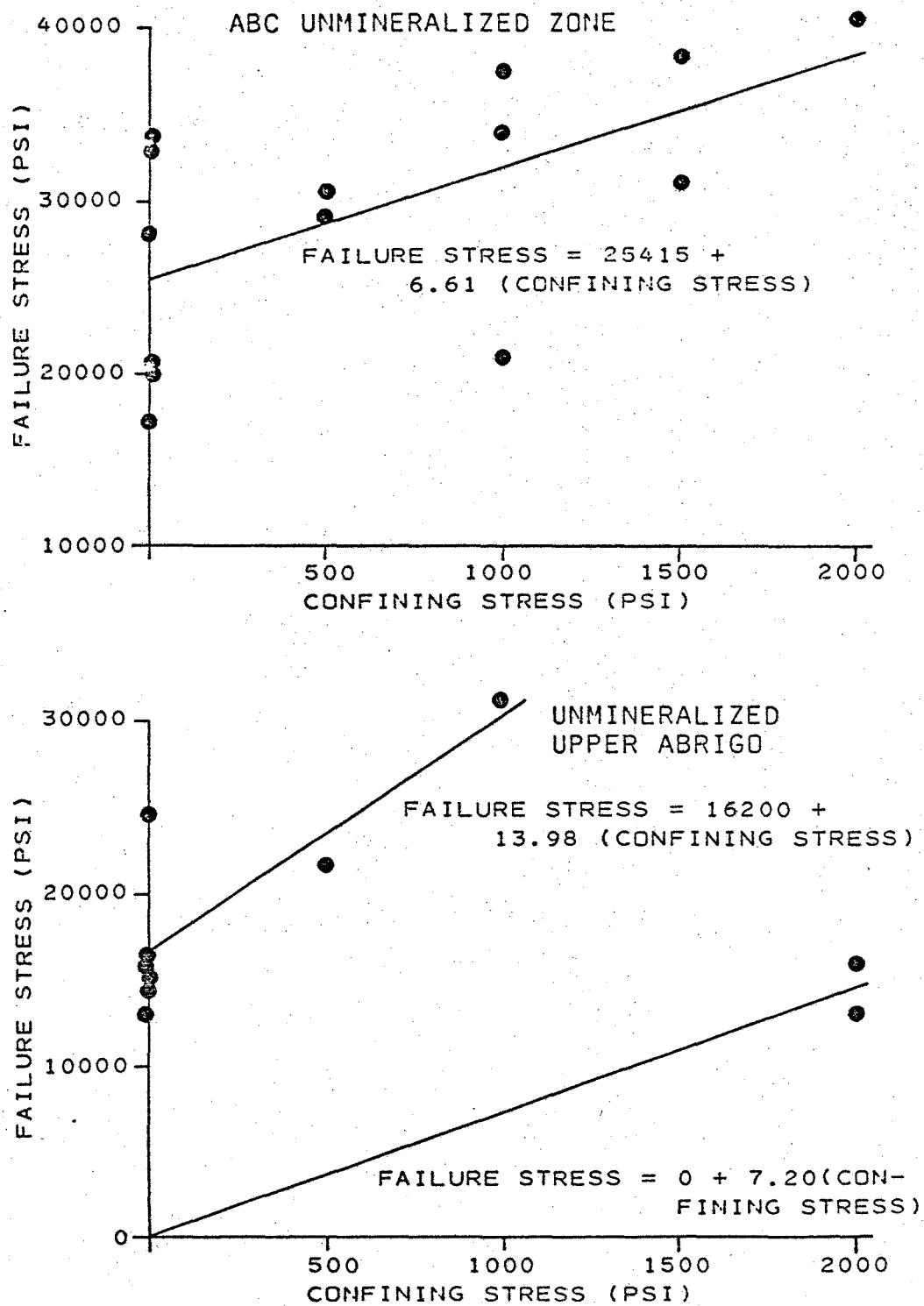
Figure 16. Failure stress versus confining stress for ABC zone and upper Abrigo

(Obert and Duvall, 1967):

$$\emptyset = \tan^{-1} \frac{m-1}{2\sqrt{m}} \tag{2}$$

$$S_c = \frac{\text{uniaxial compression}}{2\sqrt{m}} \tag{3}$$

The mean and 95% confidence interval for the internal angle of friction and cohesion of the ABC zone and upper Abrigo is given in Table 14. Two results have been reported for the upper Abrigo because samples C-7 and C-9, which failed along major structures, probably had little to no cohesion. If this assumption is correct, the friction angle for these cohesionless samples is within the range of the friction angle of the remaining upper Abrigo samples.

In the previous section it was concluded that the three rock units could be considered as one for this initial design. Combining all samples except C-7 and C-9, the internal angle of friction is 55.6° and the mean cohesion is 3,090 psi (Fig. 17, Table 14).

Rock-on-Rock Shear Strength

The results of a direct shear test from a rock-on-rock cut fracture represents the shear strength of an unfilled planar fracture. This shear strength is used to calculate the rock-on-rock friction angle and rock-on-rock cohesion. Two specimens from the ABC zone were tested. The normal stress versus shear stress curves for the specimens are shown in Figure 18. These curves indicate that the shear strength is not linear above 225 psi. The power curve proposed by Jaeger (1971) may be a better representation of the shear strength curve (Fig. 18); however, the

● ABC ZONE

✕ UNMINERALIZED UPPER ABRIGO

▲ MARTIN

FAILURE STRESS = 20156 + 10.42 (CONFINING STRESS)

Figure 17. Failure stress versus confining stress for combined rock units

Table 14. Internal friction angle and intact rock cohesion

| Rock Unit | n | Internal Friction Angle | | | Intact Rock Cohesion | | |
| | | Mean | 95% Confidence Limit | | Mean | 95% Confidence Limit | |
			Upper	Lower		Upper	Lower
ABC Zone	13	47.5°	57.7°	7.7°	4,960 psi	11,100 psi	3,690 psi
Upper Abrigo 1 [a]	7	60.11	67.1	50.9	2,170	5,130	1,390
Upper Abrigo 2 [b]	2	49.1	--	--	0	--	--
Martin [c]	5	--	--	--	--	--	--
Combined ABC Zone, Upper Abrigo 1, and Martin	25	55.6	60.8	45.9	3,090	4,040	2,590

a. Samples C-8 and C-10.

b. Samples C-7 and C-9, which failed along major structures.

c. Martin tested at zero confining stress only.

SPECIMEN 1

$$T = 2.7 + N(\tan 27.7)$$
(ONLY FOR N < 200 PSI)

$$T = 1.3\ N^{0.8}$$

SHEAR STRESS, T (PSI)

NORMAL STRESS, N (PSI)

SPECIMEN 1

$$T = 5.2 + N(\tan 28.3)$$
(ONLY FOR N < 200 PSI)

$$T = 1.5\ N^{0.8}$$

SHEAR STRESS, T (PSI)

NORMAL STRESS, N (PSI)
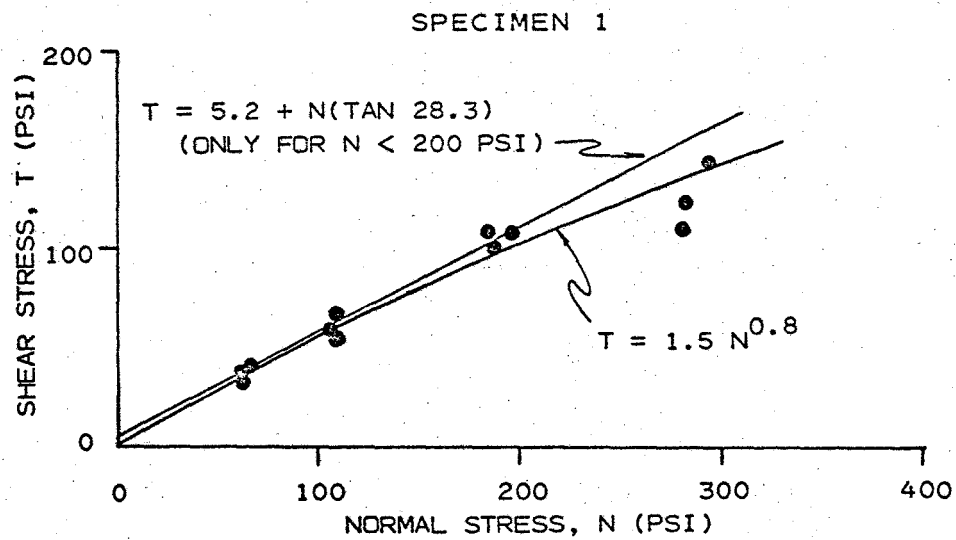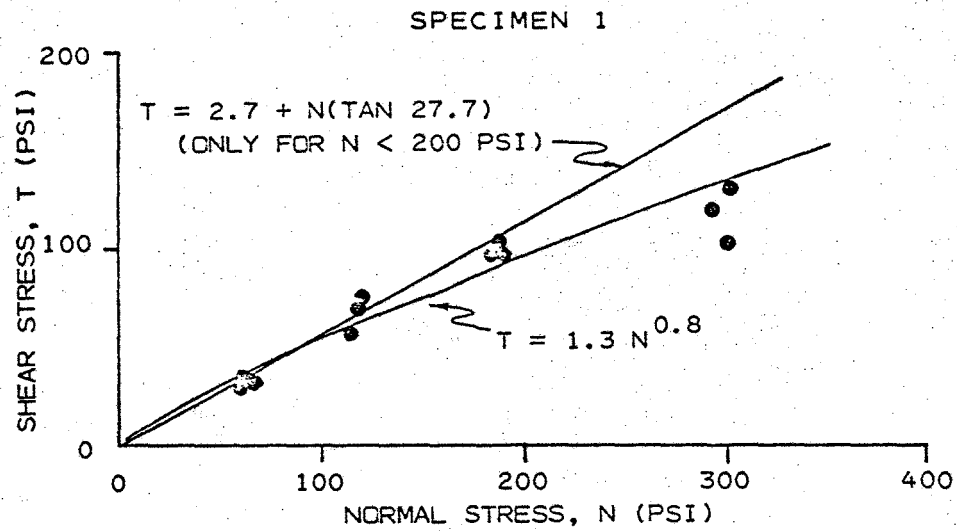
Figure 18. Rock-on-rock direct shear for ABC zone

design analysis is not presently equipped to handle this relationship.
The mean and 95% confidence interval of the rock-on-rock friction angle
and cohesion are given in Table 15 for each specimen. Combining the
two specimens, the average rock-on-rock friction angle is 28 degrees
and the average rock-on-rock cohesion is 4.0 psi (Table 15).

Table 15. Rock-on-rock friction angle and cohesion for ABC zone

Specimen No.	n (normal loads)	Rock-on-Rock Friction Angle			Rock-on-Rock Cohesion		
			95% Confidence Limit			95% Confidence Limit	
		Mean	Upper	Lower	Mean	Upper	Lower
1	4	27.7°	30.9°	24.4°	2.7 psi	12.3 psi	-7.0 psi
2	4	28.3	30.3	26.2	5.2	11.4	-1.1
Combined		28.0	29.8	26.1	4.0	9.5	-1.6

CHAPTER 5

ROCK MASS PROPERTIES

Having tested the rock substance and calculated the character-istics of the structural features it is necessary to integrate the two and describe the rock mass properties. The exact method of integrating the rock substance strength with the fracture strengths is not well defined. One approach is to classify the rock according to its strength and structural properties. Another approach is to model the rock mass and determine the amount of intact rock and the amount of fractured rock. The main problem with the classification approach is that most design analyses require specific strength properties. Classification does however provide a means of qualitatively describing the rock mass. The model method does provide a specific rock mass strength(s) but no single model includes all variables.

Classification of Rock Mass

Many methods of classification are available. For this study Deere's (1968) (Table 16) and Coates' (1970) (Table 17) classifications are used. Using Deere's classification the rock mass at Marble Peak is described as follows:

ABC Zone: A high to very high strength, a medium to high modulus ratio (Fig. 19), and a close joint spacing.

Upper Abrigo: A medium to high strength, a high modulus ratio (Fig. 19), and a close joint spacing.

52

Table 16. Engineering classification of rocks, after Deere (1968)

I. Strength Classification

Description	Uniaxial Compressive Strength (psi)
very high strength	32,000
high strength	16,000—32,000
medium strength	8,000—16,000
low strength	4,000—8,000
very low strength	< 4,000

II. Modulus Ratio (E/σ_{VH}) Classification

Description	Modulus Ratio
high modulus ratio	500
average modulus ratio	200—500
low modulus ratio	200

III. Joint Spacing Classification

Description	Joint Spacing
very close	< 2 in.
close	2 in.—1 ft
moderately close	1 ft —3 ft
wide	3 ft —10 ft
very wide	> 10 ft

IV. Rock Quality Designation (RQD)

Description	RQD (%)
very poor	0—25
poor	25—50
fair	50—75
good	75—90
excellent	90—100

Table 17. Engineering classification of rocks, after Coates (1970)

I. Rock Strength Classification

Description	Uniaxial Compressive Strength (psi)
very strong	>25,000
strong	10,000—25,000
weak	5,000—10,000
very weak	< 5,000

II. Rock Deformation Classification

Description	% Strain
elastic	<25% total strain irrevocable
yielding	>25% total strain irrevocable

III. Continuity of Formation

Description	Layer Spacing
massive	>6 ft
layered	<6 ft

IV. Fracture Spacing

Description	Block Size
blocky	1 ft —6 ft
broken	3 in.—1 ft
very broken	<3 in.
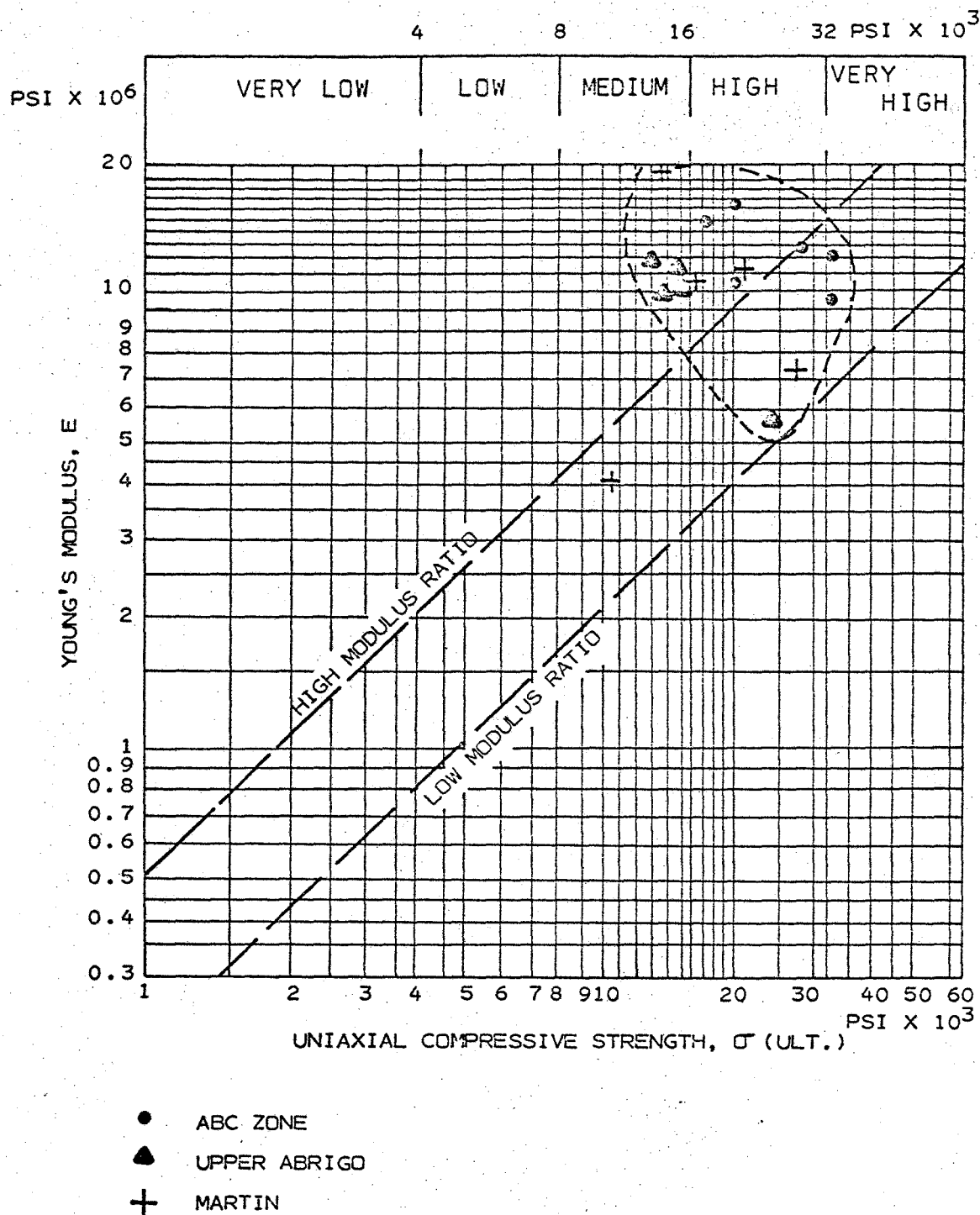
Figure 19. Strength modulus plot for ABC zone, upper Abrigo, and Martin

Martin: A medium to very high strength, a medium to high modulus ratio (Fig. 19), and a close joint spacing.

In addition, Deere proposed a rock quality designation (RQD), which is a modified core recovery. The RQD is calculated by summing the core lengths greater than twice the diameter (4 in. for the Control Property) and dividing by the total length of core inspected. A list of diamond drill holes, rock types, footage interval below the collar, and RQD is reported in Table 18. Based on a weighted average, the results are:

Rock Type	% RQD
Martin	70
Upper Abrigo	70

Using Coates' classification the rock mass at Marble Peak would be described as follows:

ABC Zone: A strong to very strong, elastic, layered, and broken to very broken rock.

Upper Abrigo: A strong, elastic, layered, and broken to very broken rock.

Martin: A strong to very strong, elastic, layered, and broken to very broken rock.

Although both classifications express the rock mass qualitatively, neither can presently be used in a design calculation. As additional information is obtained about pillar stability and roof support, it will be possible to develop a design classification for the mine.

Table 18. Rock quality designation for six drill holes in ABC zone

Diamond Drill Hole No.	Rock Formation	Footage Interval	RQD %
6	Martin	756—776	79
	Upper Abrigo	776—790	88
37	Martin	286—300	60
	Upper Abrigo	372—379	31
45	Upper Abrigo	674—689	82
	Upper Abrigo	700—705	93
69	Martin	514—523	50
	Upper Abrigo	523—539	81
	Upper Abrigo	617—623	81
70	Upper Abrigo	502—509	40
	Upper Abrigo	547—553	100
	Upper Abrigo	553—568	46
72	Martin	237—240	100
	Upper Abrigo	245—258	59
	Upper Abrigo	336—341	60

Estimate of Rock Mass Strength

Failure Modes

The rock mass strength is not only dependent on the rock sub-stance and fracture strength but also the orientation, length, and spacing of fractures. Studies by Donath (1961) and John (1969) indicate that a continuous structure oriented approximately 30 degrees from the direction of loading causes the greatest weakening of the rock mass, while struc-tures normal or parallel to loading have little effect on rock strength (Fig. 20). Assuming the load on the pillar to be normal to the dip of bedding, all but the Bedding fracture set have an orientation that will
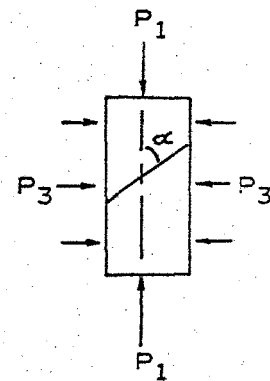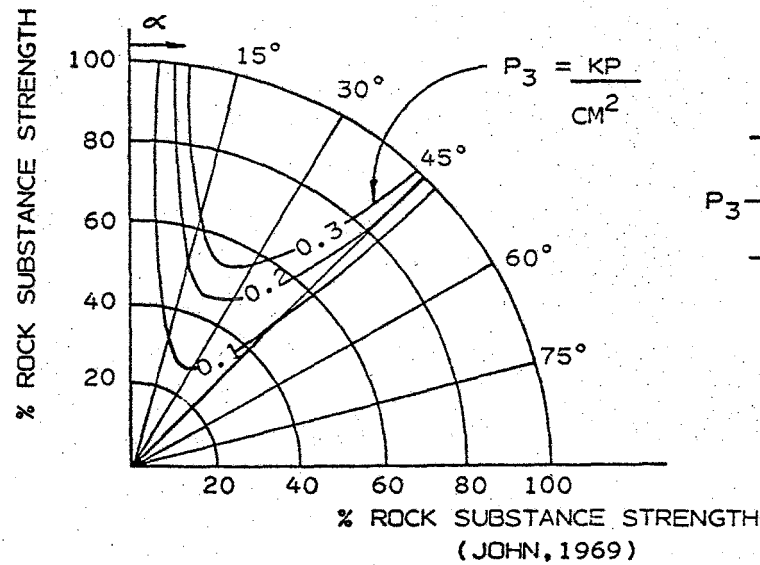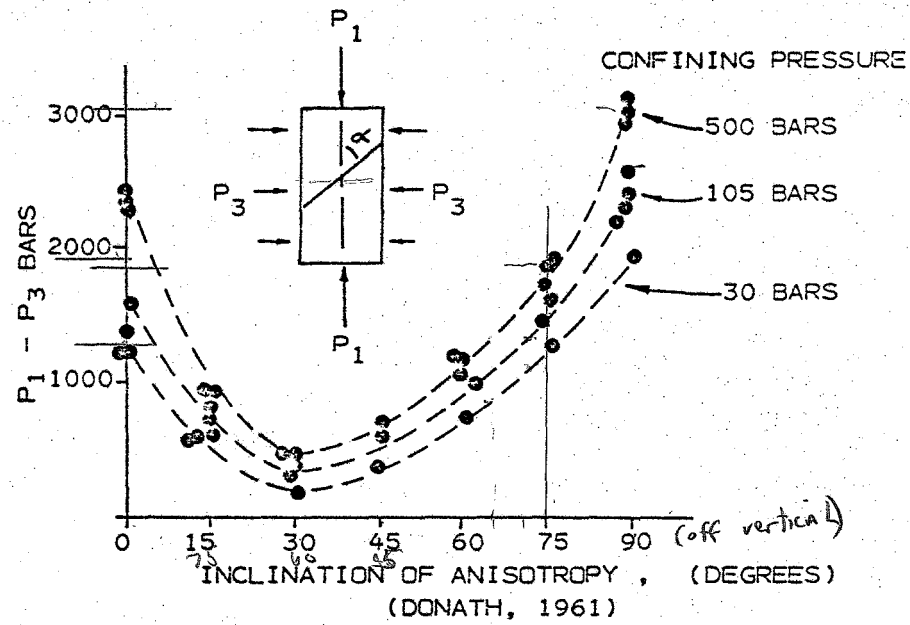
Figure 20. Rock strength versus structure orienta[tion]

reduce the pillar rock strength. If the fracture lengths do not cut completely through the pillar, the rock mass strength will also be determined by the percentage of intact rock along the plane. The structure analysis resulted in distributions of fracture lengths (Figs. 10 through 14). The probability of a fracture's length being greater than 10 feet and greater than 20 feet for the predominant joint sets is:

Set	Probability Length $>$ 10 ft	Probability Length $>$ 20 ft
Bedding	10.2%	2.6%
Northeast Flat	9.4	.9
East-West	1.6	.0
Northeast	4.5	.2
Northwest	4.8	.2

This analysis indicates that the chance of failure on a continuous joint is low for pillar widths greater than 20 feet. Faults have higher probabilities for lengths greater than 20 than do joints, but faults occur less frequently than joints. Although a single joint may significantly reduce the rock mass strength for pillar widths less than 20 feet, a combination of joints can provide a more continuous failure path. The two most probable geometries formed from a combination of joints are the wedge and the step path.

Table 19 lists the bearing, plunge, and dihedral angle for the possible wedges formed by the intersection of the predominant fracture sets. The size of these wedges depend on the distribution of fracture lengths. Since the probability of fracture lengths greater than 20 feet is

Table 19. Bearing, plunge, and dihedral angle of potential wedges

Joint Sets	Bearing	Plunge	Dihedral Angle
Bedding & East-West	90°	35°	90°
Bedding & Northeast	53	29	116
Bedding & Northwest	142	23	69
Bedding & Northeast Flat	35	22	106
North-South & Northeast	180	83	130
North-South & Northwest	180	83	40
North-South & Northeast Flat	0	44	64
East-West & Northeast Flat	270	34	51
Northeast & East-West	90	82	140
Northwest & East-West	270	83	130
Northwest & Northeast Flat	314	50	89

less than 1 percent, the wedge will have no more effect on the rock strength than the single fracture. Four of the joint sets have steep dips resulting in steep plunges. These wedges will slide out if the friction angle is the only resistance. Because the lengths are discontinuous, "small" to "medium" size wedges can be expected to slide out and reduce the rock mass strength of the pillar.

The combination of joints that is likely to result in the lowest percentage of intact rock is the step path (Fig. 21). The step path is defined by a steep (45° to 90°) joint set and a flat (20° to 60°) joint set that have approximately the same strike. The angle of the step path

BETA ANGLE

SHEAR ROCK BRIDGE

TENSION ROCK
BRIDGE

PATH FOLLOWED
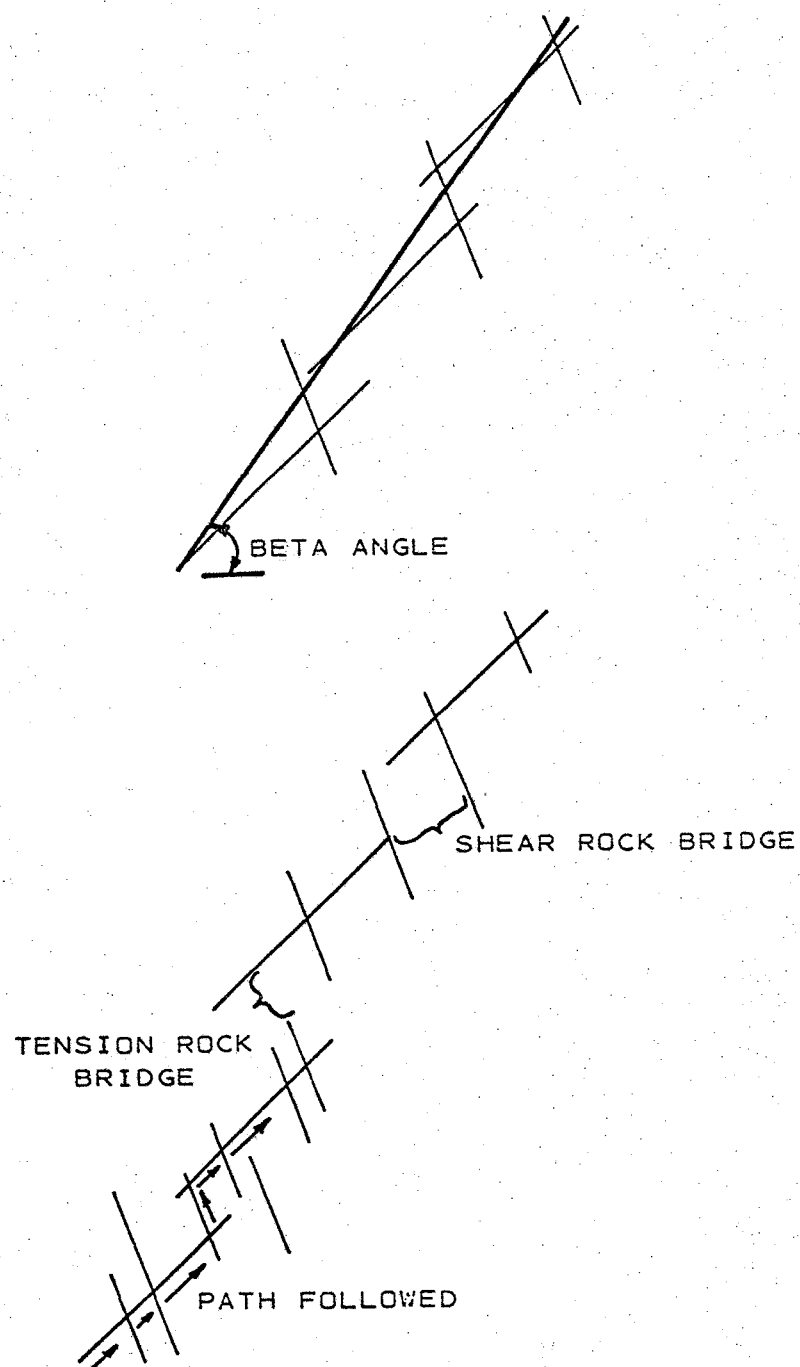
Figure 21. Geometry of a step path

(beta angle) and the extent of a continuous step path depend on the distribution of fracture dip, length, and spacing. This combination of joints will result with the lowest percentage of intact rock and will therefore be discussed in more detail.

Step Path Model

A step path computer model was developed by Call and Nicholas (1974) for slope design. The model determines the path of lowest shear strength by randomly sampling the distributions of fracture lengths, spacings, and dips. When the fracture length is short relative to fracture spacing, rock bridges form (Fig. 21). For the open-pit slope analysis, it is presumed that a rock bridge under shear stress will probably not fail but that a bridge under tensile stress will fail because the tensile strength of the rock substance is lower than the shear strength. Moreover, if the pillar core is under a triaxial stress field (Wilson, 1972) the tensile and shear rock bridges may have similar strengths. Therefore, the chance of failure is equal for both types of rock bridges. Because the design analyses are based on shear failure, it will be assume that both rock bridges will fail in shear.

The assumptions upon which the minimum resistance step path computer program is based are:

1. At least two fracture sets exist that characterize a step geometry. The sets have similar strikes with one set having a flatter dip (20° to 60°) with the steeper set dipping 45° to 90°.

2. Fracture set characteristics—dip, length, and spacing—can each be described by mathematical distributions.

3. The overlap of fractures is represented by a uniform distribution.

4. The two-dimensional analysis represents the three-dimensional picture.

5. Under a tensile stress, a preexisting fracture will propagate up to the first fracture it intersects but not beyond.

6. The flattest path will be followed; that is, the step path will follow up a flat joint to the steep joint farthest out (Fig. 21). The path will then travel out the step joint until it meets another flat joint moves up that joint (Fig. 21).

The input data required to generate the model are:

1. Distribution of fracture length, spacing, and dip for each joint set.

2. Height of pit face or pillar.

3. Number of iterations.

4. A series of random numbers.

Output comprises the beta angle and the sum total of rock bridges that would have to fail by shear stresses. With these data plus the height of the pillar the percentage of intact rock is estimated.

Results of Step Path Analysis

The Marble Peak area has two possible step paths: (1) the Northeast and Northeast Flat fracture sets and (2) the North-South and Bedding fracture sets. Because the North-South set was missing in the detail lines mapped, length and spacing distributions do not exist for

this set. Therefore, the step path model was run on only the Northeast and Northeast Flat joint systems. To determine % intact rock for a given pillar height, the model was run at pillar heights ranging from 5 to 50 feet. Because there is no unique step path, 100 iterations were made for each pillar height. This resulted in the distribution of beta angles and % intact rock shown in Figure 22. Figure 23 shows the median and 20% and 80% cumulative frequency limits for beta angles and % intact rock.

The distribution of beta angles ranges between lognormal and normal (Fig. 22c). The median beta angles range between 50.6 and 54.7 degrees and appear to increase with pillar height up to a pillar height of 15 feet where they become relatively constant (Fig. 23b).

The % intact rock distribution ranges between lognormal and negative exponential of the cumulative frequency (Fig. 22b). The median values range between 13.3 and 23.3 percent showing a general increase in % intact rock with increased pillar height up to 20 feet and then becoming relatively constant (Fig. 23a). The average of the median % intact rock is 20 percent with a standard deviation of 4 percent.

Strength Calculation

Given the results in the above section, an estimate can be made of the rock mass strength. The value of the rock mass friction angle can be estimated by proportioning the intact rock friction angle and the friction angle of fracture. The following equation demonstrates how this is done:

$$RxM\phi = (\%IRx/100)(IRx\phi) + (\%Frx/100)(F\phi) = 37° \qquad (4)$$
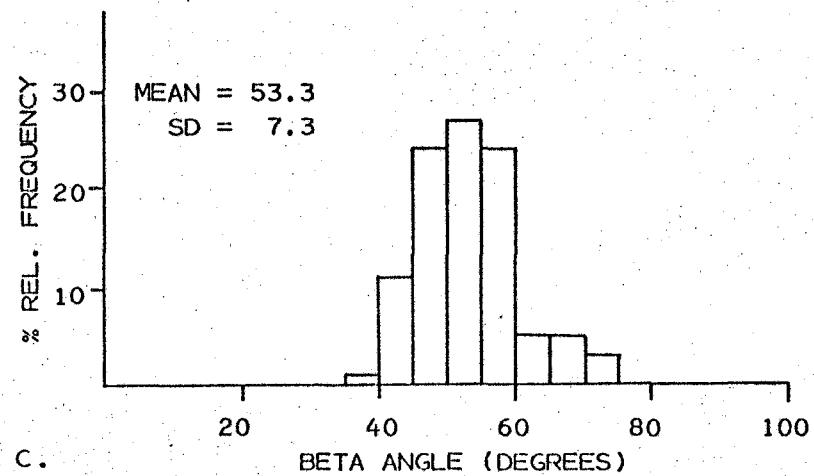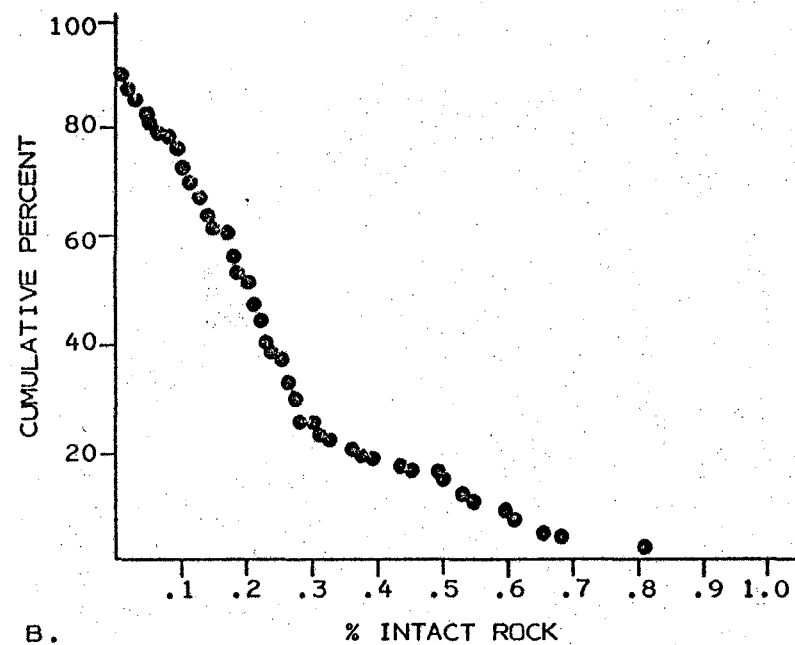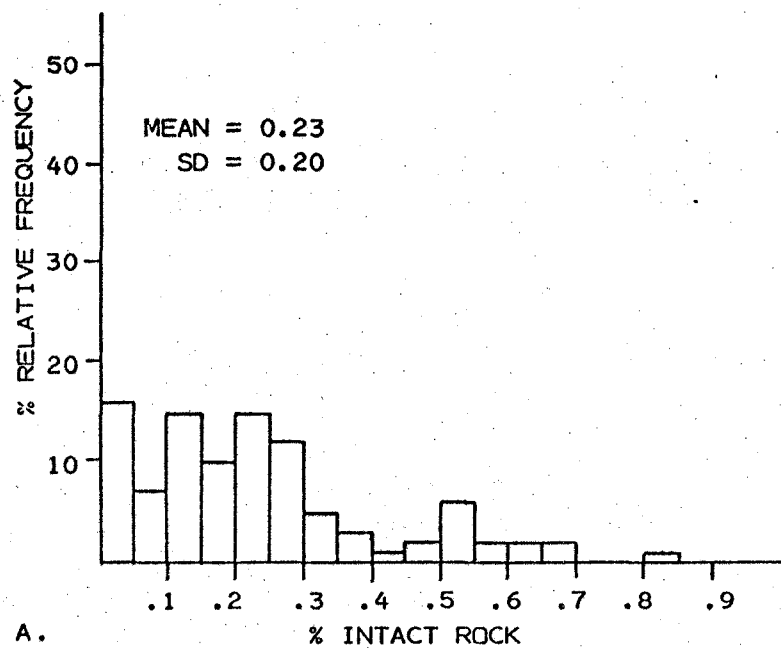
Figure 22. Example distributions of percent intact rock and beta angles from minimum resistance step path program
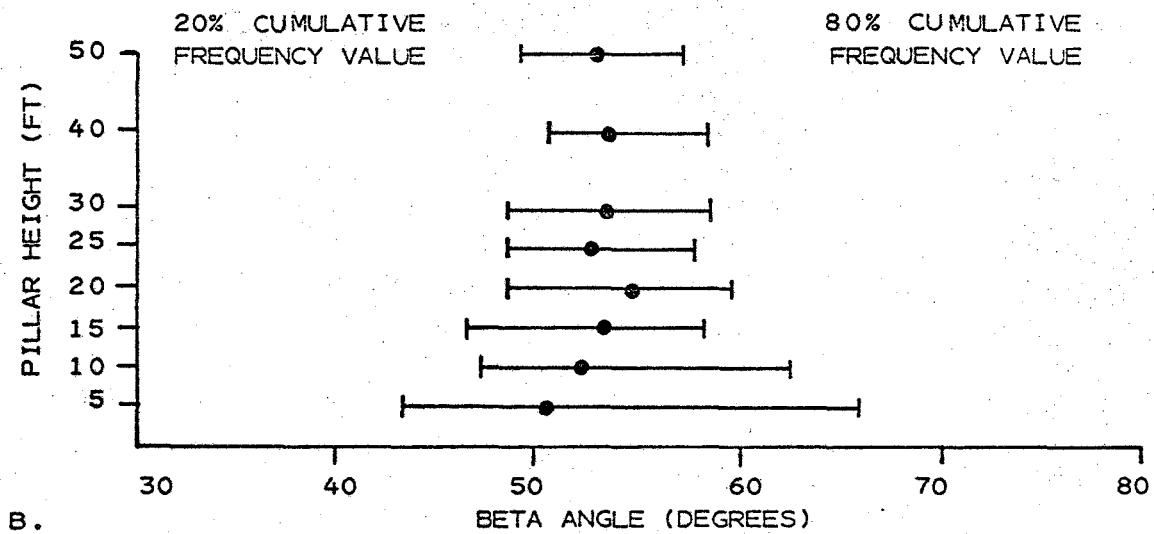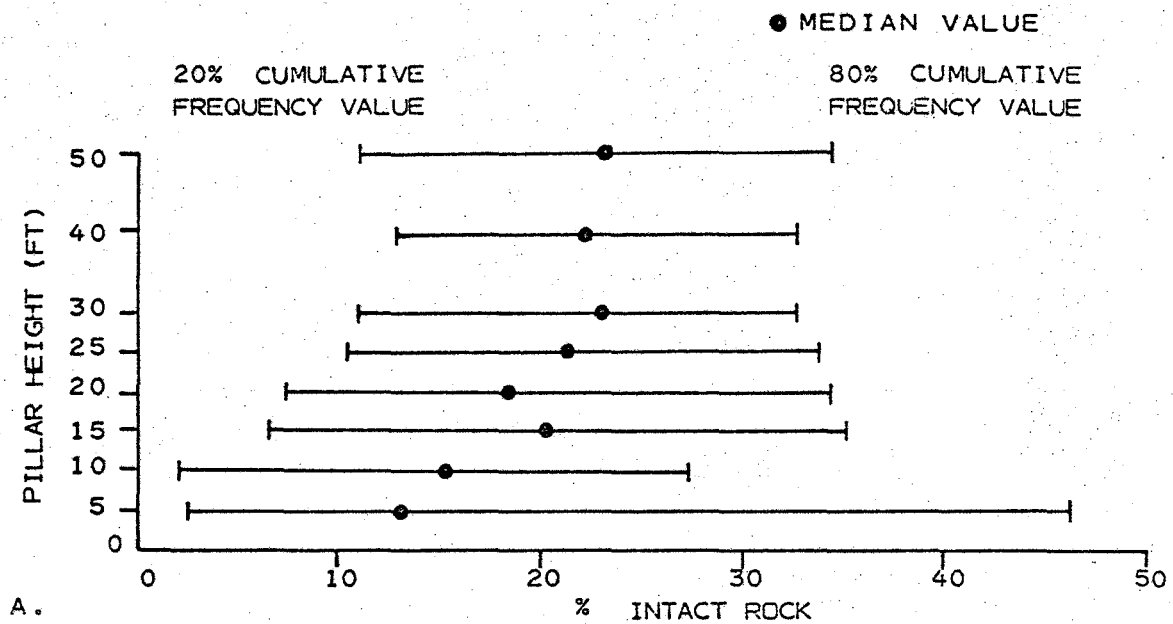
Figure 23. Median and 20% and 80% cumulative frequency
values fro percent intact rock and beta angles

if: RxM∅ = rock mass friction angle

           %IRx = percent intact rock = 20%

           IRx∅ = intact rock friction angle (internal angle of friction)

                = 55.6°

           %FRx = percent of fractured rock = 80%

           F∅   = friction angle of fracture = 32°.

The friction angle of the fracture comprises the rock-on-rock friction angle (28°) and the roughness angle (4°) measured in the structural mapping.

The rock mass cohesion is calculated by a similar equation:

$$RxMC = (\%IRx/100)(IRxC) + (\%FRx/100)(RRxC) = 620 \text{ psi} \quad (5)$$

if: RxMC = rock mass cohesion

           %IRx = percent intact rock = 20%

           IRxC = intact rock cohesion = 3,090 psi

           RFRx = percent fractured rock = 80%

           RRxC = rock-on-rock cohesion = 4 psi.

These results are only estimates and are based on median values for the Marble Peak area. Therefore the design should account for variability of the rock mass strength.

CHAPTER 6

ESTIMATION OF IN SITU STRESS FIELD

The pre-mine stress, or in situ stress, is composed of stresses due to gravity and tectonic forces. Voight (1967) proposed that the in situ stress can be classed according to the following segments:

1. Gravitational

    a. Current

2. Tectonic

    a. Current

    b. Residual.

The current gravitational stress is the stress due to the weight of the overburden. Coates and Grant (1966) reported measurements showing that the vertical stress is greater than that predicted by the overburden. This suggests that a residual gravitational stress segment should be added to the gravitational portion of Voight's classification.

If the gravitational stress is considered the only driving force, assuming a zero lateral strain, the horizontal stress σ_H predicted by elasticity is:

$$\sigma_H = \frac{\nu}{1 - \nu} \sigma_{ovb} \tag{6}$$

where ν = Poisson's ratio

σ_{ovb} = density x overburden thickness.

Because Poisson's ratio generally ranges between 0.15 and 0.25, the horizontal stress should range between 1/3 to 1/2 the vertical stress.

68

Heim (1878) proposed that the in situ stress field becomes hydrostatic due to creep, that is, $\sigma_{ovb} = \sigma_H$ = density x height of oberburden. It is argued that as sediments are deposited the stress field is hydrostatic and therefore should remain that way. Also, since an intrusion is predominantly liquid as it is formed, hydrostatic stresses are developed.

Contradictory to the hydrostatic concept, measurements have shown the horizontal stress is generally greater than the vertical stress (Fig. 24). The difference between the predicted horizontal stress by the above methods and those measured can be explained by tectonic stresses. Current tectonic stresses are difficult to measure. Seismic activity is an indication that a current tectonic stress exists, but it is not necessary (Voight, 1967). Structure orientation is also thought to relate the current tectonic stresses but Bielenstein and Eisbacher (1969) showed this was not always the case. The residual tectonic stresses are defined by Voight (1967, p. 332) as "self-equilibrating stress components that remain in a structure if external forces and moments are removed." The existence of residual stresses is best exemplified by the exfoliation of the Half Dome in Yosemite Park, California.

Methods for Measuring Stress

In order to design a mine it is necessary to know or else to be able to reasonably estimate the in situ stress field, that is, the loading condition anticipated. The best available technique for measuring the in situ stress is one of the overcoring stress relief methods. This technique involves drilling three holes at least two times the drift width and then overcoring these holes, that is, releasing the stress while

OA: $\sigma_v = \sigma_{h1} = \sigma_{h2} = \sigma_{o.b.}$

OE: $\sigma_{h1} = \sigma_{h2} = \left[v/(1-v)\right]\sigma_v = \left[v/(1-v)\right]\sigma_{o.b.}$

● : $1/2(\sigma_{h1}+\sigma_{h2})$ measured by Hast in Scandinavia

●C: $1/2(\sigma_{h1}+\sigma_{h2})$ measured by Coates and Grant in Canada

●H: $1/2(\sigma_{h1}+\sigma_{h2})$ measured by Hoskins in Australia

XH: σ_v measured by Hoskins in Australia

●M: σ_{h1} measured by Moye in Australia

XM: σ_v measured by Moye in Australia

●B: $1/2(\sigma_{h1}+\sigma_{h2})$ measured by Barron in South Africa,a=1.38,b=0

XB: σ_v measured by Barron in South Africa using a=1.38,b=0

●BR: $1/2(\sigma_{h1}+\sigma_{h2})$ measured by Barron in South Africa, a=1.1,b=-0.75

XBR: σ_v measured by Barron in South Africa using a=1.1,b=-0.75

●P: $1/2(\sigma_{h1}+\sigma_{h2})$ measured by Pallister in South Africa,a=1.1,b=-0.75

XP: σ_v measured by Pallister in South Africa using a=1.1, b=-0.75

Figure 24. Summary of in situ stress measurements made in virgin rock—after Jaeger and Cook (1969)

monitoring the strain. The overcoring stress relief method requires so-
phisticated equipment and is expensive.

A similar method is to overcore an isolated block of rock and
measure the residual strains that are translated into residual stresses.
The concept of residual stresses is not new but its acceptance is not
universal. To determine the in situ stress fields Voight (1967) proposed
that these residual stresses can be added to the stresses predicted by
gravity. However, if there is a current tectonic stress present it will
not be included. The residual stress method does have the advantage
of low cost and is relatively easy to perform.

Because the geologic structure is the result of all the stress
fields that have acted on the rock, it is reasonable to assume that the
stress field could be estimated from the geologic structure. J. F. Abel
(oral commun., 1974b) has developed a flow chart to estimate the orienta-
tion and magnitude of the stress field given the rock type and basic
structural data. He developed this flow chart by combining the theories
of fracture propagation and the results of in situ stress measurements
and their correlation with the geology (rock type and structural features).
As Abel admits, this method is only an estimate, but for lack of any
other data, "It's the best we got."

Residual Stress Relief Analysis

Assumptions

The stress relief technique entails overcoring a strain gage and
measuring the change in strain. The strain measurements made after cor-
ing are the results of instantaneous strain recovery and time-dependent

strain recovery. However, all the strain is not recovered as long as the core is intact.

Because the magnitude and orientation of stresses are calculated from the strain measurements, critical assumptions must be made. These assumption are (Gentry, 1972, p. 22):

1. Probably all rocks exhibit non-elastic (time-dependent) strain.

2. The total measured elastic and non-elastic strains are proportional to the total strain which existed in the rock prior to stress relief as long as the rock can be considered rheologically isotropic.

3. The values of the Modulus of Elasticity and Poisson's ratio determined by laboratory methods are identical to the in situ values.

4. Strain and stress ellipses calculated from the measured 'released' strains are oriented and of proportional magnitudes to the stress field which existed in the rock prior to stress-relief overcoring. This also assumes the rock is rheologically isotropic.

Sample Collection and Testing Procedure

An oriented block of approximately 0.7 ft^3 volume was collected from the ABC zone on the 6400-foot elevation (Fig. 7). Three planes on the rock were monitored with 45-degree strain rosettes. The orientation of the planes monitored were:

Strike	Dip	Set
N. 2° E.	42° SE	Bedding
N. 28° W.	62° SW	Northwest
N. 62° W.	85° SW	East-West (Northwest)

The testing procedure used was similar to that used by Gentry (1972). A detailed explanation of this procedure is given in Appendix D, but a brief explanation here is necessary for a better understanding of the results. Forty-five-degree strain gage rosettes were glued to the rock on each of the three planes. The strain gages were read until the strain values stabilized and were then overcored but not broken free from the rock. The gage and core on the bedding plane broke free from the block because of a fracture. Again strain measurements were made until the strains stabilized. Finally, all cores were broken free from the block and strain measurements were made until stabilization occurred. While breaking the core from the block the northwest plane was destroyed.

Test Results

Figure 25 (in pocket) shows the strain versus time graph for each of the planes monitored. The N. 2° E. and N. 28° W. gages stabilized within 800 hours; however, the N. 62° W. plane took 1100 hours. The period of time that was used to calculate the average strain values before coring, after coring, and after core release are shown in Figure 25. The average strains corrected for temperature for these periods are listed in Table 20.

Given the strains in three directions, Young's modulus, and Poisson's ratio, the stress magnitude and orientation can be calculated for the plane in which the strains were measured. Because these stresses are calculated from strains on a single plane, they are called the secondary principal stresses. The standard equations used to calculate the

Table 20. Summary of residual stress relief analysis

Plane Monitored		Stabilization Period	Average Strain Readings (temperature corrected)			Secondary Principal Stresses (psi)			Secondary Principal Stress Orientation (degrees)			
									Max		Min	
Strike	Dip		ϵ_1	ϵ_2	ϵ_3	Max	Min	Max Shear	Bearing	Plunge	Bearing	Plunge
N 2 E	42 SE	Before coring	-81.36	29.33	-210.90	-401	-4483	2040	N 8 W	9	N 82 E	42
		After coring	13.83	135.80	-117.20	1303	-3031	2167	N 8 W	9	N 82 E	42
		After core released	-43.20	102.07	-179.04	584	-4298	2441	N 6 W	7	N 84 W	42
N 28 W	62 SW	Before coring	-50.53	-69.59	-100.10	-981	-1530	278	N 67 W	50	S 24 W	56
		After coring	-56.53	-5.45	37.85	360	-673	517	S 16 W	51	N 76 W	54
N 62 W	85 SW	Before coring	59.21	-5.29	-418.90	224	-6234	3229	S 2 W	84	N 88 W	79
		After coring	300.33	-2.81	-256.05	3417	-2677	3047	S 86 W	81	S 4 E	84
		After core release	285.71	-100.02	-400.44	2813	-4730	3771	S 87 W	80	S 3 E	84

stresses from the strains are taken from Hetenyi (1954) and are listed in Table 21. The maximum, minimum, and maximum shear secondary principal residual stresses are listed in Table 20 for each plane monitored and for each period of strain stabilization. By definition, a positive value means compression and a negative value means tension.

Because mining will generally follow the plane of bedding, the orientation and magnitude of the stress in this plane is critical to the design. The maximum residual stress in the bedding plane is approximately parallel to the strike of bedding, and the minimum stress is approximally down the dip of bedding (Table 20). This orientation does not change throughout the three stages of monitoring. The maximum residual stress has a magnitude of 580 psi and the minimum stress has a magnitude of - 4300 psi. Using Voight's (1967) concept, the current gravitational and tectonic stresses should be added to the residual stress to obtain the complete in situ stress field. It is beyond the scope of this study to determine the current tectonic stresses, and they are therefore assumed to be zero. Based on a depth of 620 feet and a Poisson's ratio of 0.26, the vertical and horizontal stresses due to gravity are 680 psi and 250 psi, respectively. This stress ellipsoid, due to gravity, results in a stress vector in the dip direction of 310 psi. Adding the gravity stress to the residual stress results in a stress parallel to the strike of bedding of 830 psi and the stress in the downdip direction of - 3990 psi. This dip direction tensile stress indicates the potential of rock burst; however, the stress magnitudes are questionable. Gentry, (1972, p. x) made this conclusion about the residual stress magnitude after running seven specimens: "Indications are that more confidence can be placed

Table 21. Standard equations for principal stress and strain calculations for a three-gage 45-degree rosette--After Hetenyi (1954)
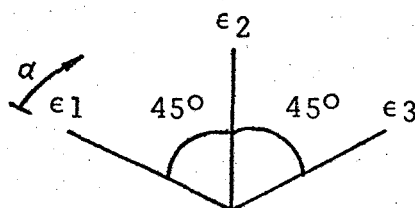
ϵ = strain measurement of a gage

E = Young's modulus

v = Poisson's ratio

$A = 1/2(\epsilon_1 + \epsilon_3)$

$B = 1/2(2(\epsilon_1 - \epsilon_2)^2 + 2(\epsilon_2 - \epsilon_3)^2)^{1/2}$

or

$((\epsilon_1 - A)^2 + (\epsilon_2 - A)^2)^{1/2}$

$\tan 2\alpha = (2\epsilon_2 - \epsilon_1 - \epsilon_3)/(\epsilon_1 - \epsilon_3)$ or $(\epsilon_2 - A)/(\epsilon_1 - A)$

$\epsilon_{max} = A + B$

$\epsilon_{min} = A - B$

$A' = AE/(1 - v)$

$B' = BE/(1 + v)$

$\sigma_{max} = A' + B'$

$\sigma_{min} = A' - B'$

$\tau_{max} = B'$

in residual stress orientations than in magnitude." Therefore, before any conclusion about rock burst is made, additional residual stress relief testing is required.

The three-dimensional residual stresses are calculated using a computer program written by the U.S. Geological Survey. The program calculates the three principal residual stresses utilizing the change in strains of all planes monitored, Young's modulus, and Poisson's ratio. The program requires the three planes monitored to be orthogonal. Because the three planes monitored for this study were not orthogonal, they were rotated on paper to fulfill this orthogonal requirement.

The results of the three-dimensional stress analysis are given in Table 22. As was found by Gentry (1972), the orientation of the stress field does not change radically through the testing program but the magnitudes do. Adding the stresses due to gravity the in situ stress field is

Stress	Bearing	Plunge	Magnitude
Maximum	S. 67° W.	15°	1590 psi
Intermediate	S. 24° E.	1	300
Minimum	N. 69° E.	76	-4750

The validity of these results is questionable for the following reasons:

1. The planes in which strain measurements were made were not orthogonal.

2. The gage on the N. 28° W. plane was destroyed before the core release strain measurements could be made.

Table 22. Results of three-dimensional residual stress analysis

Test Period	Maximum Stress			Intermediate Stress			Minimum Stress		
	Bearing	Plunge	Magnitude	Bearing	Plunge	Magnitude	Bearing	Plunge	Magnitude
Before Coring	S. 55° W.	9°	128 psi	S. 36° W.	8°	- 2797 psi	N. 14° E.	79°	- 6213 psi
After Coring	S. 60° W.	12	1508	N. 30° W.	4	977	N. 86° E.	79	- 3372
Release from Block	S. 67° W.	15	1335	S. 24° E.	1	49	N. 69° E.	76	- 5435

3. The rock is not isotropic but contains alternating beds of diop-

side, epidote, and garnets.

If this test were run again, two changes would be made. First, the block would be collected from the Martin near the Abrigo contact because the Martin is more isotropic than the upper Abrigo. Second, the block would be cut with one plane parallel to bedding and the other two orthogonal to the bedding plane.

Estimate of Stress Field Based on Geology

Anderson (1951) has discussed the stress field necessary to create a fault based on the Coulomb and Mohr theories. Anderson assumes one of the principal stresses is vertical at "moderate" depths because the earth's surface is free to move. Therefore, four stress fields are possible.

Relative Stress Field	Resultant Faults
$\sigma_V = \sigma_{H_1} = \sigma_{H_2}$	none
$\sigma_V \gtrsim \sigma_{H_1}$ and σ_{H_2}	normal
$\sigma_{H_1} \gtrsim \sigma_V \gtrsim \sigma_{H_2}$	strike-slip or reverse
$\sigma_{H_1} \gtrsim \sigma_{H_2} \gtrsim \sigma_V$	thrust

where σ_V = overburden stress and σ_{H_1} and σ_{H_2} = horizontal stresses. These faults are the results of a build-up of stresses; however, after the faulting has occurred the build-up of stresses has been dissipated and the stress orientations have been shifted. Because the faults occur due to the

stress field, it appears logical that the new stress field can be related to the resultant faults. Abel (1974a) has proposed a guide to estimate the in situ stress field based on the following parameters:

1. Rock type (igneous, metamorphic, or sedimentary).

2. Structural history (most recent or major fault and fault type).

3. Orientation of structures (faults, joints, foliation, bedding).

4. Joint spacing.

5. Bed thickness.

6. Elastic properties (Young's modulus and Poisson's ratio).

The guide used to estimate the in situ stress field is given in Appendix E. Abel developed this flow chart by correlating the above parameters with the results of in situ stress measurements. This method provides a quick, cheap estimate of the in situ stress. However, Abel admits that this is just an estimate of the in situ stress and that it has a high probability of being incorrect.

Input Parameters

The use of the stress flow chart requires knowledge of the geology in the area and in some cases the elastic properties of the rock. The following paragraphs will briefly discuss the parameters used in the analysis at Marble Peak (Table 23).

The rock types in the ABC zone is a hydrothermally altered shaly limestone. There has been approximately complete replacement of the limestone in the mineralized zone (Fritts, 1974b), implying a metamorphic classification. However, not all segments of the Paleozoic section in the Marble Peak area have been metamorphosed and some still

Table 23. Input parameters required for Abel's method of estimating in situ stress field

Strike, Dip, and Median Spacing of Joint Sets

Joint Set	Strike	Dip	Median Spacing (ft)
Bedding	N 11 E	46 SE	0.79
Northeast Flat	N 25 E	35 NW	.65
Northeast	N 50 E	83 SE	.69
Northwest	N 38 W	67 SW	.99
East-West	N 87 W	85 SW	.96
North-South	N 15 E	60 NW	unknown

Bed Thickness

Rock Unit	Bed Thickness (ft)
Horquilla	600
Escabrosa	580
Martin	250
Upper Abrigo (only)	75
Entire Abrigo	450

Elastic Properties of Engineering Rock Units

Rock Unit	Young's Modulus (psi)	Poisson's Ratio
Martin	11.0×10^6	0.28
ABC Zone	14.0	.27
Upper Abrigo	10.6	.26

maintain their sedimentary characteristics. It is therefore probable that the rock type should be classed as metamorphic although the analysis will also include a sedimentary rock type.

The structural history in the Marble Peak area is extremely complicated. The major structure in the area is the Geesman fault, which strikes east-west and dips 70° S. Determining the most recent structure is a complex problem that requires a separate and detailed discussion.

Since the joint systems parallel the fault systems, the orientations obtained from the combined detail lines (Table 23) will be used. One structure that was not observed in the detail line was the North-South set. For its orientation the results from Continental Copper's underground geology map will be used. The joint spacing will be the median spacing determined from the detail line mapping. Bed thicknesses are from Fritts (1974b). Elastic properties are those determined from laboratory testing of specimens from core samples.

Structural History of Marble Peak

The structural history of the Marble Peak area has been reported by Peirce (1958) and DuBois (1959), among others. All investigators agree that the end of the tectonic history culminated in a period of faulting. The Geesman fault is known to cut all rock types and it is therefore considered to be younger than all deposition and emplacement.

One method of determining the relative age of fault systems is to define which faults displace other faults. The following observations were made from Continental Copper's surface geology map. The East-West fault set is generally displaced by the Northwest and North-South

fault sets. This indicates that the East-West set is the oldest of these
three fault systems. The Northeast fault set is generally not displaced
by another fault system; instead, it butts up against other faults but
does not displace them. One East-West fault set is displaced by a
North-South set as elsewhere, but the East-West system also displaces
a Northwest and Northeast fault set. This special case indicates that
there was later movement along preexisting faults. This analysis in-
dicates that no conclusion can be made as to the youngest fault system
because of recurrent movement along older faults.

Some intuition about the sequence of faulting may be obtained
from the type of filling in the fracture sets since they parallel the fault
systems. Table 24 lists the joint systems and percentage of filling for
the ABC zone and the Martin in the area of the three detail lines. Assum-
ing the bedding joints existed from the beginning of hydrothermal activity,
they should contain all the types of filling. This does occur. The North-
east Flat set appears to have the same filling types and percentages as
the Bedding set, indicating similar age. The East-West joint set is pre-
dominantly filled with epidote. Whether the Northeast Flat or East-West
set is the oldest is difficult to determine. One may argue that the epi-
dote came first and filled the fractures thereby preventing the fractures
from being filled with the other filling types, or it may be argued that the
epidote was the last filling and that the East-West set was formed main-
ly after the chlorite, quartz, and mineralization. The Northwest set con-
tains little filling except for epidote, indicating that it occurred after the
East-West set. The Northeast joint set contains little filling at all,

Table 24. Summary of filling types and percent filling of joint sets

Joint Set	None	Chlorite	Quartz	Calcite	Mineralized	Epidote	Iron Oxide	Garnet
Bedding	55%	10%	4%	4%	6%	6%	8%	2%
Northeast Flat	68	15	17	22	15	5	0	5
East-West	36	9	4	4	13	43	2	0
Northwest	54	2	7	35	4	10	0	6
Northeast	64	7	2	29	3	2	0	0
North-South				unknown				

indicating that it was the last to form. The North-South set was not ob-
served; therefore, no relationship could be determined based on its
filling.

The presence of slickensides on faulted dikes filled with the
most recent intrusive material (diabasic diorite) led Fritts (1974b) to
conclude that the Northwest fault system is probably the youngest. How-
ever, the East-West and North-South fault systems also show similar
signs indicating similar age (Fritts, 1974b). Another interpretation re-
lated to the dikes is the absence of dikes parallel to the Northeast fault
system. The absence of dikes parallel to this fault system could indi-
cate that it was formed after the other fault systems had been filled with
dike material.

It is therefore difficult to determine the most recent fault sys-
tem from this evidence, but based on the available information it is be-
lieved that either the Northwest or Northeast fault system is the young-
est.

In addition to the relative ages of the fault systems, the type
of faulting (normal, reverse, or strike-slip) is required. The East-West
and North-South systems are predominantly normal faults, although some
strike-slip movement probably occurred (Fritts, 1974b). The Northeast
and Northwest fault systems are all predominantly strike-slip faults
(Fritts, 1974b), and he believes that the Northeast Flat system is a
thrust fault system. Because the type of faulting is not clear-cut, the
two probable fault types will be analyzed. Table 25 lists the fault sys-
tems with their most probable and alternate fault type.

Table 25. Probable fault type for each fault system

Fault System	Fault Type	
	Probable	Alternative
East-West	Normal	Strike-sli
Northeast Flat	Thrust	Normal
Northeast	Strike-slip	Normal
Northwest	Strike-slip	Normal
North-South	Normal	Strike-slip

Estimate of in Situ Stress

After the input parameters required for Abel's (1974a) estimation of the in situ stress field have been defined, the analysis can be made. Table 26 lists the postulated stress fields based on a metamorphic rock type and Table 27 is based on a sedimentary rock type.

In my opinion the case of a metamorphic rock with a strike-slip Northeast fault system is probably the most correct. In addition, a northeast fault exists at the location where the block for the residual stress analysis was collected. These conditions predict that the principal stress bears N. 50° E., plunges 0 degrees, and has a magnitude less than or equal to three times the overburden load; the intermediate stress bears N. 40° W., plunges 7 degrees, and has a magnitude less than twice the overburden load; and the minimum stress bears S. 40° E., plunges 83 degrees, and has a magnitude less than or equal to 1.5 times the overburden load (Table 26, Figure 26). However, if the Northwest fault system is younger than the Northeast, the orientations are similar

Table 26. Possible stress fields based on a metamorphic rock type

	Stress Field								
	Major Stress			Intermediate Stress			Minimum Stress		
Fault System	Bearing	Plunge	Magnitude	Bearing	Plunge	Magnitude	Bearing	Plunge	Magnitude
East-West									
Normal	N 87°W	0	$= 2\,\sigma_{ovb}$	S 3°W	85°	$= 1.5\,\sigma_{ovb}$	N 3°E	5°	$= \sigma_{ovb}$
Strike-slip			$= 3\,\sigma_{ovb}$	N 3°E	5°	$= 2\;\sigma_{ovb}$	S 3°W	85°	$= 1.5\,\sigma_{ovb}$
Northeast Flat									
Normal	N 50°E	0	$= 2\,\sigma_{ovb}$	N 40°W	33	$= 1.5\,\sigma_{ovb}$	S 40°E	57	$= \sigma_{ovb}$
Reverse			$= 3\,\sigma_{ovb}$	S 40°E	57	$= 2\;\sigma_{ovb}$	N 40°W	33	$= 1.5\,\sigma_{ovb}$
Northwest									
Normal	N 38°W	0	$= 2\,\sigma_{ovb}$	S 52°W	66	$= 1.5\,\sigma_{ovb}$	N 52°E	24	$= \sigma_{ovb}$
Strike-slip			$= 3\,\sigma_{ovb}$	N 52°E	24	$= 2\;\sigma_{ovb}$	S 52°W	66	$= 1.5\,\sigma_{ovb}$
North-South									
Normal	N-S	0	$= 2\,\sigma_{ovb}$		90	$= 1.5\,\sigma_{ovb}$	E-W	0	$= \sigma_{ovb}$
Strike-slip			$= 3\,\sigma_{ovb}$	E-W	0	$= 2\;\sigma_{ovb}$		90	$= 1.5\,\sigma_{ovb}$
Northeast									
Normal	N 50°E	0	$= 2\,\sigma_{ovb}$	S 40°E	83	$= 1.5\,\sigma_{ovb}$	N 40°W	7	$= \sigma_{ovb}$
Strike-slip			$= 3\,\sigma_{ovb}$	N 40°W	7	$= 2\;\sigma_{ovb}$	S 40°E	83	$= 1.5\,\sigma_{ovb}$

Table 27. Possible stress fields based on a sedimentary rock type

Fault System	Major Stress			Intermediate Stress			Minimum Stress		
	Bearing	Plunge	Magnitude	Bearing	Plunge	Magnitude	Bearing	Plunge	Magnitude
East-West									
Normal	S 74° E	42°	$= \sigma_{ovb}$	N 78° W	48°	$= \sigma_{ovb}$	N 16° E	5°	$= \sigma_{ovb}$
Strike-slip			$= 1.5\,\sigma_{ovb}$			$= \sigma_{ovb}$			$= \sigma_{ovb}$
Northeast Flat									
Normal	N 19° E	3	$= \sigma_{ovb}$	N 72° W	33	$= \sigma_{ovb}$	S 65° E	57	$= \sigma_{ovb}$
Reverse			$= 1.5\,\sigma_{ovb}$			$= \sigma_{ovb}$			$= \sigma_{ovb}$
North-South									
Normal	South	15	$= \sigma_{ovb}$	North	85	$= \sigma_{ovb}$	E-W	0	$= \sigma_{ovb}$
Strike-slip			$= 1.5\,\sigma_{ovb}$			$= \sigma_{ovb}$			$= \sigma_{ovb}$
Northwest									
Normal	S 22° E	31	$= \sigma_{ovb}$	N 79° W	47	$= \sigma_{ovb}$	N 52° E	24	$= \sigma_{ovb}$
Strike-slip			$= 1.5\,\sigma_{ovb}$			$= \sigma_{ovb}$			$= \sigma_{ovb}$
Northeast									
Normal	N 54° E	32	$= \sigma_{ovb}$	S 37° W	57	$= \sigma_{ovb}$	N 40° W	7	$= \sigma_{ovb}$
Strike-slip			$= 1.5\,\sigma_{ovb}$			$= \sigma_{ovb}$			$= \sigma_{ovb}$

except that the maximum and intermediate stresses are reversed (Table 26, Figure 26).

In Situ Stress Field for Pillar Analysis

Two methods, residual stress relief and Abel's estimate based on geology, have been used to evaluate the in situ stress field. If both methods are valid, their results should be comparable. A comparison of stress orientations predicted by the residual method and by Abel's method is shown in Figure 26. The maximum stress orientation obtained from the two methods are amazingly similar. Based on these two separate analyses the in situ stress field to be considered is:

Stress	Bearing	Plunge	Magnitude
Maximum	N. 50° E.	0°	3.0 σ_{ovb}
Intermediate	N. 40° W.	0°	1.5 σ_{ovb}
Minimum		90°	1.0 σ_{ovb}

Given the proposed stress field, the magnitude of stresses parallel to the strike of bedding, downdip of bedding, and normal to bedding can be calculated. Based on an average bedding dip of 30 degrees, the magnitude of the stresses in the above orientation are:

Orientation	Magnitude
Parallel to strike of bedding	1.72 σ_{ovb}
Downdip of bedding	1.33 σ_{ovb}
Normal to bedding	1.24 σ_{ovb}

These stress magnitudes are not unequivocal but are the best estimates at this time. It is certainly better to use them than to assume the stress field predicted by gravity loading only.
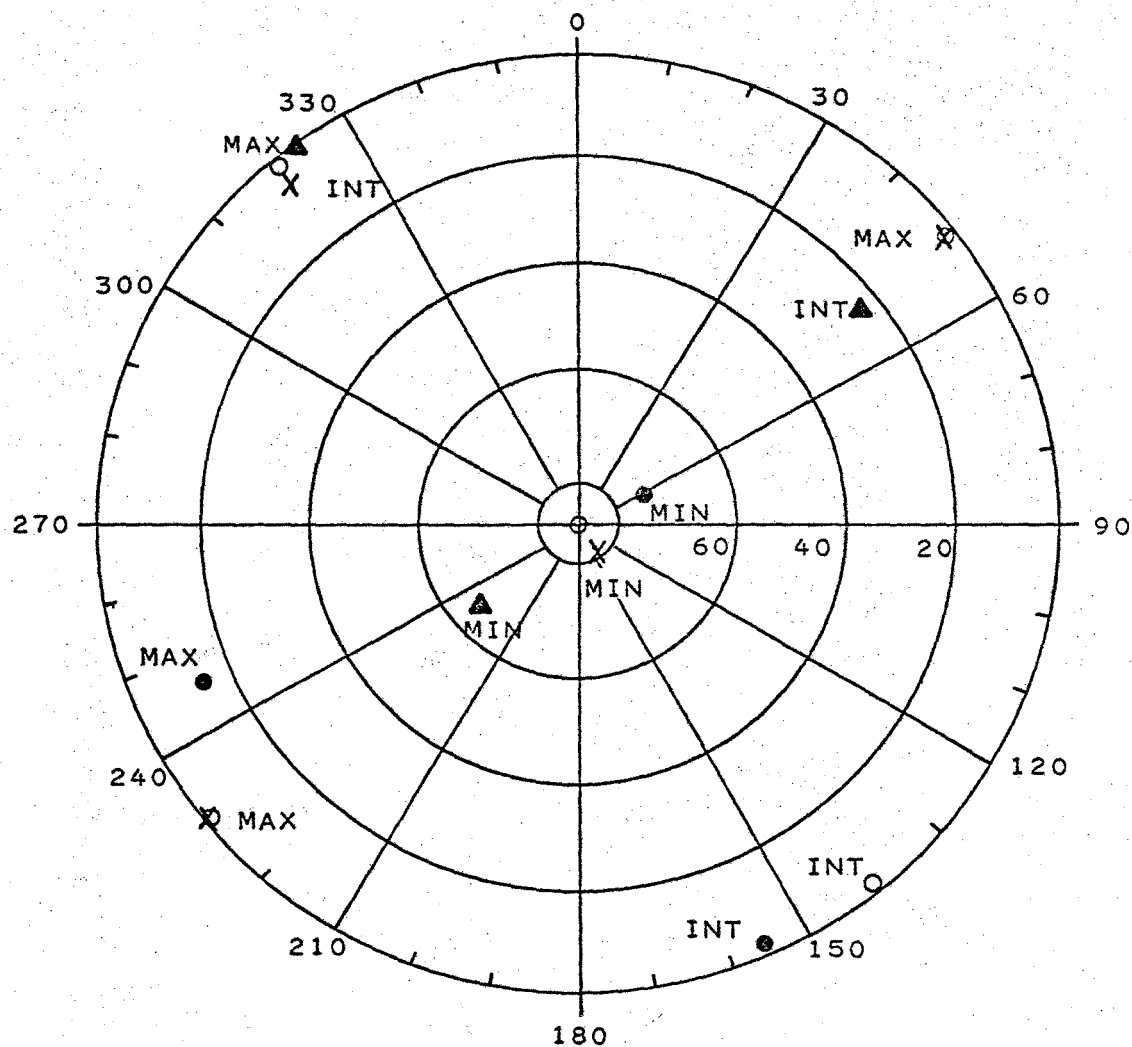
MAX = MAXIMUM STRESS   ● RESIDUAL STRESS ANALYSIS

INT = INTERMEDIATE STRESS   X ABEL'S METHOD BASED ON
                                NORTHEAST SET WITH STRIKE-
MIN = MINIMUM STRESS   SLIP MOVEMENT

                              ▲ ABEL'S METHOD BASED ON
                                NORTHWEST SET WITH STRIKE-
                                SLIP MOVEMENT

                              O STRESS FIELD USED FOR
                                STOPE & PILLAR ANALYSIS

Figure 26. Stereo net plot of stress field

CHAPTER 7

STOPE AND PILLAR ANALYSIS

The preceding six chapters have discussed values for the rock mass strength and a definition of the in situ stress field. These values can now be used to compare a number of pillar design methods. Before the pillar design comparison can be made, however, the orientation of the pillars, the dimensions of the room, and the method of calculating the load on the pillar must be discussed.

Pillar Orientation

Pillar should be oriented to permit easy mining while minimizing failure along the weakest structures. Pillar orientation will depend on the strength of the structures and their orientation relative to the maximum loading stress. Based on the results of the pre-mine stress field analysis for the Control Property, the maximum loading is normal to the dip of bedding.

Pillar orientations being considered at the Control Property are: (1) a vertical wall (Figure 27a) or a wall normal to the dip of bedding (Figure 27b) is possible for the wall parallel to the strike of bedding and (2) long axis of pillar in strike direction of bedding or long axis in dip direction of bedding. In terms of operational considerations, the preferred pillar orientation is a long axis in dip direction of bedding and vertical walls parallel to strike of bedding. Based on the weakest joint sets and the estimated pre-mine stress field, pillars with long dip

WEST   EAST

EXPLANATION
——— BEDDING PLANE
          FRACTURE
—··— NORTHEAST FLAT
          FRACTURE
——— NORTHEAST FRACTURE

A.
VERTICAL
WALLS

B.
WALLS NORMAL
TO BEDDING

CROSS SECTION LOOKING NORTH
ALONG STRIKE OF BEDDING

SOUTH ————————————————— NORTH

C. CROSS SECTION LOOKING
UP DIP OF BEDDING
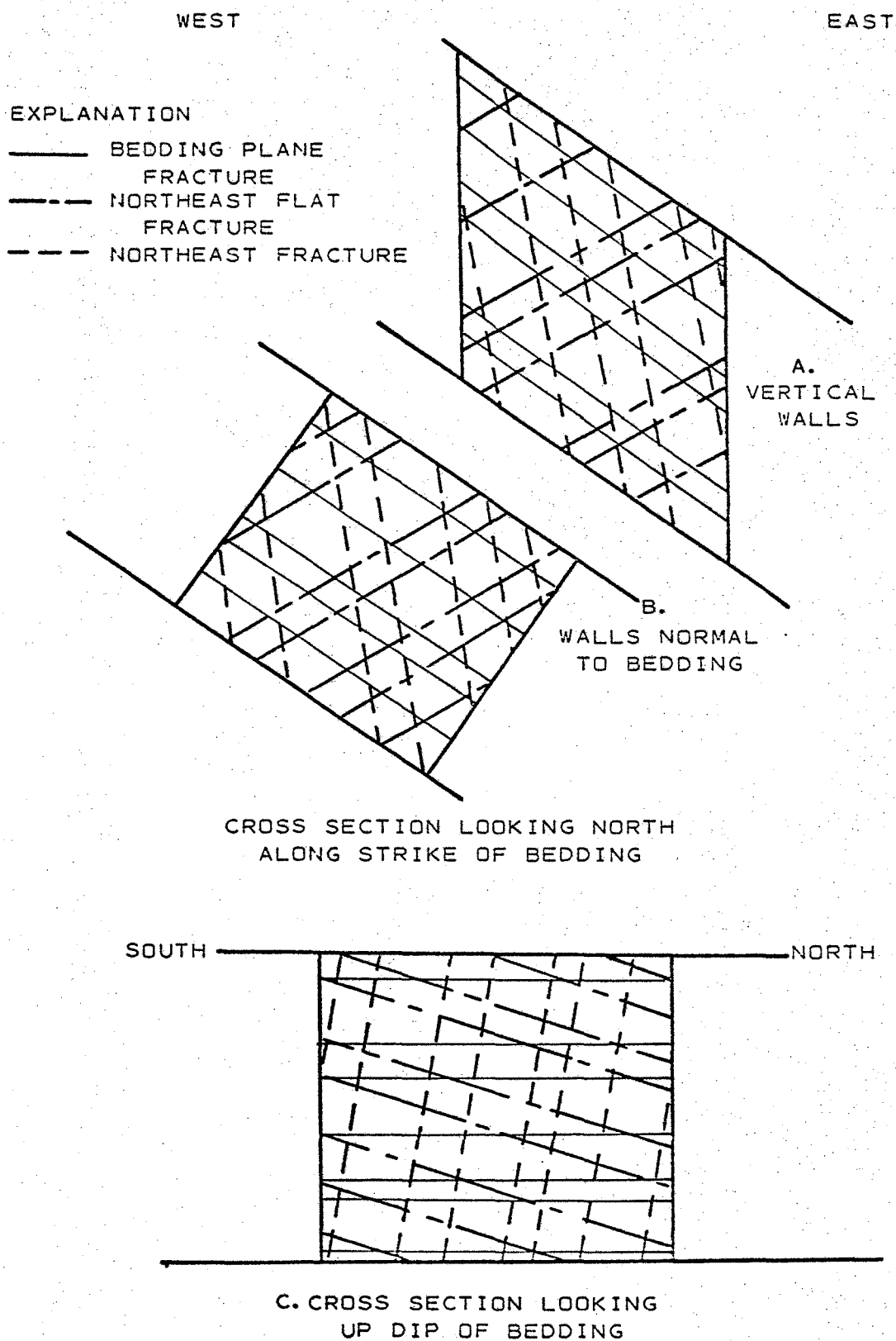
Figure 27. Relationship between critical structures and pillar
orientation

lengths and walls normal to dip of bedding will be the most stable (Figure 27).

Vertical pillar walls in strike direction of bedding will have stress concentrations resulting in a shear stress approximately parallel to the Northeast Flat set (Figure 27a). This pillar will also be destressed on the updip and downdip sides resulting in failure along the Northeast set. Walls parallel to strike and normal to dip of bedding do not develop the stress concentrations as in the vertical pillar walls. Minor shearing along the Northeast and Northeast Flat set can be expected for pillar walls normal to bedding (Figure 27b). Therefore, the wall parallel to the strike and normal to the dip of bedding is probably more stable than the vertical wall. The wall normal to the dip of bedding is difficult to mine; however, the vertical wall will probably fail, resulting in a stable pillar with walls normal to bedding.

Based on the structure sets, the pillar with the long axis in the dip direction of bedding is more stable than the pillar with the long axis in the strike direction of bedding. The long axis in the strike direction will expose a large area in which shearing of the Northeast Flat set can occur (Figure 27b), while the weakest structures are not critically oriented for the wall bearing in the dip direction of bedding (Figure 27c).

The pillar orientation to be analyzed will have the long axis in the dip direction of bedding and the walls parallel to the strike of bedding will be normal to its dip.

Room Dimensions

The room dimensions to be determined are the height, width, and length. Room height is determined predominantly by ore thickness. In some cases, there may be a limit due to equipment. At Marble Peak the mineralized zones range between 10 and 70 feet in true thickness. For the purpose of comparison, a 30-foot-high room will be analyzed.

The length and width of the room depend on the stability of the roof. If the room is much longer than its width, the stability is determined by the width. The roof above a mine opening can be divided into three zones that show different effects due to the load. The three zones and the roof response are:

1. Surface: ground may subside.

2. Intermediate: pressure arch forms.

3. Immediate roof: ground will deflect in a beam or plate action
   or, if transverse fracturing, may have voussior arch action
   (W. H. Evans, 1941).

As the room is mined the load above the room is transferred to the pillars. This load transfer forms the pressure arch. Rock under the pressure arch is therefore destressed except for its own weight. If the area is bedded or has a structure parallel to the roof, these beds will separate and respond like beams or plates. Because of the increased load on the pillars they will strain, which will then result in a minor deformation of the surface (subsidence). The intermediate and immediate roofs have the greatest control on the actual room size, whereas the surface zone depends on closed proximity to the surface with respect to the size of the orebody

and the pillar's stiffness. The ABC zone's thickness in relation to depth
is small, so the surface zone will not be discussed.

Intermediate Roof

The pressure arch is formed as the room is mined and the ver-
tical load is transferred to the abutments (exterior pillars) (Figure 28).
The rock under the pressure arch is destressed, i.e., has overburden
stresses removed, except for its own weight. The ability of the rock to
transfer the load normal to the length of rooms depends on the magnitude
of the stress normal to the arch (usually related to depth), the shear and
compressive strength of fractures, and the strength of the abutments.
Field measurements from European coal mines have indicated a relation-
ship between depth and arch distance (Figure 29). The raw data collected
by Alder, Potts, and Walker (1951) show that the arch distance predicted
by the curve in Figure 29 is conservative. Therefore this relationship
can be applied to this study because the rock mass strength at Marble
Peak is more competent than most coal beds. The height of these pres-
sure arches are a third to a half of the length of the pressure arch. Field
studies have demonstrated that when the predicted maximum pressure
arch width is less than half the width of the mining zone, the pillars in
the central part of the mining zone will have to carry the entire load of
rock to the surface.

Immediate Roof

Where the back is defined by a bedding plane or a joint set
parallel to the roof, the beds will separate from the back. This area is
called the immediate roof. The immediate roof can be modeled after a

LARGE SCALE
PRESSURE ARCH

SMALL SCALE
PRESSURE ARCH
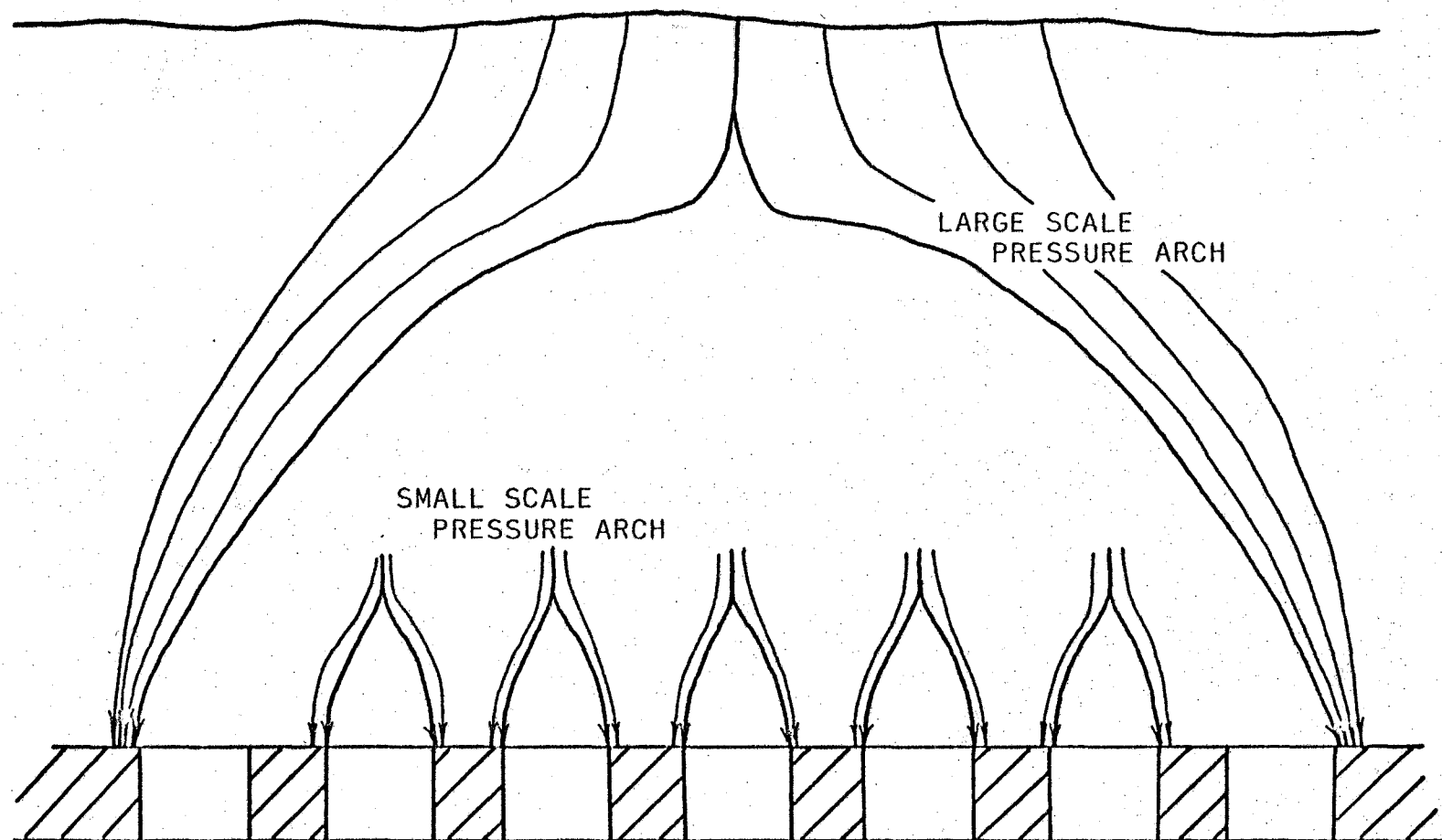
Figure 28. Proposed pressure arches formed in a room-and-pillar design
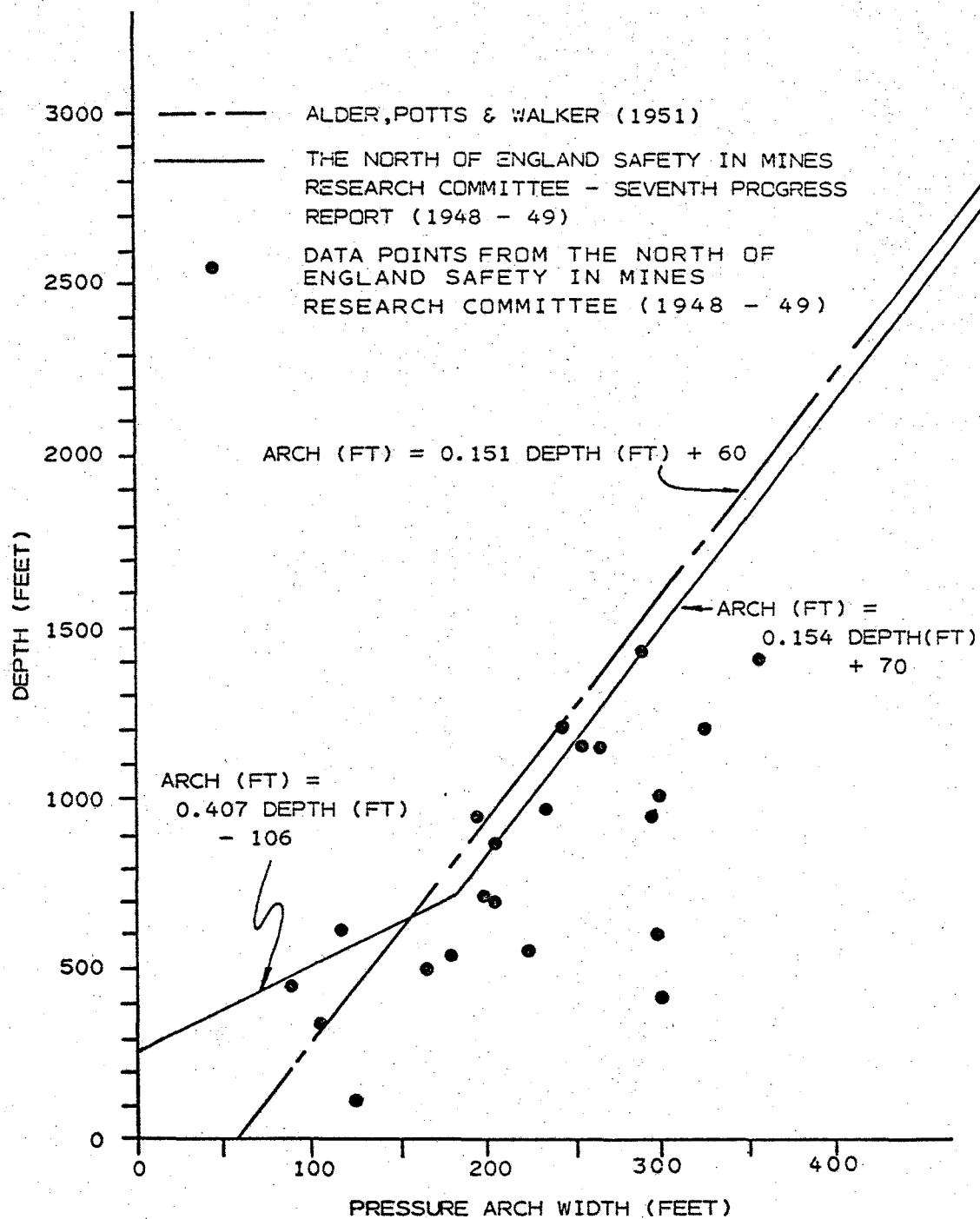
Figure 29. Maximum expected pressure arch distance versus depth—After Alder, Potts, and Walker (1951) and The North of England Safety in Mines Research Commitee (1948-49)

uniformly loaded fix-end beam. The beam analysis is an elastic analysis
and therefore the following assumptions are required:

1. Rock is homogeneous, isotropic, and elastic.

2. Beam is straight with a uniform cross-sectional area.

3. Loads and reactions are perpendicular to the axis of the beam
and are in the same plane.

4. Beam span is at least twice the beam thickness.

It is possible to relax these assumptions somewhat without destroying
the confidence in the answer (Alder and Sun, 1968).

Failure of the beam will occur in tension at the center and in
shear at the ends. The beam is likely to fail in tension first because the
rock is seaker in tension than in shear. Analyzing the beam equation
(Figure 30) for the axial bending stress at the center of the beam results
in the following equation:

$$\text{axial bending stress} = \gamma L^2/4h \tag{7}$$

where γ = density of rock

L = beam length

h = beam thickness

The beam thickness is determined by the bedding or joint spacing. The
axial bending stress should not exceed the rock substance tensile
strength. Obert, Duvall, and Merrill (1960) recommend that the axial
bending stress should not exceed 1/4 to 1/8 the tensile strength; i.e.,
the safety factor of the beam should range between 4 and 8.

Another approach proposed by Abel (1974b) is to assume the rock
mass tensile strength equals zero and the in situ stress counteracts the
bending stress in the beam (Figure 30). Because the rock is fractured
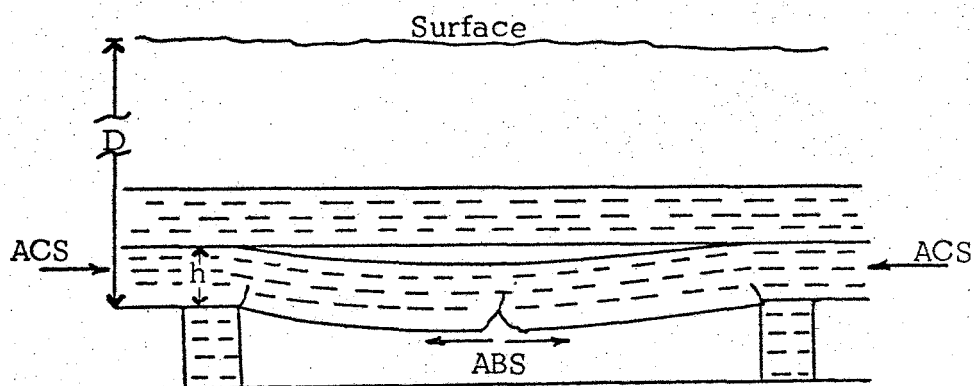
Explanation

b = unit width

h = beam thickness

L = beam length

γ = density

D = depth of overburden

$S_R = \dfrac{\text{horizontal stress}}{\text{vertical stress}}$

w = load/running unit = γhb

I = moment of inertia = $bh^3/12$

c = centroid = h/2

M_c = moment at center = $wL^2/24$

ABS = axial bending stress = $c\,M_c/I$

$= \dfrac{h}{2} \cdot \dfrac{\gamma hbL^2}{24} \cdot \dfrac{12}{bh^3} = \dfrac{\gamma L^2}{4h}$

ACS = $\gamma \cdot D \cdot S_R$

If net stress = 0, axial confining stress = axial bending stress, or

$$\frac{\gamma L^2}{4h} = \gamma \cdot D \cdot S_R$$

and

$$L = 2\,(D \cdot h \cdot S_R)^{1/2}$$

Figure 30. Uniformly loaded fixed-end beam analysis used to estimate room width

it is realistic to assume that the rock mass tensile strength is zero. The concept that the in situ stress acting in the plane of the beam will hold the blocks together appears logical and feasible. Therefore, the net stress at the center of the beam is:

Net stress = Axial confining stress - Axial bending stress. (8)

Solving for a net stress of zero, the length of the beam equals (Figure 30):

$$L = 2 \ (D \cdot h \cdot S_R)^{1/2}. \tag{9}$$

Stability Analysis of the Roof

The major concern of the miner is the stability of the immediate roof. Once the maximum stable room width has been determined then the intermediate roof can be analyzed in terms of the pressure arch.

The immediate roof in the ABC zone can be analyzed by using the beam analysis because the roof will parallel the bedding. The thickness of the roof is equal to the thickness of the bedding or bedding joints. Based on the distribution of bedding joint spacing (Figure 10), the median value is 0.79 feet. To design on this spacing would require that 50 percent of the roof thickness would be less than 0.79 feet and the roof would therefore have a high probability of failure. My opinion is that by using a 75 percent probability that the spacing is greater would be more realistic. This results in a spacing of 0.12 feet, which is below the modal spacing value (0.4 feet).

Using the basic beam equation and varying the room width, a curve is developed (Figure 31). Obert et al. (1960) recommend that the tensile strength should be between four and eight times the bending
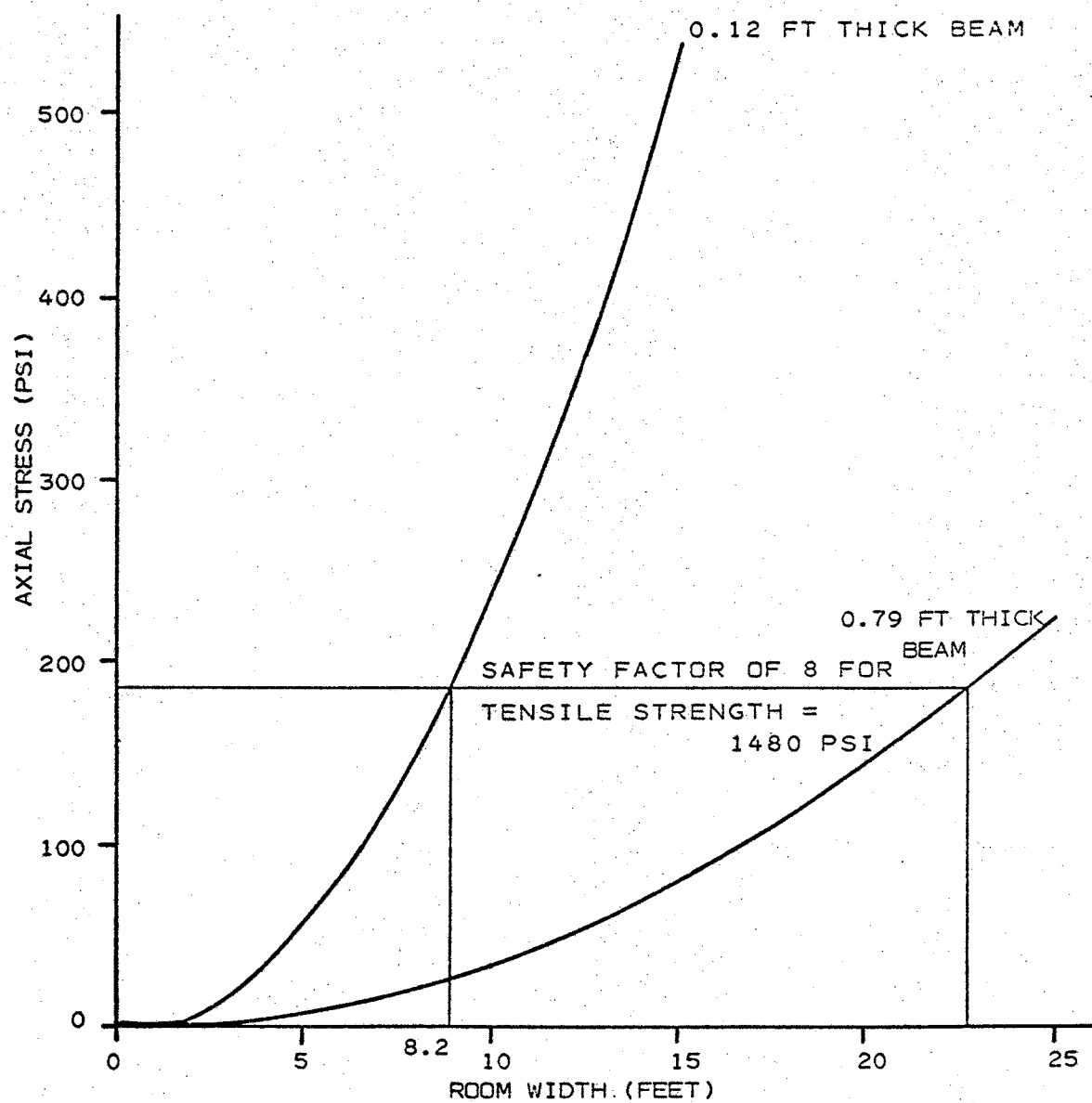
Figure 31. Axial beam stress versus room width

stress. Based on the mean tensile strength of 1265 psi, a 0.12-foot bedding joint spacing, and a tensile strength eight times the bending stress, the predicted room width is 8.2 feet (Figure 31). Using the same conditions but with a median spacing of 0.79 feet, the predicted room width is 21.1 feet.

Using Abel's approach that the rock mass tensile strength is zero and the beam is held together by the in situ stress in the plane of the beam, a curve of room width versus depth can be developed. Based on the stress field estimation the horizontal stress in the plane of the beam is equal to 1.72 σ_{ovb}. Figure 32 shows the room depth versus room width for a beam 0.12 feet thick and 0.79 feet thick. Because the horizontal stress is questionable (Chapter 6), Figure 32 also shows depth versus room width assuming that the horizontal stress in the plane of the beam equals the overburden stress. The decrease in the in situ stress results in a significant reduction in room width for a given depth.

The present workings in the study area are nominally 18 feet wide for a depth ranging between zero and 620 feet. This width has required little to no bolting, which indicates a stable condition. Obert et al.'s (1960) method, based on a 0.12-foot beam thickness, underestimates the room width (Figure 31), while for a beam thickness of 0.79 feet, their method predicts that an 18-foot-wide room would be stable. Abel's (1974b) analysis, using a 0.12-foot beam thickness and a horizontal stress equal to 1.72 σ_{ovb}, predicts that an 18-foot room width would be stable at a depth of 400 feet (Figure 32). Using the same beam thickness but changing the horizontal stress to equal the overburden stress predicts that the 18-foot room width should not be stable above a depth
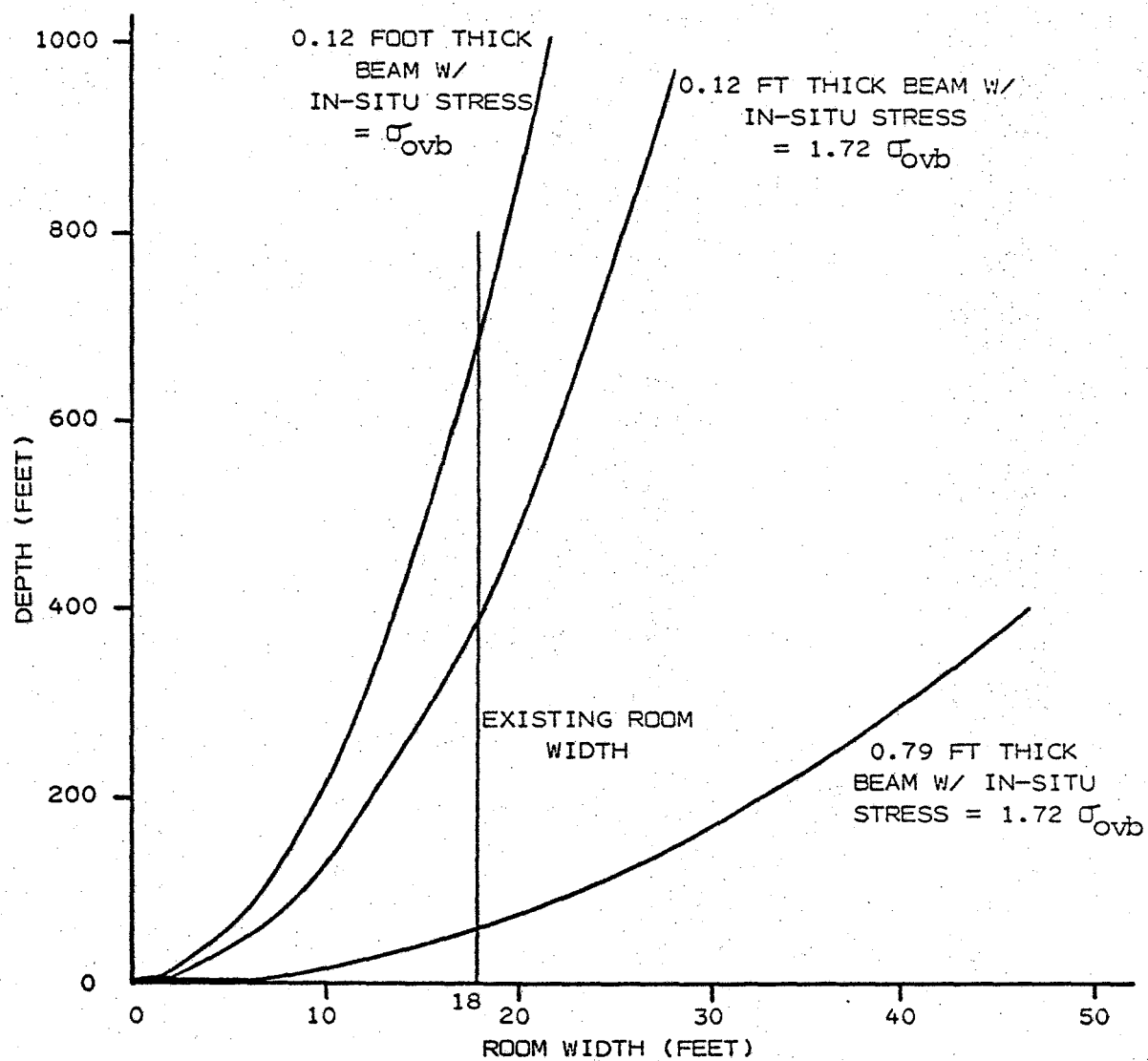
Figure 32. Depth versus room width

of 700 feet. However, we know that the roof is stable above 700 feet; therefore, the beam is either thicker than estimated or the stress in the plane of the beam is greater than the overburden load. Obert et al.'s (1960) approach is based on a wide set of experience and is therefore only a general solution. Their recommendation of a safety factor of four to eight is to account for variations in rock strength. Because their approach is a general solution, its use could result in an overdesign or an underdesign of the roof stability.

Abel's approach of assuming zero rock mass tensile strength and assuming that the axial confining stress counteracts the axial bending stress appears logical. To assume that the rock mass tensile strength is zero is reasonable because the rock is fractured and the fractures are generally unfilled. The difficulty with this method is in determining the axial confining stress. Because this method best approximates how the immediate roof reacts, it will be used to determine the room widths. Using Figure 32 for a 0.12-thick beam and an axial confining stress of 1.72 σ_{ovb} counteracting the tensile axial bending stress, the following room widths have been chosen:

Depth (feet)	Room Width (feet)
0-500	18
500-700	20
700-900	24

Once the width of the stable immediate roof is known, or estimated, the intermediate roof can be analyzed. The intermediate roof can be considered on two scales. On the small scale the load must be

transferred between the pillars (Figure 28), and on the larger scale the load must be transferred across the entire mined zone (Figure 28). Based on the pressure arch data in coal, the maximum arch lengths for 250, 500, and 700 feet are estimated to lie between 0 to 98 feet, 98 to 136 feet, and 169 to 179 feet, respectively. It is obvious from this analysis that the load will be able to arch between the pillars. Therefore those room widths calculated for the immediate roof will probably be the limiting dimensions.

In terms of the large-scale pressure arch, the load must be transferred the strike length since it is generally the minimum plan dimension. Using an average strike length of 300 feet the maximum pressure arch is exceeded until a depth of approximately 1500 feet is reached (Figure 29). Below the depth of 1500 feet the pillars only have to carry the load under the pressure arch. However, above 1500 feet the central pillars will have to be capable of carrying more load. By calculating the load on the pillar using the tributary-area-load method, the pillars are expected to carry the full overburden load. This alleviates the problem of exceeding the pressure arch because the pillar is designed to carry the maximum load.

Measure of Pillar Stability

Safety Factor

The stability of the pillar depends on the load-carrying capacity of the pillar and the load applied to it. Until recently the most common description of the pillar stability is the safety factor. The safety factor is defined as follows:

$$\text{Safety Factor} = \frac{\text{Load-carrying capacity of pillar}}{\text{Load on pillar}} \qquad (10)$$

From this equation, if the safety factor is less than one, the stresses on the pillar will be greater than the pillar strength and failure should occur. If the method of calculating the pillar's load-carrying capacity was absolute and if the stress field were known, a safety factor of one would be sufficient for pillar stability. However, as was discussed in the previous chapters, the rock mass strength and the in situ stress field are not deterministic values but have some distribution or are not well defined. To account for the uncertainty in these input values, the past approach has been to require a safety factor greater than one.

The safety factor required is highly dependent on personal opinion and past experience. A number of people knowledgeable in pillar design have expressed their opinions as to what safety factor is sufficient. Salamon (1967) found that by calculating the safety factor based on his pillar design, 50 percent of the stable pillars had a safety factor against tributary-area loads between 1.3 and 1.75, with 1.5 as the median (Figure 33). Holland and Gaddy (1957), who employ an experience-based pillar design method similar to Salamon's, recommend a minimum safety factor of 1.8 for "average" conditions; for critical areas they suggested a safety factor of 2.0 or even 2.2 may be required. Recently, Holland (1973) has suggested if strong support is "near by" or if a retreat mining system is used where the effects on the surface are not important, a safety factor between 1.3 and 1.4 is sufficient. If surface considerations are required, where the effects on the surface are critical, a safety factor of 1.6 is now suggested by Holland (1973).
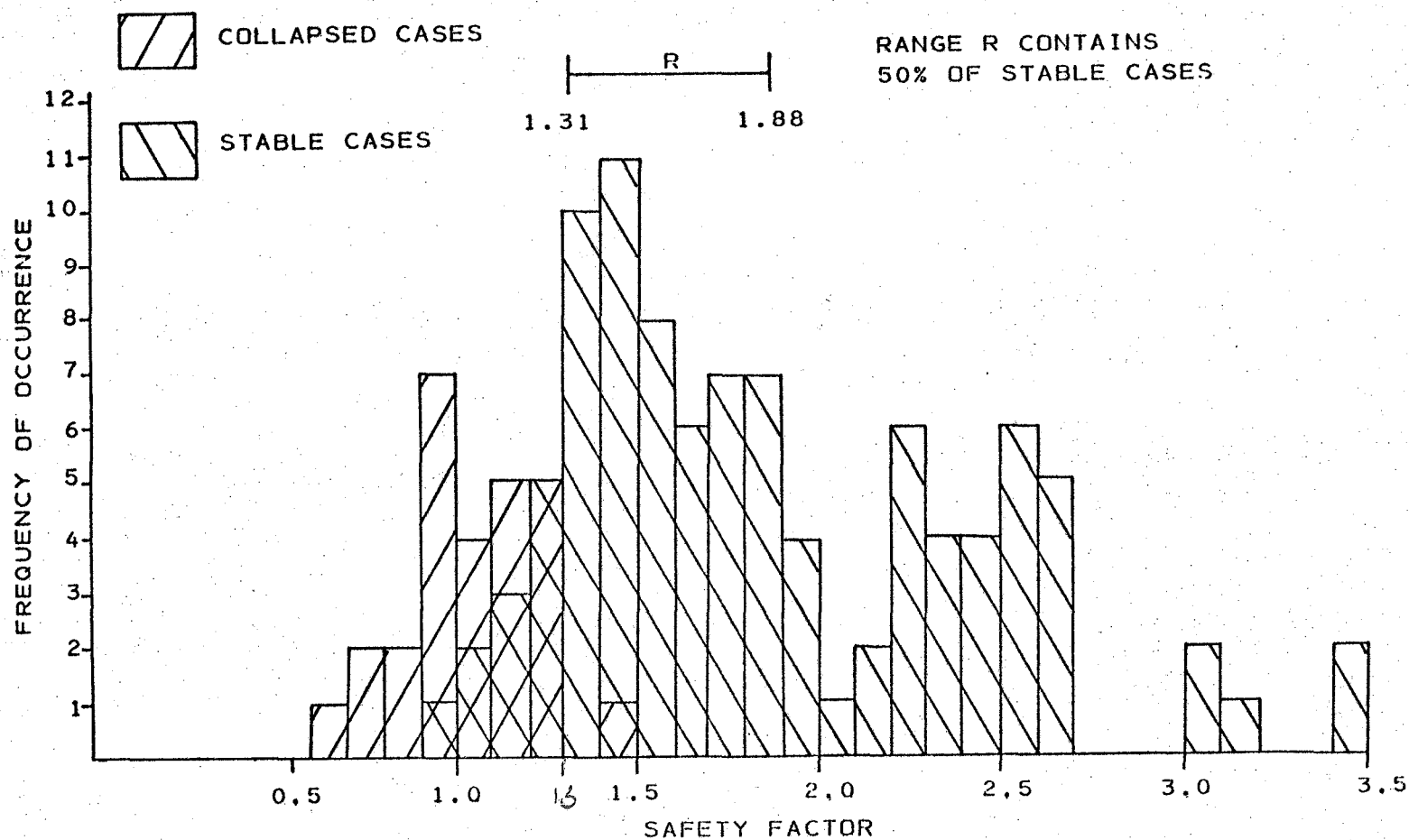
Figure 33. Histogram of safety factors for existing coal pillars--After Salamon (1967)

Ashwin (1972) implies that a safety factor of 1.5 is required. Obert et al. (1960) recommend a safety factor of 2.0 to 4.0 for competent rock. It is obvious that there is no agreement as to what is the correct safety factor, which adds an additional problem to pillar design.

Probability of Failure

More recently, the approach of probability has been applied to pillar design. Coates and Gyenge (1973) have proposed a method to calculate the probability of failure. Given a distribution of stresses on the pillar and a distribution of pillar strengths, the overlap area of these two curves represents those cases where pillar failure will occur (Figure 34). The overlap area can be related to the total area under the pillar strength distribution, which is then the probability of failure. The difficulty of this method is in defining the pillar strength and pillar stress distributions. Given the probability of failure, it can be related to the cost of failure; thereby an optimum risk can be calculated.

The probability of failure approach is more appealing than the safety factor method. The probability of failure accounts for the natural variations in rock strength and applied stress, whereas the safety factor method is a deterministic solution. For the purpose of comparing different pillar design methods the safety factor approach will be used.

Calculation of Load on Pillar

The tributary-area load method will be used to calculate the load on the pillar. By definition the tributary-area load means that each pillar carries the entire overburden load half way to the next support (Figure 35). The tributary-area load is calculated from the equation:

DISTRIBUTION OF LOAD
ON PILLAR (L_p)

DISTRIBUTION OF PILLAR
STRENGTHS (S_p)

PROBABILITY
OF FAILURE
EQUALS SHADED
AREA

0

$S_p - L_p$
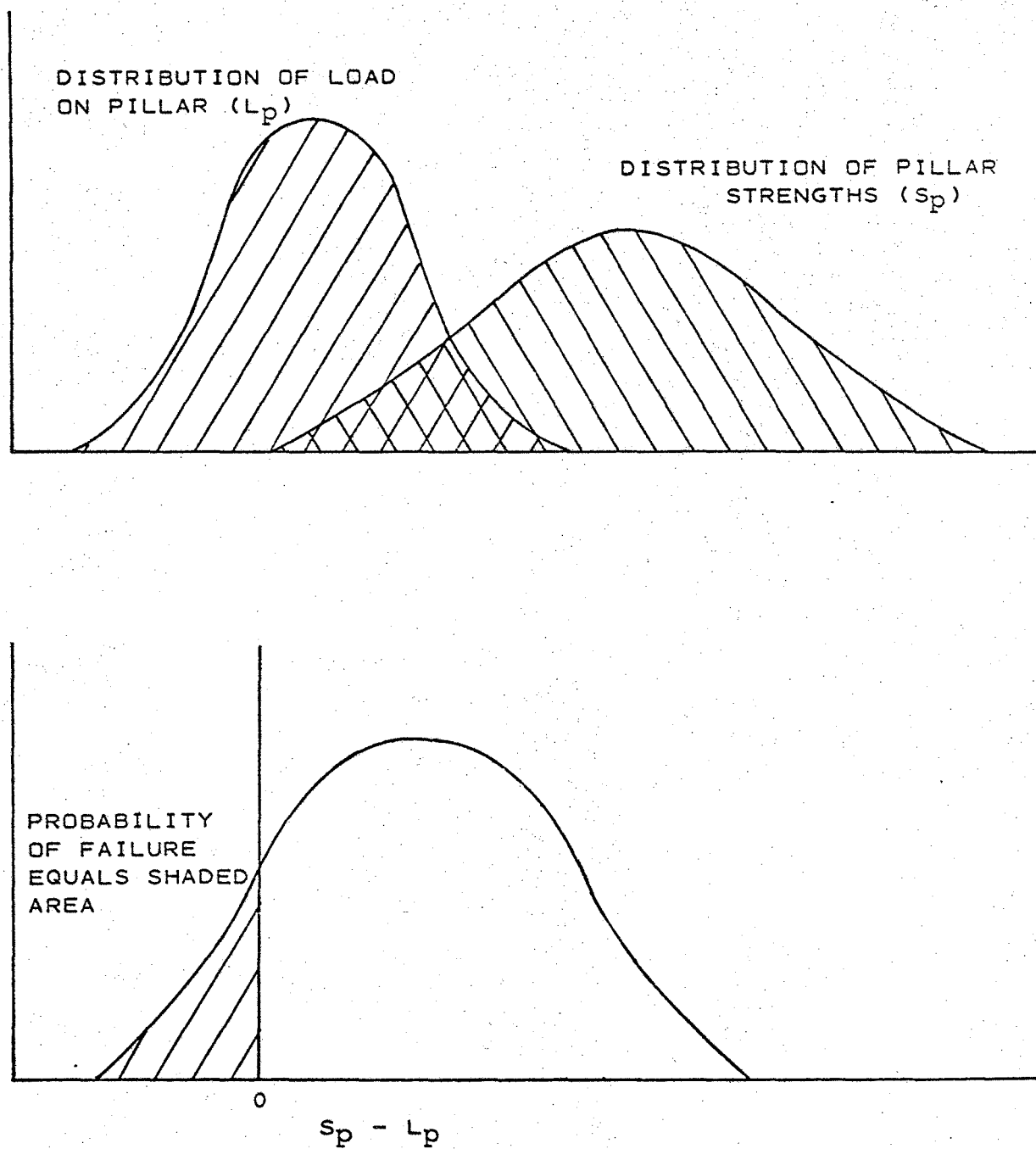
Figure 34. Method of calculating probability of failure—After
Coates and Gyenge (1973)

SURFACE
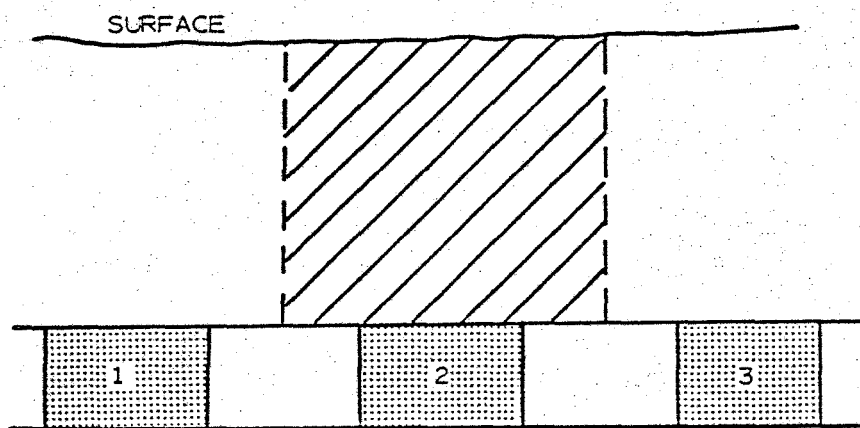
HATCHED AREA IS CROSS SECTION OF
TRIBUTARY - AREA   LOAD ON PILLAR 2
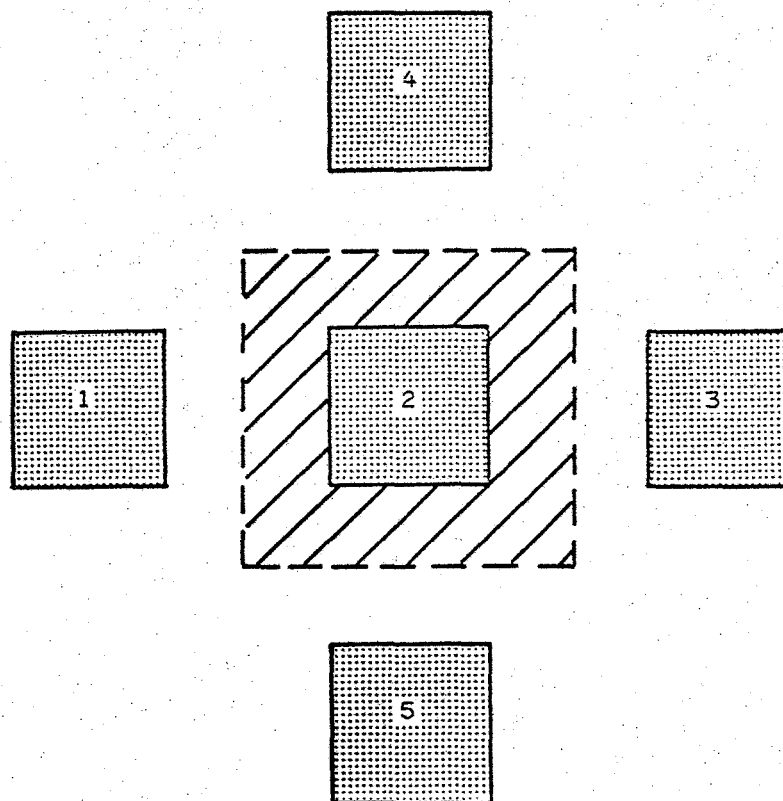
HATCHED AREA IS PLAN SECTION OF
TRIBUTARY - AREA   LOAD ON PILLAR 2

Figure 35. Tributary-area load

$$TAL = (RmW + PW)(CcW + PL)\,\sigma \qquad\qquad (11)$$

where: TAL   = tributary-area load (lb)

RMW = room width (ft)

CcW = crosscut width (ft)

PW   = pillar width (ft)

PL   = pillar length (ft)

σ = in situ stress (psf) normal to roof.

This method predicts the maximum load that can be applied to the pillar.

For this analysis, the applied load will be assumed normal to bedding because the mineralization parallels the bedding. The dip of the bedding ranges between zero and 60 degrees, with a median of approximately 30 degrees. The magnitude of the estimated in situ stress normal to bedding under the average conditions at the Control property is $1.24\ \sigma_{ovb}$.

Comparison of Methods for Calculating the Load-carrying Capacity of a Pillar

There presently exist numerous methods for calculating the load-carrying capacity of a pillar. Most work to date has been done in terms of coal mining. For the purpose of this study the following methods will be discussed and compared: (1) Obert, Duvall, and Merrill, (2) Skinner, (3) Bieniawski, (4) Salamon and Munro, and (5) Wilson. These methods are based on different concepts or entirely different approaches to similar concepts.

To permit comparison between the results obtained by the different methods, the values listed in Table 28 will be used for each method. Because the size effect is an important parameter, two pillar

Table 28. Basic input parameters for pillar design comparison

Parameter	Value
Depth	50 ft
Dip of beds	30°
In situ stress normal to bedding	1.24 σ_{ovb} psf
Room width	20 ft
Crosscut width	20 ft
Square pillar	
Pillar width	37 ft
Pillar length	37 ft
Pillar height	30 ft
Tributary-area load	166,700 tons
Recovery	57.9%
Rectangular Pillar	
Pillar width	25 ft
Pillar length	60 ft
Pillar height	30 ft
Tributary-area load	184,100 tons
Recovery	58.3%

geometries will be examined: a square pillar (37 x 37 feet) and a rectangular pillar (25 x 60 feet). Approximately the same tonnage of ore will be mined from these two pillar designs.

The Obert, Duvall, and Merrill Method

Obert, Duvall, and Merrill (1960) believed that the strength of the pillar is equal to the uniaxial compressive strength of a core sample with the same width-to-height ratio as the pillar. To use this method the following assumptions or conditions must be fulfilled:

1. The rock is competent; i.e., "rock which, because of its physical and geological characteristics is capable of sustaining openings without any structural support except pillars and walls left during mining (stulls, light props and roof bolts are not considered as structural support)" (Obert et al., 1960, p. 5).

2. The pillar carries the stress equally throughout. This is based on elastic studies which shows that as the ratio between the room width and the pillar width increases the average stress approaches the maximum stress and becomes more uniform.

3. The pillar can be considered stable if the safety factor is at least between two and four.

Because all of the core testing is not done at the same width-to-height ratio as the pillar testing, Obert et al. have developed the following equation to correct for this difference in ratios:

$$C_s = C_1(0.778 + (0.222d/h)) \qquad (12)$$

where: C_s = compressive strength of specimen if $d/h \neq 1$

C_1 = compressive strength of specimen if $d/h = 1$

d = diameter of specimen

h = height of specimen.

Recommended limits for d/h for this equation are $0.25 \leq d/h \leq 4$. Because the samples are usually tested at some other ratio than 1:1, equation (1) can be solved, as follows:

$$C_p = C_c \frac{0.778 + (0.222(d_p/h_p))}{0.778 + (0.222\ d_c/h_c)}$$

for normalizing to 2:1

$$C_c = C_L / \left(\frac{1.222}{.778 + .222(\%)} \right) \quad (13)$$

corrected   lab   of lab specimen

where: C_p = compressive strength of specimen with a width-height

ratio of the pillar

C_c = compressive strength of specimen with a width-height

ratio of the core tested

d_p = diameter of pillar

h_p = height of pillar

d_c = diameter of core specimen

h_c = height of core specimen.

If $d_c = 1.86$ in., $h_c = 3.72$ in., and $C_c = 19,920$ psi, the compressive strength of the square pillar is 23,570 psi. The load-carrying capacity is then:

(area of pillar) x (compressive strength of pillar)   (14)

= (37 ft x 37 ft) (23,570 psi x 144/2000)

= 2,323,248 tons

and the safety factor (SF) for the tributary-area-loaded square pillar is:

$$SF = 2,323,248/166,700 = 13.9.$$

A similar analysis can be made for the rectangular pillar. The minimum pillar length will be used for the pillar diameter to correct the compressive strength of the rectangular pillar. The reason for this choice is that testing has indicated that the compressive strength for a constant height depends on the minimum sample width and not its length (Denkhaus, 1962). The pillar strength based on the mean uniaxial compressive strength is 21,580 psi and the load-carrying capacity for a pillar 25 x 60 feet is 2,330,640 tons. The safety factor is then 12.7.

The safety factors for these two pillar dimensions far exceed the required safety factor suggested by Obert et al. (1960). Although this method is very easy to apply, one of the major problems is the assumption that the compressive strength of the pillar equals the compressive strength of a core sample with the same width-to-height ratio. However, the core samples represent the rock substance strength while the pillar is made up of the rock mass. Obert et al. assume that the pillar can carry the load uniformly across the pillar; however, this is unlikely because the edge of the pillar has sustained blast damage that weakens the rock mass strength.

The Skinner Method

Working on anhydrites, Skinner (1956) developed a method to calculate pillar strength based on the weakest link theory. This theory is based on the idea that the strength of a chain is no greater than the strength of the weakest link. Skinner postulates that a pillar is made up

of N number of unit blocks and that if each of these units was tested, their strengths would fit a distribution. The weakest block of the distribution would represent the strength of the pillar. Skinner showed that his test results of anhydrite were best represented by either a normal or a Weibull distribution. The Weibull distribution requires test results of samples of various volumes and it will therefore not be used for this analysis. The equation for the normal distribution of pillar strength (S) is

$$S = \bar{X} - \mu(2 Ln N)^{1/2} + 1/2 \; (Ln \, Ln \, N + Ln \, 4 \pi (2 \, Ln \, N)^{-1/2} \quad (15)$$

where: $\bar{X}$ = mean strength of unit blocks

μ = standard deviation of unit blocks

N = number of unit blocks that make up the pillar.

Skinner's testing shows that as the sample volume increases the sample strength decreases (Table 29). This result helps to justify that the larger samples have lower strengths because their number of flaws is greater than that of a smaller sample.

Table 29. Effect of size on compressive strength for anhydrite--After Skinner (1956)

| Sample Side Length (in.) | Uniaxial Compressive Strength (psi) | |
	Mean	Standard Deviation
1	32,510	4,600
2	25,360	2,580
4	24,270	2,050
10	16,800	2,680

Before Skinner's method can be used, the core strengths have to be corrected to the same width-to-height ratio as the pillar. This correction was made using Obert et al.'s (1960) equation (equation Table 30 lists the corrections for the two pillar dimensions. The normal distribution equation (equation 15) will have to be used because only samples of similar size were tested. The mean and standard deviation of the unit block for the square pillar are 24,800 psi and 9,600 psi, respectively. The number of unit blocks (N) that make up the pillar is calculated as follows:

$$N = \frac{\text{Pillar Dimensions}}{\text{Unit Core Block}} = \frac{(37 \times 37 \times 30 \times 12^3) \text{ in.}^3}{(1.86 \times 1.86 \times 1.51) \text{ in.}^3} \qquad (16)$$

$$= 13,585 \times 10^3$$

Using these parameters in the normal distribution equation (equation 15), the calculated square pillar strength is -30,200 psi. Because the pillar strength cannot be negative, the strength of the square pillar is zero. This method can also be approached graphically by plotting the sample strength versus the cumulative probability of failure. The divisor for calculating the cumulative probability is the total number of samples plus one (N + 1). This is used because for a small sample size there are probably specimens stronger and weaker than the ones tested.

Table 30 lists the cumulative probabilities with the associated strengths. Figure 36 shows the core strength versus cumulative probability of failure plot for the square pillar. It is obvious that the data fit a two-segment line. The cumulative probability of the weakest unit block failing for a 37 x 37 x 30-foot pillar is 1/N, which equals

Table 30. Corrected compressive strengths and associated cumulative probabilities

Core Uniaxial Compression Strength (psi)	Square Pillar (37 x 37 x 30 feet)		Rectangular Pillar (25 x 60 x 30 feet)	
	Corrected Strength (psi)	Cumulative Probability	Corrected Strength (psi)	Cumulative Probability
33,500	39,630	0.94	36,290	0.94
33,100	39,160	.89	35,860	.89
28,000	33,130	.83	30,330	.83
26,600	31,470	.78	28,810	.78
24,500	28,990	.72	26,540	.72
20,500	24,250	.67	22,210	.67
20,500	24,250	.61	22,210	.61
20,400	24,140	.56	22,100	.56
17,300	20,470	.50	18,740	.50
16,700	19,760	.44	18,090	.44
16,100	19,050	.39	17,440	.39
15,000	17,750	.33	16,250	.33
15,000	17,750	.28	16,250	.28
14,500	17,160	.22	15,710	.22
13,500	15,970	.17	14,620	.17
13,000	15,380	.11	14,080	.11
10,500	12,420	.06	11,370	.06
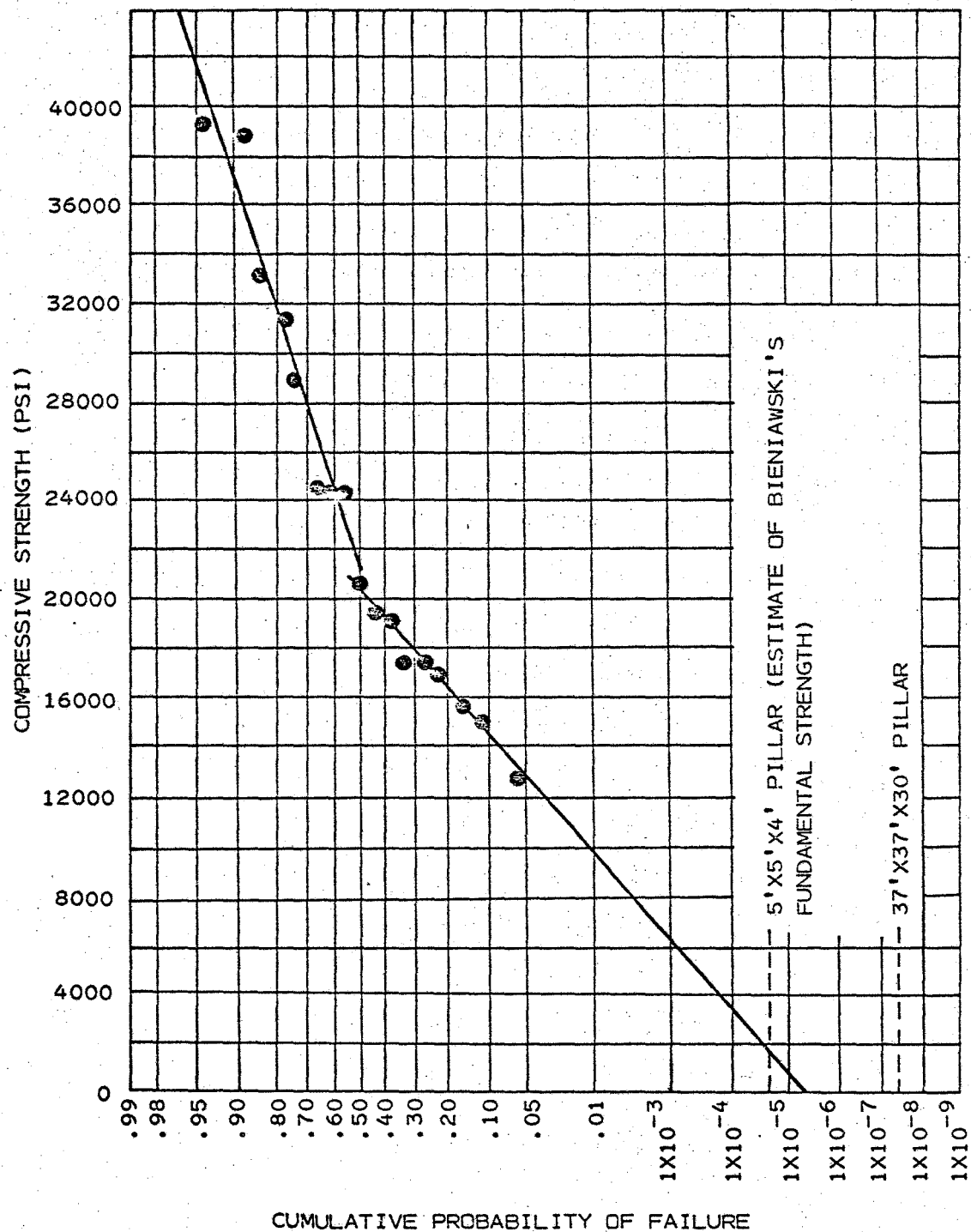
Figure 36. Square pillar strength based on the Skinner method

7.36×10^{-8}. Figure 36 shows that the pillar strength is still zero, hence the safety factor equals zero.

This approach can be applied to the rectangular pillar. Using a pillar width of 25 feet, the corrected compressive strengths and cumulative probabilities are listed in Table 30. The mean corrected compressive strength is 22,700 psi with a standard deviation of 8,800 psi. The number of unit blocks in the pillar is:

$$N = \frac{(25 \times 60 \times 30 \times 12^3) \text{ in.}^3}{(1.86 \times 4.46 \times 2.23) \text{ in.}^3}$$
$$= 4,203 \times 10^3.$$

This results in a pillar strength of $-25,900$ psi, which means that the predicted strength for the rectangular pillar is zero. Plotting the data on the cumulative probability paper shows that the strength is still zero (Fig. 37).

The obvious disadvantage of this method is the result of a negative pillar strength, which Skinner admits. The concept of the weakest link does have some validity; however, the location of this weakest link should also be considered. If the weakest link is located in the center of the pillar it is confined and should therefore have a higher strength than represented by a uniaxial test. Also, one unit block may fail in a pillar but the other units may be able to carry the additional load because they are stronger. Skinner found that the normal and Weibull distributions produced the same result; however, he was testing an anhydrite, which may be a special case. If a rock strength testing program could have been carried out that tested different volumes,
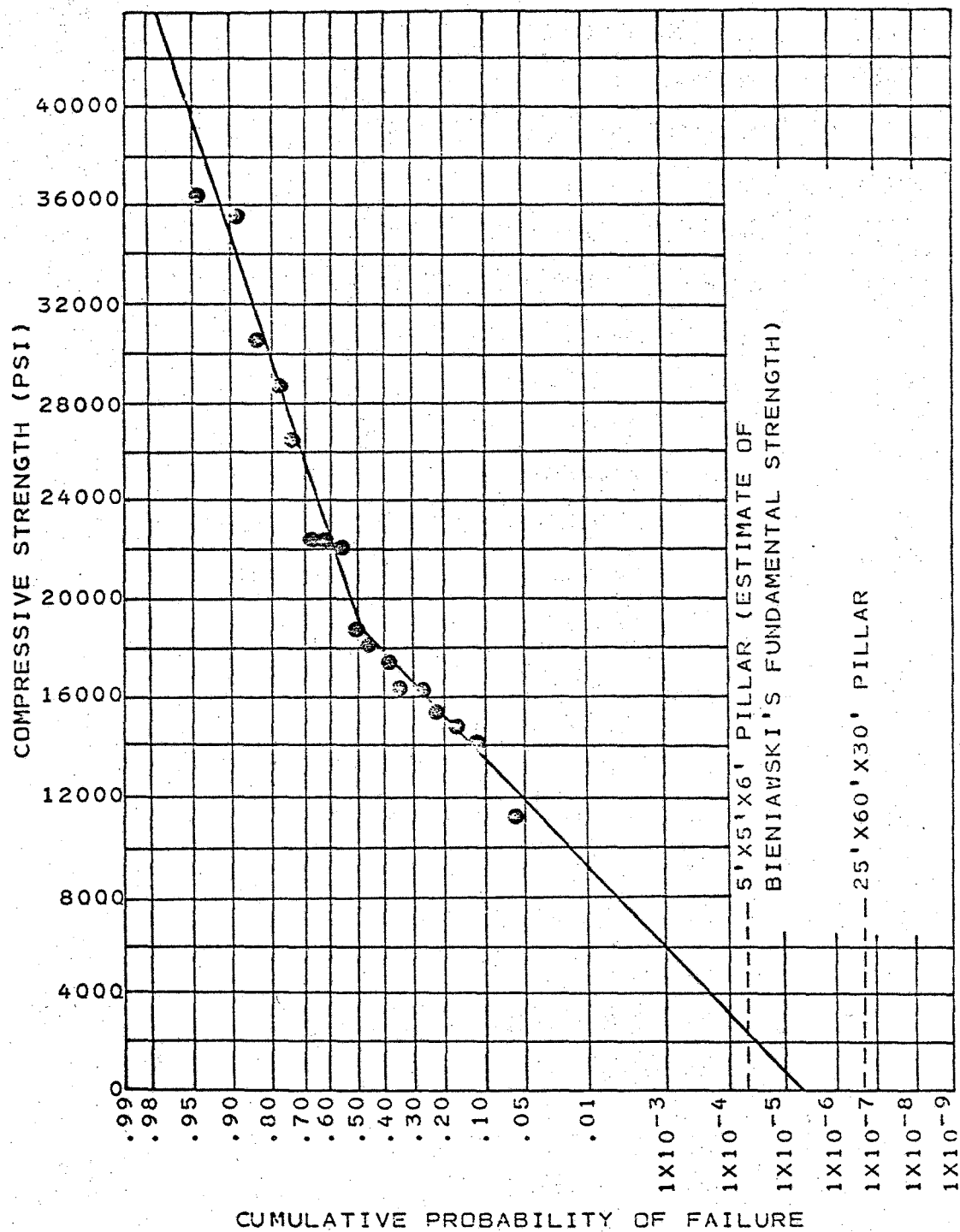
Figure 37. Rectangular pillar strength based on the Skinner method

the Weibull distribution could have been used which may have produced results other than those obtained by using a normal distribution.

The Bieniawski Method

Bieniawski (1968) also based his method on the idea that the strength decreases as the volume increases. This fact was observed in Skinner's test results (Table 29). Bieniawski proposed further that there is a fundamental strength within the rock mass and that the increase in volume beyond this point does not change the rock mass strength. He produced a strength versus sample size curve (Fig. 38) from data from testing cubical coal samples ranging from 0.75 to 60 inches on a side. He divided this curve into three segments: segment a, constant strength; segment b, reduced strength; and segment c, constant strength. The equations for pillar strength for each of the curve segments that fit Bieniawski's data are:

1. Curve segment a, $S = 24,620$ psi $\hspace{4em}$ (17)

2. Curve segment b, $S = 1,100(W^{0.16}/h^{0.55})$ psi, where $\hspace{1em}$ (18)

    W = pillar width (ft) and h = pillar height (ft).

3. Curve segment c, $S = 400 + (200W/h)$. $\hspace{4em}$ (19)

The equation for curve segment c is the fundamental strength equation.

From the strength versus volume curve (Fig. 38), Bieniawski concluded that the fundamental strength was reached at 5 feet. Both the square and rectangular pillars being analyzed are greater than 5 x 5 x 5 feet, hence Bieniawski's fundamental strength curve can be applied. The The strength of the square pillar is

$$S = 400 + (200 \times 37/30) = 647 \text{ psi.}$$
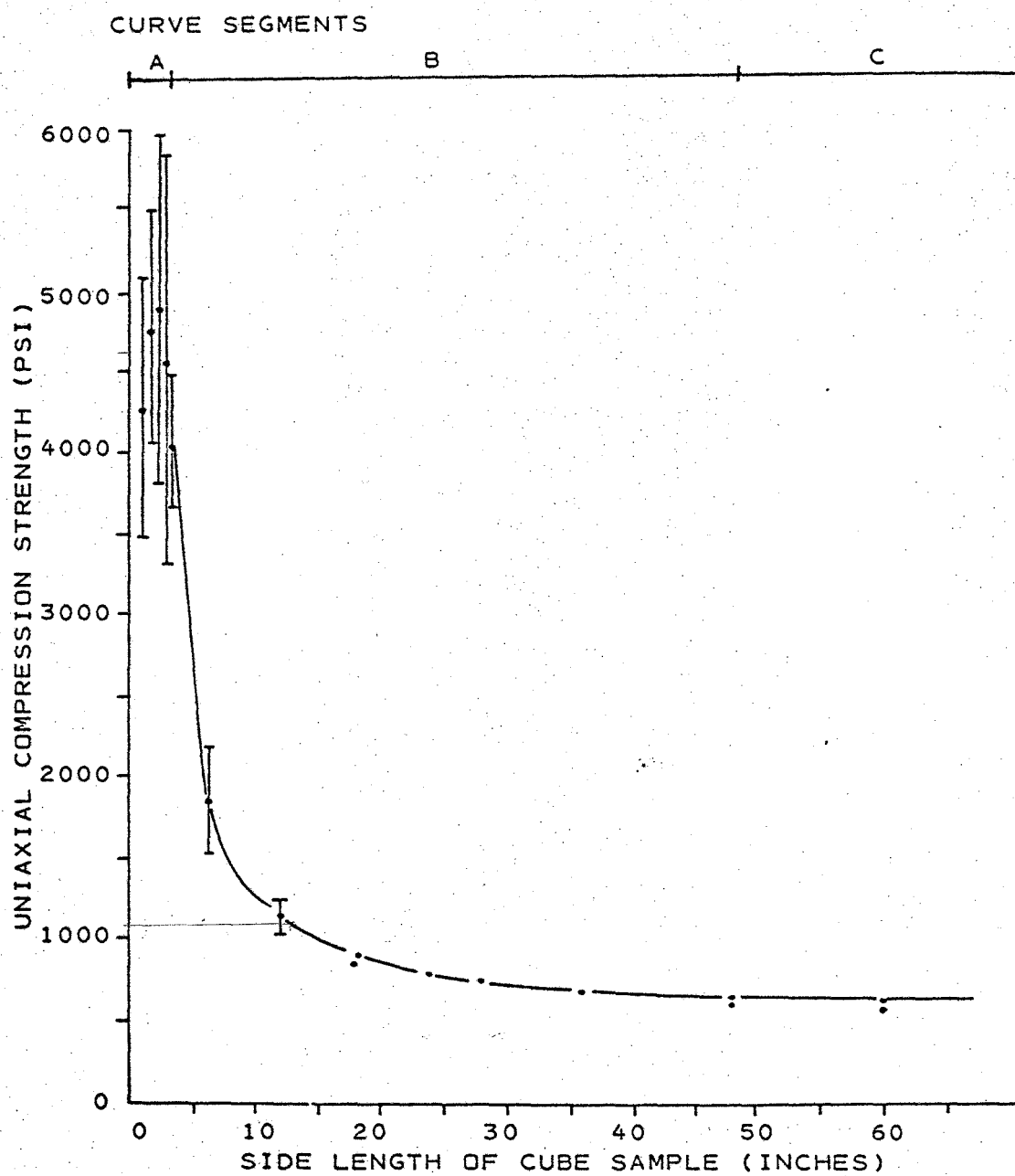
Figure 38. Uniaxial compressive strength of coal versus side length of cube-shaped samples—After Bieniawski (1968)

This results in a load-carrying capacity of 63,774 tons or a safety factor of 0.4. Using a pillar width of 25 feet for the rectangular pillar, the pillar strength is 567 psi, the load-carrying capacity is 61,236 tons, and the safety factor is 0.3.

The obvious disadvantage of using Bieniawski's fundamental strength equation at Marble Peak is that it is based on coal which does not have the same strength parameters as the rock at Marble Peak. The fundamental strength of the ABC zone rock might be obtained by using the curves generated from Skinner's method. Assume that the fundamental rock strength is reached at 5 x 5 x 4 feet for the square pillar and 5 x 5 x 6 feet for the rectangular pillar. The cumulative probability of the weakest specimen for the square pillar is 3.02×10^{-5}. From Figure 36, the pillar strength is 1800 psi; i.e., the load-carrying capacity is 177,420 tons and the safety factor is 1.1. For the rectangular pillar the cumulative probability of the weakest specimen is 7.4×10^{-5}, which from Figure 37 results in a fundamental strength of 2,200 psi. This fundamental strength equals a load-carrying capacity of 237,600 tons or a safety factor of 1.3 for the rectangular pillar.

Bieniawski's (1968) concept that some fundamental strength is reached as the volume of the specimen increases seems logical. The factor yet to be determined is the size at which the fundamental strength is reached. Fundamental strength has to be a function of rock substance strength, the length, spacing, and orientation of the joints, and the shear strength of the joints. Because Bieniawski's test analysis was based on coal, the fundamental strength for the ABC zone is probably different. He states that his average spacing was 0.22 feet, which is

similar to the results obtained at Marble Peak; however, the rock substance strength is greater at Marble Peak. I. Evans (1970) made the point that Bieniawski's fundamental strength was reached at the size of the largest sample tested and that we do not know what happens beyond a side length of 5 feet. His point that a 5-foot side length may not be the size at which the fundamental strength is reached is well taken. However, in studying Bieniawski's curve, the change in pillar strength is minimal for an increase in pillar size above 3 x 3 x 3 feet. This concept of a fundamental strength, i.e., the number of flaws per volume is constant, was observed in the step path analysis, which showed that the median percentage of intact rock did not vary significantly above a pillar height of 15 feet (Fig. 26). If 5 x 5 x 5 feet is the size of a pillar at which all rock types reach their fundamental strength, this strength can be calculated using Skinner's method of the weakest link.

The Salamon and Munro Method

Salamon and Munro (1967) measured 125 room-and-pillar coal mines in South Africa with varying depths, pillar heights, pillar widths, and extraction ratios. The pillars measured were both stable and collapsed. They assumed the distribution of safety factors for these pillars fit a lognormal distribution with a median of one. Using a power function to describe the pillar strength and assuming a tributary-area load, they estimated the unknown factors of the strength equation with a "likelihood function."

The general strength equation used by Salamon and Munro (1967) is:

$$q \qquad \text{Pillar Strength (S)} = K h^A W^B \qquad (20)$$

where: K = strength of 1 ft^3 rock (psi)

h = pillar height (ft)

W = pillar width (ft)

A and B are constants.

Assuming the tributary-area load to be the load on the pillar, the safety factor (SF) is calculated as follows:

$$SF = \frac{K h^A W^B}{\gamma H \left(\frac{W+b}{W} \right)^2} \times 144 \qquad (21)$$

where γ = rock density (lb/ft^3)

H = thickness of overburden (ft)

b = room width (ft).

In the above equation, the unknowns are K, A, and B.

Salamon and Munro proposed that distribution of pillar safety factors is lognormal with the median at one because the safety factor is limited by zero on one side, unlimited on the other, and most designs require a minimum safety factor of one for stability. With this assumption they obtained the safety factor distribution with a median of one using a "likelihood function" and maximizing K, A, and B based on the 125 observations. The results of Salamon and Munro's (1967, Table II) analysis are:

K = 1,322

A = - 0.6609

B =   0.4590

Their results are based on square pillars.

Using Salamon and Munro's (1967) equation, the strength (S) of a square pillar as defined in Table 28 can be calculated as follows:

$$S = 1,322 \; (30^{-0.6609})(37^{0.4590}) = 732 \text{ psi}$$

The load-carrying capacity for the square pillar is 72,152 tons, which equates to a safety factor of 0.4. For a rectangular pillar the strength is 612 psi (66,096 tons load-carrying capacity), which results in a safety factor of 0.4.

Because Salamon and Munro's strength equation is based on coal, its use at the Control property is probably not valid. However, if we can assume that the A and B values of the strength equation do not change from one rock type to another but that the unit cube strength does, the equation can be changed to account for rock strength in the ABC zone. The strength of the one foot unit cube can be estimated from Skinner's method. The cumulative probability for the weakest specimen in a unit cube is 3.72×10^{-3}, which results in a value for K of 7,500 psi (Fig. 39), and Salamon and Munro's equation for the ABC zone now becomes:

$$S = 7,500 \; h^{-0.6609} w^{0.459},$$

which gives a square pillar strength of 4,156 psi (409,649 tons load-carrying capacity), resulting in a safety factor of 2.47. The rectangular pillar strength is 3,471 psi, which equals a load-carrying capacity of 374,895 tons. The safety factor for the rectangular pillar is 2.04.

Salamon and Munro's method of calculating the constants and unit cube strength are very attractive for those areas where existing pillars are present. The assumption that the distribution of safety factors
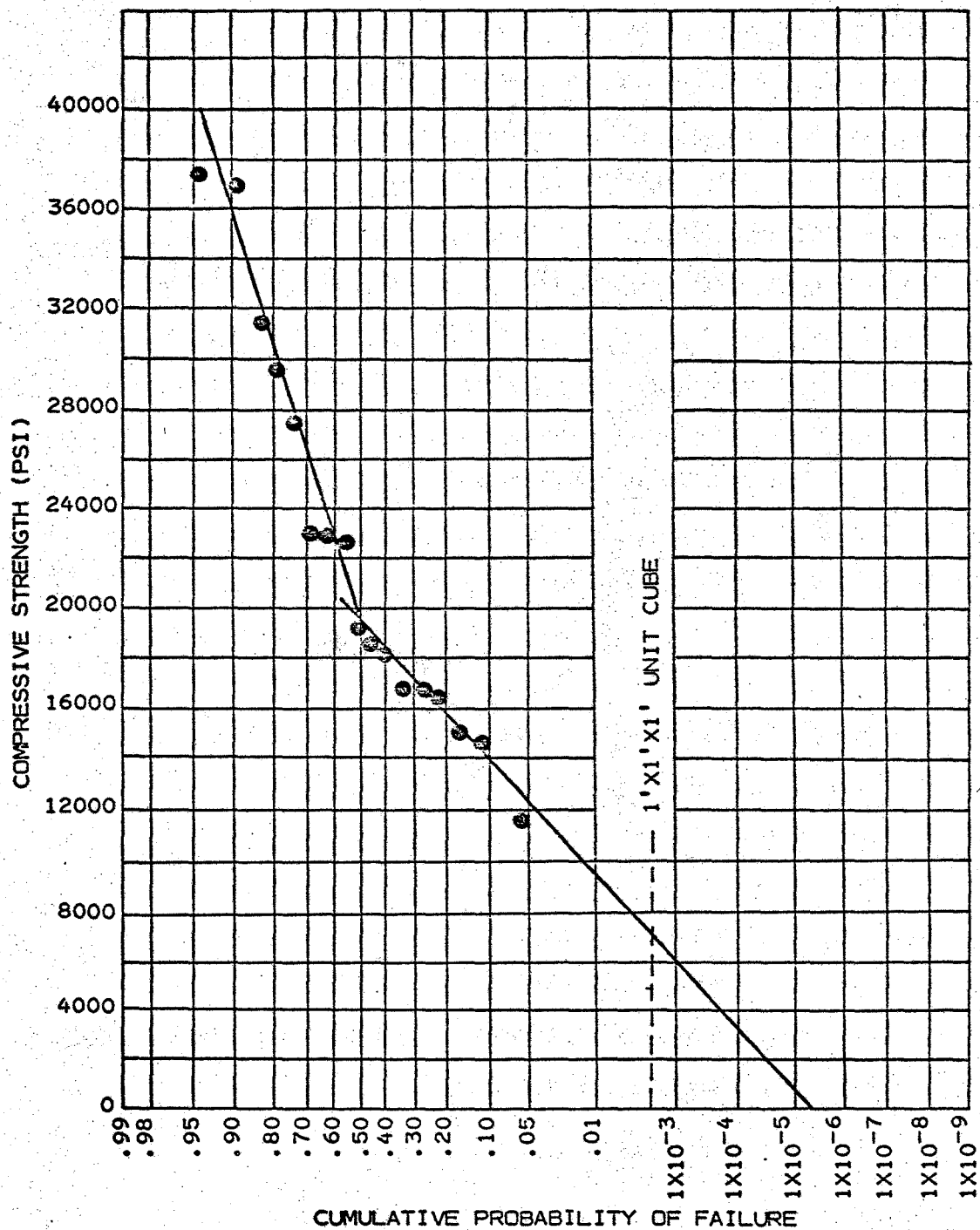
Figure 39. Strength of a one-foot cube based on the Skinner method

has its median at one is probably incorrect. As discussed in the section on the measure of pillar stability, the recommended safety factors are at least 1.4, therefore perhaps this should be the median of the distribution. Assuming the exponents remain constant for any rock type, the unit cube strength can be estimated from Skinner's method.

The Wilson Method

Wilson (1972) contends the pillar is divided into two zones, an inner core and a surrounding yield zone. The inner core carries most of the load and is subject to a triaxial stress condition while the yield zone carries little load but confines the inner core (Fig. 40). The yield zone is characterized by being highly fractured at the edge of the pillar. These blocks do not all fall out because of friction on the ends and interlocking of the blocks. Wilson shows how with friction only as the horizontal stress increases inward to the pillar core. This is analogous to the passive pressure of a retaining wall. The magnitude of the confining stress does not increase all the way to the center of the pillar, but it increases until the magnitude of in situ stress is reached. The distance into the pillar where the maximum pillar stress is reached, i.e., the distance into the edge of the confined core is calculated as shown in Table 31. Wilson contends that the rock mass cohesion (S_c) is one psi for coal.

By calculating the area under the stress distribution, knowing the pillar width, length, and height, and the maximum stable vertical stress (S_{MV}), the load-carrying capacity can be calculated. Wilson (1972) assumes the stress distribution can be simulated by a simple

CAVED   ROOM   PILLAR   ROOM   CAVED

A) CROSS SECTION

YIELD ZONE   PILLAR   YIELD ZONE

CORE

B) PROBABLE STRESS DISTRIBUTION

PRACTICAL
STRESS LIMIT

MAXIMUM VERTICAL
PILLAR STRESS

COVER LOAD

C) HYPOTHETICAL STRESS DISTRIBUTION
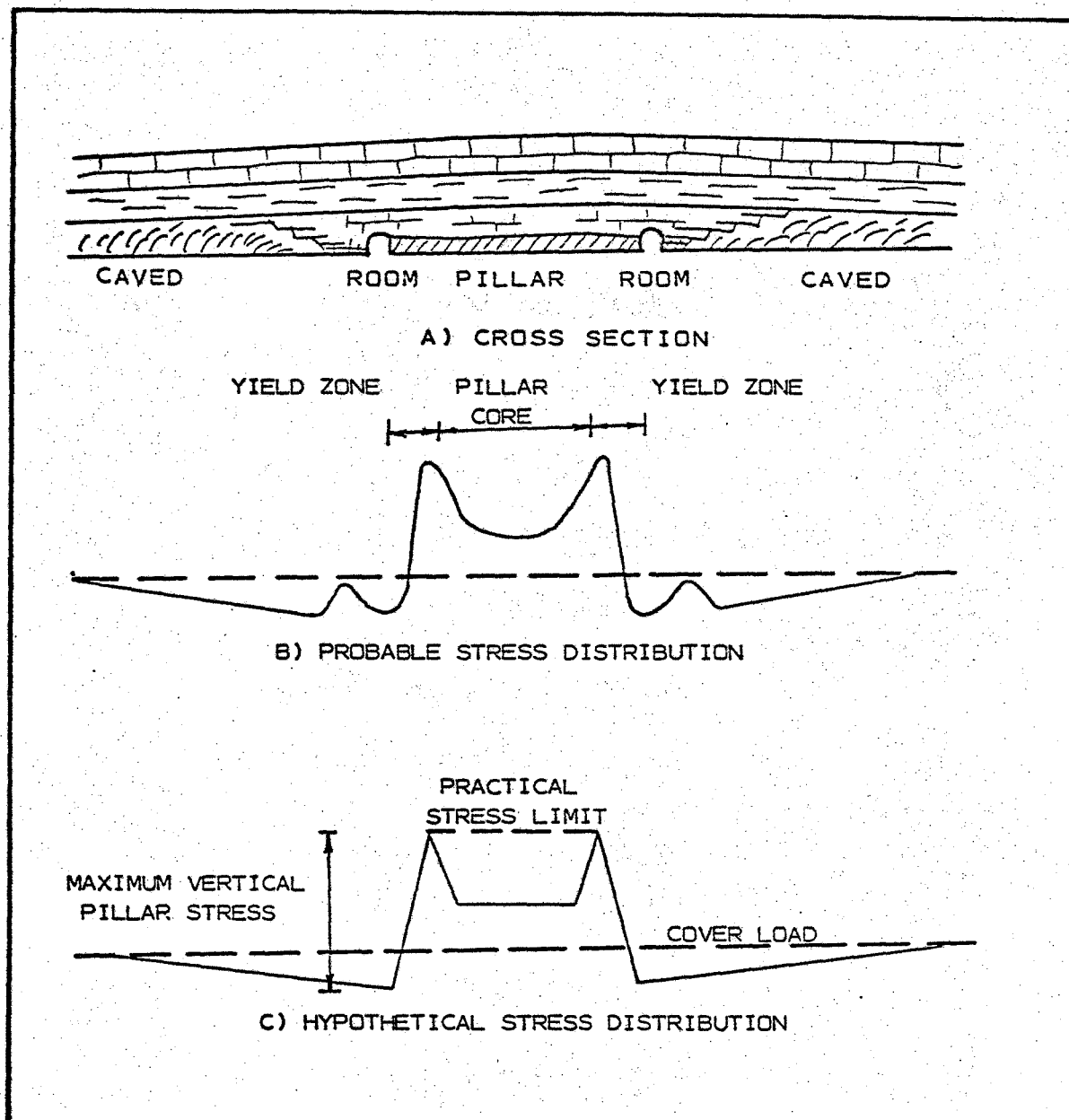
Figure 40. Wilson's concept of how pillars carry load—After
Wilson (1972)

Table 31. Wilson's equations for calculating load-carrying capacity of pillars--After Wilson (1972)

Load-carrying capacity for wide pillars: $P > 2Y_M$

Square pillars

$$LCC = 7.2 \times 10^{-2} S_{MV} (P^2 - 2PY_M + 1.33 Y_M^2) \text{ tons}$$

Rectangular pillars

$$LCC = 7.2 \times 10^{-2} S_{MV} (PL - PY_M - LY_M + 1.33 Y_M^2) \text{ tons}$$

Long pillars

$$LCC = 7.2 \times 10^{-2} S_{MV} (P - Y_M) \text{ tons per foot of run}$$

Load-carrying capacity for narrow pillars: $P < 2Y_M$

Square pillars

$$LCC = 7.2 \times 10^{-2} S_{MV} \frac{P^3}{6Y_M} \text{ tons}$$

Rectangular pillars

$$LCC = 7.2 \times 10^{-2} S_{MV} \frac{P^2}{2Y_M} \left(\frac{L}{2} - \frac{P}{6} \right) \text{ tons}$$

Long pillars

$$LCC = 7.2 \times 10^{-2} S_{MV} \frac{P^2}{4Y_M} \text{ tons per foot of run}$$

where: LCC = load-carrying capacity of pillar (short tons)

S_{MV} = maximum stable vertical pillar stress (psi)

$$= (6.94 \times 10^{-3} S_R g H) \tan B + S_c$$

Y_M = distance into pillar (ft) at location of maximum stable pillar stress and edge of confined core

$$= \frac{M}{(\tan B)^{1/2} (\tan B - 1)} \ln \frac{S_{MV}}{S_c}$$

Table 31. Wilson's equations--<u>Continued</u>

tan B = passive pressure coefficient = $(1 + \sin\phi)/(1 - \sin\phi)$

P = pillar width (ft)

L = pillar length (ft)

M = pillar (seam) height (ft)

ϕ = rock mass friction angle

H = thickness of overburden (ft)

g = density (lb/ft^3)

S_c = confining stress acting at edge of pillar (psi); rock mass cohesion

S_R = (horizontal stress)/(vertical stress)

truncated pyramid (Fig. 40). Wilson states that whose width is less than $2Y_M$ will have no inner core. It is doubtful that this pillar can be considered long-term stable; however, the load-carrying capacity can be calculated. Table 31 gives the equations for calculating the load-carrying capacity of pillars of different shapes for the cases where the pillar width is less than and greater than $2Y_M$.

The input parameters used for this analysis are:

1. Pillar geometry from Table 28.
2. Estimate of rock mass friction angle $(\phi) = 37$ degrees (Chapter 5).
3. Rock mass cohesion $(S_c) = 620$ psi (Chapter 5).
4. Horizontal stress ratio $(S_R) = 1.72$.

The load-carrying capacity for the square pillar is calculated as follows:

$$S_{MV} = (6.94)(1.72)(165)(500)\frac{1+\sin 37}{1-\sin 37} \times 10^{-3} + 620$$

$$= 4\ 604.62 \text{ psi}$$

$$Y_M = \frac{30}{\left(\frac{1+\sin 37}{1-\sin 37}\right)^{1/2}\left(\frac{1+\sin 37}{1-\sin 37} - 1\right)} \ln \frac{4604.62}{620} = 9.92 \text{ ft}$$

$$LCC = (7.2 \times 10^{-2})(4604.62)(37^2 - 2 \times 37 \times 9.92$$
$$+ 1.33 \times 9.92^2) = 253,970 \text{ tons.}$$

The safety factor of the square pillar determined by using Wilson's method is 1.5.

A similar analysis for the rectangular pillar would give:

$$S_{MV} = 4604.62 \text{ psi}$$
$$Y_M = 9.92 \text{ ft}$$
$$LCC = 261,218 \text{ tons}$$

and the safety factor for the rectangular pillar would be

$$SF = 1.4.$$

Wilson's method accounts for the way in which the pillar carries the load for most pillar geometries and the rock mass strength for the particular rock type. The difficulty of this method is in evaluating the input parameters. The rock substance properties can be measured and the rock fabric properties can be measured, but combining the two to obtain the rock mass strength is extremely difficult and perplexing.

Summary

Five basic methods for calculating the load-carrying capacity of pillars were analyzed. In addition, two methods that combine two of the basic pillar methods were analyzed. Although each of the basic methods are based on different approaches, it is possible that the results can still be the same. Table 32 shows that the following methods yield approximately the same results:

1. The Bieniawski and the Salamon and Munro.
2. The Wilson, the Bieniawski in combination with the Skinner, and possibly the Salamon and Munro in combination with the Skinner.

Because all the methods do not result with the same load-carrying capacity, those methods that are most applicable to the study area must be chosen. The basis of each pillar method and its validity in terms of the Marble Peak will be briefly discussed.

The Obert, Duvall, and Merrill method assumes that given competent rock, the pillar strength is equal to the strength of a core

Table 32. Load-carrying capacities and safety factors based on different
pillar design methods

Method	Square Pillar		Rectangular Pillar	
	LCC, tons	SF	LCC, tons	SF
Obert, Duvall, and Merrill	2,323,248	13.9	2,330,640	12.7
Skinner	0	0	0	0
Bieniawski				
Equation	63,774	0.4	61,236	0.3
Skinner curve	177,420	1.1	237,600	1.3
Salamon and Munro				
Equation	72,152	0.4	66,096	0.4
Skinner curve	409,649	2.47	374,895	2.0
Wilson	253,970	1.5	261,218	1.4

specimen with the same width-to-height ratio. Obert et al. (1960) also
assume that the load is carried uniformly across the pillar. They recom-
mend a safety factor of two to four to account for variations in the rock
strength and the load on the pillar. This method is suitable for rock that
has little or no structure; however, this is not the condition at Marble
Peak where the rock mass has a significant amount of structural discon-
tinuities. Therefore, the assumption that the rock substance strength
equals the rock mass strength is invalid at Marble Peak. To use a safety
factor of four to account for this difference in strength may result in an
overdesign in some cases and an underdesign in other cases.

Skinner's (1956) approach of the weakest link results with a load-carrying capacity less than zero, which is unrealistic. The concept that the strength of a chain is determined by the weakest link and that the longer the chain the greater the chance of having a weak link is not unreasonable. However, every link in a chain depends on the next, whereas a portion of a pillar may fail but the remaining part may be able to carry the extra load. Therefore the Skinner method results with a highly conservative answer.

Bieniawski (1968) assumed that as the size of a pillar increases the pillar reaches a fundamental strength; i.e., the number of flaws per volume of material is constant. This concept appears reasonable, but the determination of the volume of material at which the fundamental strength is reached is difficult. Bieniawski stated that for coal the fundamental strength was reached at a five-foot cube, which was the largest specimen tested. This may or may not be the exact size at which the fundamental strength is reached for othe rock types. The five-foot cube is certainly of the order of magnitude at which the fundamental strength is reached. Because the fracture spacing (0.2 ft) of the coal Bieniawski tested and the fracture spacing (0.2 ft) of the ABC zone are relatively the same, it can be assumed that the five-foot cube is the volume at which the fundamental strength is reached for the ABC zone. The strength of the five-foot block can be estimated by using the Skinner method. Although this approach seems reasonable, the estimated size at which the fundamental strength is reached is questionable and the Skinner method probably results in a conservative strength.

Salamon and Munro's (1967) approach of back analyzing existing pillars and developing an equation that best fits the strength distribution of the pillars is good. By assuming that the exponents for the height and width of a pillar are the same for the ABC zone as for coal, an estimate of the strength of a cubic foot of rock can be made by using Skinner's method. Although the Skinner method underestimates the strength of a pillar, it is reasonable to use this method to estimate the strength of a unit cube because the unit cube size is much closer to the specimen size than it is to the pillar size. The Salamon and Munro method is valid as long as there are existing pillars to work with; however, if there are no existing pillars and the rock type is not similar to coal, this method is not applicable. The Salamon and Munro method can be modified by predicting the strength of a unit cube by Skinner's method, but whether the exponents remain the same for different rock types is not known.

Wilson's (1972) approach is that the pillar carries most of the load in its inner core and the outer core carries little load but confines the inner core. His method requires input of rock mass friction angle and cohesion, which are difficult to measure or calculate. The method allows for pillars other than square. While all methods account for width-height ratio, none accounts for length-width ratio except to say that it should not exceed 10:1.

From this analysis it is my opinion that the Wilson method is the most applicable for the ABC zone rock. The Wilson method best accounts for the way in which a pillar carries its load, and it uses the parameters that are applicable to the property. A combination of the

Bieniawski and Skinner methods or of the Salamon and Munro and Skinner methods results in similar values for the load-carrying capacities as obtained in the Wilson method. However, these combination have not been checked with actual results.

Pillar-width Nomograph

A nomograph, using the Wilson method, can be used to determine the pillar width given the following (Abel, 1974b):

1. Depth (thickness of overburden).

2. Room width.

3. Crosscut width.

4. Room length.

5. Room height.

6. Rock mass properties.

Figure 41 is an example of the nomograph. The following is a guide for its use:

Step

1   Determine height of pillar and choose corresponding nomograph (30 ft)

2   Determine depth to be analyzed (600 ft)

3   Determine maximum tributary-area load (210,000 tons)

4   Specify required safety factor (1.6)

5   Calculate required load-carrying capacity (210,000 x 1.6 = 336,000 tons)

6   Read pillar width for depth and load-carrying capacity (32.5 ft)
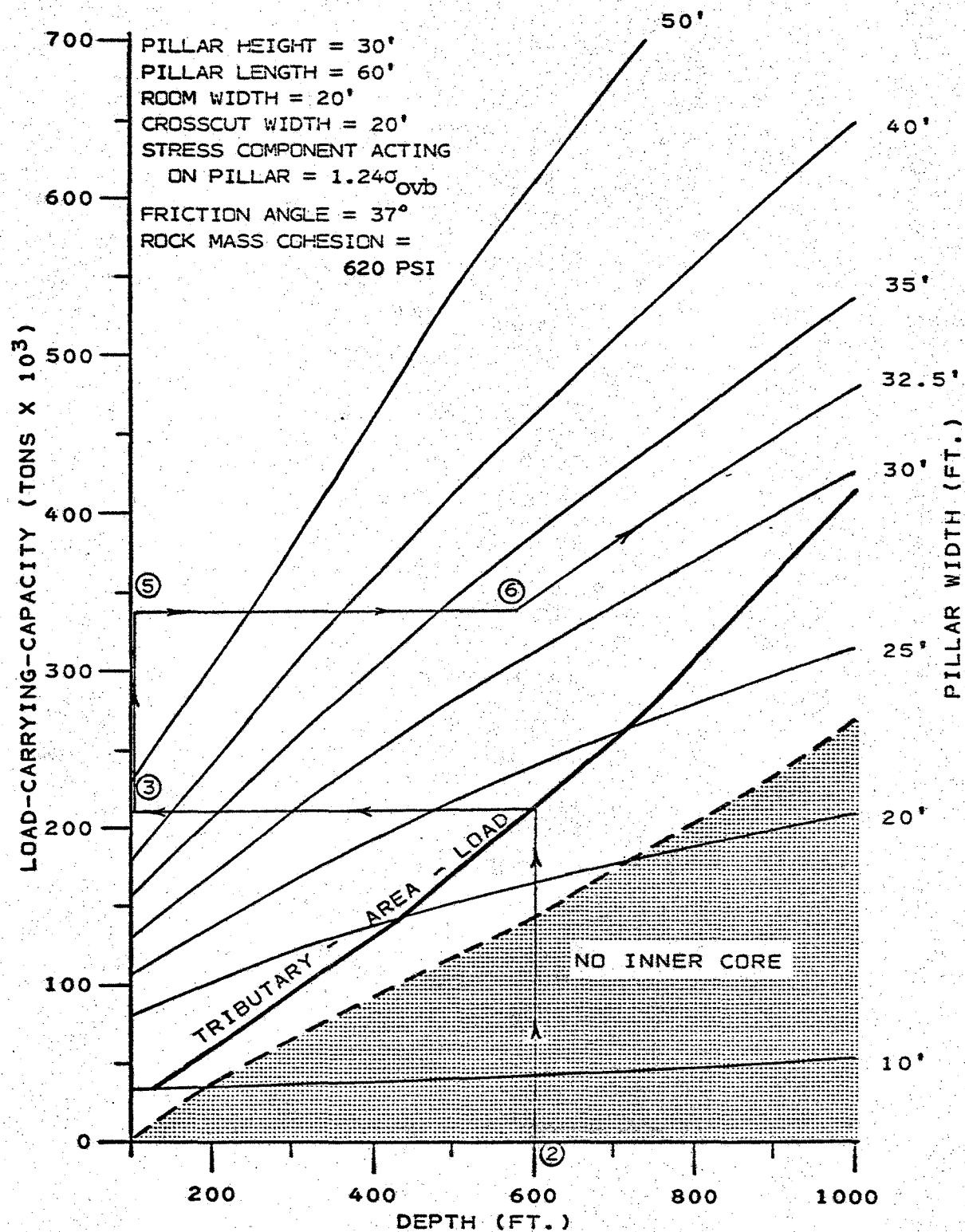
Figure 41. Nomograph to predict pillar width using the Wilson method

CHAPTER 8

SUMMARY AND CONCLUSIONS

Rock Mass Strength and in Situ Stress Field

Based on statistics and engineering judgment, the rock proper-
ties for the ABC zone, the upper Abrigo, and the Martin were pooled.
The pooled rock properties described the rock mass in the ABC zone area
as a high-strength (16,000 to 32,000 psi), elastic, layered, broken to
very broken, hydrothermally altered limestone. An estimate of the rock
mass shear strength was made using the minimum resistance step path
analysis and the shear strengths from rock-on-rock direct shear tests
and triaxial compression tests on intact rock. The estimated rock mass
shear strength (τ) can be described as

$$\tau = 630 + \sigma_N \tan 37^\circ \text{ (psi)}. \tag{22}$$

The in situ stress field was estimated by using two indirect
methods: (1) measuring the residual stress and adding it to the gravi-
tational stress and (2) relating the stress field to the geology and struc-
ture of the area. For the pillar analysis the maximum stress was
considered to be horizontal bearing N. 50° E. and the minimum stress
to be vertical and equal to the overburden load.

Stope and Pillar Analysis

Pillar orientation is both an operations consideration and a
stability consideration. Based on structure alone, a pillar with walls
normal to the bedding dip with a long axis parallel to the dip direction

will be the most stable. For operational considerations, a vertical pillar wall will be the more advantageous. Walls normal to bedding will be used in the pillar analysis because this will probably be the final stable condition. Stope height is defined by the thickness of the mineralized zone, and stope length will be 60 feet for operational reasons.

Roof stability determines room width. Assuming that the roof acts as a uniformly loaded, fixed-end beam, the maximum roof width can be determined by comparing the stress at the center of the roof beam to either the in-situ stress acting in the same direction or the tensile strength of the rock with an appropriate safety factor. Because the rock mass tensile strength approaches zero, it is believed that comparison of the bending stress to the in situ stress is more realistic. The current 18-foot-wide openings are at a depth of 620 feet and are stable. From this information, using the beam analysis, the following room widths and depth intervals are recommended:

Depth (feet)	Room Width (feet)
0–500	18
500–700	20
700–900	24

The load on the pillar was calculated from the tributary-area method, which assumes that the entire overburden load on the pillar is carried half way to the next pillar. This probably gives a conservative estimate due to formation of a pressure arch. It is difficult to evaluate the exact geometry of this pressure arch. Using the pressure arch concept, the pillars in the center should be the widest, i.e., have the

highest safety factor, while those pillars nearest the unmined rock can have the lowest safety factor.

Of the five basic pillar design methods compared, Wilson's method, which uses rock mass shear strength based on the step path, appears to be the best method. Wilson's method attempts to account for the distribution of the load on the pillar and uses the rock mass properties. With Wilson's method, the pillar width can be determined from a nomograph for a given room length, room width, room height, and rock mass properties.

Recommended Future Work

The approach for estimating the rock mass strength using the minimum resistance step path program needs to be improved. Special concentration is required in defining the distribution of fracture overlap, improving the step path program to handle more complex decisions on the stepping procedure, a finite element analysis to determine the stress concentration at a rock bridge, and field data to check the method.

More work is needed to determine if the in situ stress can be obtained either by measuring the residual stress and adding it to the gravitational stress or by defining the stress field from the geologic structure.

For a pillar design in rock the input parameters are never absolute and the analysis should therefore be based on a probabilistic rather than a deterministic approach. The deterministic approach assumes unique input parameters which do not adequately represent the variability of the rock mass strength; therefore, a calculated safety factor greater

than one does not mean that all pillars are stable but only those with
the given parameters. The probabilistic approach can be accomplished
by adding a Monte Carlo overlay to the analysis and determining a dis-
tribution of safety factors. The probability of failure is then the per-
centage of iterations with safety factors less than one. The mine
management can then better evaluate the risk of failure versus capital
gain.

APPENDIX A

METHOD OF STRUCTURAL DATA
COLLECTION AND ANALYSIS

At this time there are two popular methods of collecting structural data: detail line and joint set mapping. The joint set mapping discussed by Call (1972) involves measuring mean orientation and fracture characteristics for each fracture set in a 10- to 15-foot zone. The detail line technique proposed by Call (1972) entails stretching a tape along the wall and measuring all fractures 6 inches or longer that intersect the tape. Because of the tape's orientation, two joint sets could be missed: the set striking nearly parallel to the tape and the set dipping less than 25 degrees. Therefore, to minimize the bias all fractures in a zone one foot above and below the tape were measured with footage marked at the projected intersection. Savely (1972) has shown that little change in the rock fabric occurs after measuring 60 joints in a complex porphyry deposit. To ensure a suffient amount of data Savely used 100 measurements as the cutoff point. Because the fracture pattern at Marble Peak is no more complex that that of the Sierrita open pit examined by Savely, 100 fracture observations should be ample. The detail line method was used in this study for the following two reasons:

1. Not enough spot samples for the joint set mapping could be taken due to limited exposure of the ore zone.

2. Joint spacing from joint set mapping is a judgment number, whereas spacing from a detail line is based on measured footage.

144

The data recorded for each joint were:

1. Distance along the tape where the joint or its projection intersect the tape.

2. Rock type.

3. Structure type, i.e., bedding plane fracture, single fracture, fault, contact.

4. Fracture orientation; care was taken to correct for magnetite affecting the readings.

5. Minimum dip; the flattest dip of the joint.

6. Planarity; a qualitative rating technique that categorizes the waviness of the joint on a scale of 3 feet or greater (Fig. A-1).

7. Continuity; a qualitative measure of intact rock (Fig. A-1).

8. Roughness; a qualitative measure similar to planarity, except the roughness is on the scale of one inch (Fig. A-1).

9. Length; the maximum traceable distance that the fracture can be observed; limited by the width of the drift.

10. Fracture thickness.

11. Fracture filling; the different fillings were noted, if any.

12. Presence of water.

13. Existence of slickensides.

14. Bookkeeping; the page and column were noted for referencing.

In addition to the above data, the line number, date, data collector, the bearing and dip of the face, and general location of sample area were noted on the data sheet.

The poles to fracture planes were plotted on a Schmidt equal area, lower hemisphere azimuthal projection net for analysis (Billings,
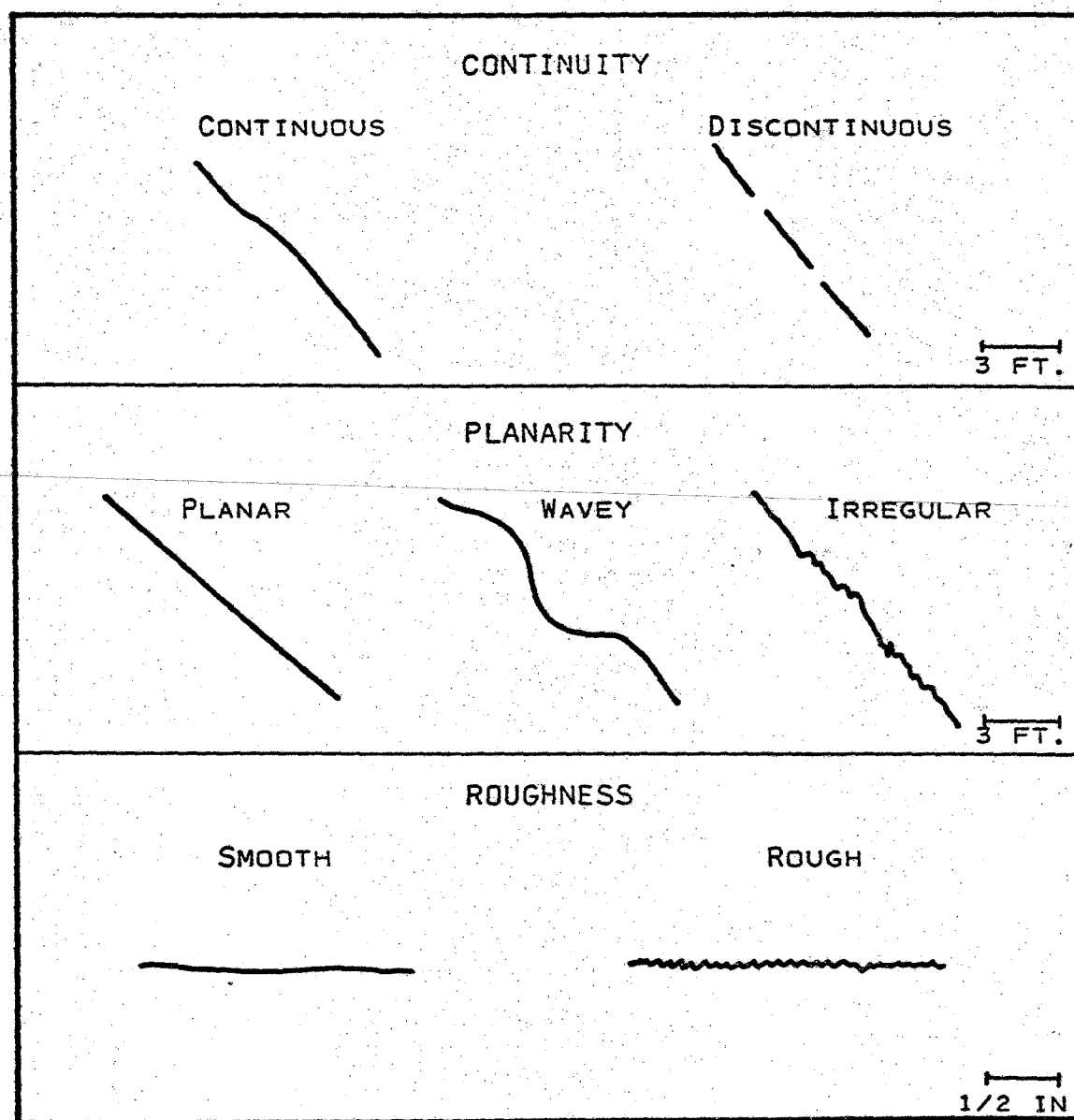
Figure A-1. Geometry of planar structural features

1942). A computer program was used to plot the 100 poles and calculate the percentage of poles per one percent area of the projection. To evaluate the randomness of pole concentrations, Poisson's exponential binomial limit were used (Pincus, 1951; Spencer, 1959). Fracture sets were defined as significant if the percentage of poles was greater than 2.8 percent. This meant the fracture sets equal to above that percentage had at least an 80 percent probability that they were not a random occurrence.

As discussed earlier, the possibility of bias occurs for fracture sets that are nearly parallel ($\pm 10^{\circ}$) to the strike of tape. This area has been called the "blind" zone by Terzaghi (1965), and she has presented a method to correct the data. However, this bias correction is not considered necessary because care was taken to observe these "blind" fractures. In addition, another check detail line will be run approximately 90 degrees to the first line.

The average orientation of each fracture set was determined by two methods: (1) the mode (highest concentration of poles) and (2) the mean vector. Because the mean vector analysis gives equal weight to each fracture, even those on the extreme limits, the modal orientation was used to represent each fracture set. The mean and mode minimum dips were also calculated for each fracture set. The planarity, continuity, and roughness factors, and fracture filling were calculated as a percentage of the total fractures for the given fracture set. The mean, mode and maximum lengths; mean, mode and minimum spacing; and mean and mode thickness were calculated for the defined fracture sets.

APPENDIX B

STANDARD PROCEDURES FOR TESTING ROCK CORES
AND CALCULATING ROCK SUBSTANCE PROPERTIES

1. Unconfined Compressive Strength

a. Specimen preparation

Drill core is cut with a diamond saw to a length-diameter
ratio between 2:1 and 3:1. The ends of the samples are ground
flat and parallel to the core axes with a Rockwell Delta surface
grinder.

b. Testing

The specimens are loaded at a nominal rate of 400 lb/s
in a Structural Behavior Engineering Laboratories, Inc. CT-500
equipped with a hemispherical seat on the upper platen and a
Coates-type Teflon seat on the lower platen. One-inch steel
disks the same diameter as the core are placed between the
core and the platen.

The maximum load at failure is recorded by a hydraulic
pressure gage.

The maximum compressive strength in pounds per square
inch is determined by dividing the maximum load by the cross
sectional area of the specimen.

2. Deformation Modulus and Poisson's Ratio

a. Specimen preparation

Same as unconfined compression.

148

b. Strain measurements

Lateral and longitudinal strains are measured with an SR-4 strain gage 90-degree rosette glued to the midpoint of the sample.

c. Load measurement

The load is measured by a load cell.

d. Data output

The load and longitudinal strain are recorded on one XY recorder to obtain the stress-strain curve from which Young's modulus is determined.

e. Testing procedure

The specimen is mounted in the testing machine in the same configuration as for the unconfined compression. The specimen is loaded to about a third the compressive strength and then unloaded to determine the permanent strain. Then the specimen is loaded to failure.

f. Computation of deformation modulus

The deformation modulus (E) is computed from the stress-strain curve as a tangent modulus where

$$E = \frac{\Delta\sigma}{\Delta\epsilon}$$

If the stress-strain curve is not linear, the modulus is computed for segments of the curve and the stress range is specified.

g. Computation of Poisson's ratio

Poisson's ratio (μ) is computed from the lateral strain-longitudinal strain curve where

$$\mu = \frac{\Delta \epsilon \text{ lateral}}{\Delta \epsilon \text{ longitudinal}}$$

If the curve is not linear, μ is computed for segments of the curve and the stress range is specified.

3. Brazilian (Indirect Tensile) Test

a. Specimen preparation

Specimen preparation consists of cutting core into pieces 1/2 to 1 inch long. The length and diameter of each core disk are recorded.

b. Testing procedure

The testing machine and accessories described for the uni-axial strength test are used. The core disks are mounted in the testing machine with the diameter ends against the platens. The load is applied at a nominal rate of 1,000 pounds per minute. The maximum is recorded after the specimen fails.

c. Computation

The tensile strength is reported for each specimen, calculated by the formula:

$$T_S = 2P/\pi DL$$

where P is the applied load, D is the diameter, and L is the length.

The mean and standard deviation of the tensile strength are reported for groups of specimens of the same rock type.

4. Triaxial Compression Strength

    a. Specimen preparation

        Same as for unconfined compression. In addition, the core and platens are sealed with shrink tubing.

    b. Testing

        Sealed core and platens are seated in a Structural Behavior Engineering Laboratories, Inc. triaxial compression cell and filled with hydraulic fluid. A vertical load of 25 percent the uniaxial compression strength is applied before the desired confining stress is applied. The vertical load is applied at a nominal rate of 400 pounds per second until failure.

    c. Load measurements

        The confining load is measured with a dial gage. The vertical load is measured by a BLH electronic load cell

    d. Data output

        The failure load for a given confining stress is recorded on the XY recorder. The failure stress is calculated by the following formula:

$$\text{Failure stress} = \frac{\text{Failure load} - \text{Confining pressure }(3.55 - \text{area of specimen})}{\text{Area of sample}}$$

5. Rock-on-Rock Cut Direct Shear Strength

    a. Specimen preparation

        Drill core is cut into two disks with heights of 1/4 and 1 inch. The two surfaces are ground to ensure at least 75 percent

contact. To prevent high stress concentrations on the edges of the disk, they are beveled.

b. Testing

A modified Soiltest direct shear machine that will accommodate up to a 2.5-in.-diameter specimen. A combination worm belt—variable speed electric motor drive gives a nominal 0.05 inch per minute loading rate. The normal load is provided through a level arm—dead load arrangement. The test is run through four to five different normals for a displacement no greater than 25 percent of the specimen diameter.

c. Load measurements

Shear load is measured using a load cell. The specimen displacement is measured using a LVDT and a 1-in. dial gage.

d. Data output

The shear load versus displacement is recorded on the XY recorder for each normal. An area correction is made, then the shear stress versus the normal stress is plotted to calculate the shear strength equation.

APPENDIX C

ADDITIONAL DATA ON PHYSICAL ROCK PROPERTIES

Table C-1. Uniaxial compression samples

Specimen No.	Drill Hole No.	Depth below Collar (ft)	Rock Type	Height/Diameter Ratio
A-1	70	552	Ore	2.1
B-2	crosscut	6400 elev.	Ore	2.1
B-3				2.1
B-4				2.1
B-5				2.0
B-6				2.1
C-1	6	789	UAL	2.2
C-2	6	789		2.1
C-3	45	705		2.2
C-4	75	671		2.1
C-5	37	377		1.9
C-6	69	535		2.1
C-7	72	256		1.9
D-1	6	773	Martin	1.9
D-6	6	773		2.0
D-3	69	521		2.1
D-4	72	239		2.2
D-5	4	711		2.1
D-6	4	711		2.0

Table C-2. Brazilian disk tension samples

Specimen No.	Drill Hole No.	Depth below Collar (ft)	Rock Type	Height/Diameter Ratio
M-1	70	552	Ore	0.50
M-2	70	552		.50
M-3	70	547		.50
M-4	crosscut	6400 elev.		.40
M-5				.46
M-6				.49
M-7				.36
M-8				.50
M-9				.45
M-10				.47
N-1	6	789	UAL	.33
N-2	6	789		.38
N-3	6	789		.41
N-4	45	705		.48
N-5	45	705		.49
N-6	75	671		.45
N-7	69	535		.41
N-8	37	379		.34
N-9	37	379		.42
N-10	37	379		.30
O-1	6	773	Martin	.41
O-2	69	521		.46
O-3	72	239		.36
O-4	72	239		.45
O-5	45	711		.28
O-6	45	711		.36

Table C-3. Triaxial compression samples

Specimen No.	Drill Hole No.	Depth below Collar (ft)	Rock Type	Height/Diameter Ratio
T-1	70	552	Ore	2.2
T-2	70	547		2.1
T-3	crosscut	6400 elev.		2.0
T-4				2.1
T-5				2.1
A-2	70	547		2.1
B-2	crosscut	6400 elev.		2.1
B-7				2.1
C-7	72	256	UAL	1.9
C-8	45	684		2.1
C-9	37	379		2.0
C-10	72	257		2.0

Table C-4. Failure stress; stiffness with its stress range; and Poisson's ratio with its stress range

Speci-men No.	Failure Stress (psi)	Stiffness (E) (psi)	Stress Range (psi)	Poisson's Ratio	Stress Range (psi)
ABC Zone					
A-1	28,000	40.0×10^6	2,500- 7,400	0.20	0-16,000
		17.5	7,400-10,000	.22	16,000-22,000
		14.0	10,000-15,800	.32	22,000-28,000
		11.8	15,800-26,500		
		6.7	26,500-28,000		
B-2	20,500	60.0	0- 3,500	.18	0-17,000
		31.4	3,500- 7,000	.27	17,000-20,500
		18.8	7,000-11,000		
		14.4	11,000-20,500		
B-3 Run 2	33,500	45.0	0- 4,000	.21	0-26,400
		24.0	4,000- 7,500	.37	26,400-33,500
		17.5	7,500-11,300		
		13.0	11,300-18,000		
		12.2	18,000-33,500		
Run 1		14.3	0- 4,500	.20	0- 7,500
		10.7	4,500- 5,800	.22	7,500-11,600
		8.3	5,800-18,700	.29	11,600-15,500
				.36	15,500-18,700
B-4	17,500	26.3	0- 6,000	.61	0- 9,500
		16.1	6,000- 9,500	.75	9,500-11,900
		12.5	9,500-14,000	.93	11,900-13,200
		10.7	14,000-17,300	1.30	13,200-14,600
B-5 Run 2	33,100	22.0	0- 4,000	.33	0- 9,000
		15.7	4,000- 7,000	.20	9,000-16,500
		10.4	7,000-25,000	.30	16,500-26,000
		9.2	25,000-33,100	.45	26,000-33,100
Run 1		28.1	0- 2,500	.25	0-10,000
		22.2	2,500- 3,900	.20	10,100-16,300
		17.5	3,900- 5,400	.24	16,300-21,400
		13.9	5,400- 7,400		
		10.0	7,400-12,500		
		9.4	12,500-21,400		

Table C-4. Failure stress--Continued

Speci-men No.	Failure Stress (psi)	Stiffness (E) (psi)	Stress Range (psi)	Poisson's Ratio	Stress Range (psi)
B-6	20,400	42.9×10^6	0- 1,500	0.19	0-16,400
		23.0	1,500- 3,700	.32	16,400-20,400
		17.9	3,700- 6,000		
		14.3	6,000- 8,000		
		11.8	8,000-15,800		
		13.5	15,800-20,400		

Unmineralized Upper Abrigo

Speci-men No.	Failure Stress (psi)	Stiffness (E) (psi)	Stress Range (psi)	Poisson's Ratio	Stress Range (psi)
C-1	15,000	20.0	0- 3,200		
		12.5	3,200- 7,400		
		9.1	7,400-15,000		
C-2	16,000				
C-3	24,500	11.5	0- 4,500	.11	0- 8,500
		8.6	4,500- 7,000	.16	8,500-12,000
		6.8	7,000- 9,200	.21	12,000-16,100
		5.7	9,200-24,100	.31	16,100-20,000
		0.5	24,100-24,500	.40	20,000-24,000
				.53	24,000-24,400
				.88	24,440-24,500
C-4	15,000	25.0	0- 3,900	.22	0-15,000
		16.7	3,900- 6,800		
		11.0	6,800- 9,300		
		9.2	9,300-14,500		
C-5 Run 2	13,000	9.2	0- 700	.24	0- 5,500
		12.9	700- 7,100	.40	5,500-10,000
		6.4	7,100-13,000	.60	10,000-13,000
				.93	13,000-13,000
Run 1		1.1	0- 500	1.6	13,000-13,000
		2.5	500- 2,100		
		3.3	2,100- 7,400		
		2.7	7,400- 9,000		
		2.3	9,000-11,200		

Table C-4. Failure stress--<u>Continued</u>

Specimen No.	Failure Stress (psi)	Stiffness (E) (psi)	Stress Range (psi)	Poisson's Ratio	Stress Range (psi)
C-6	14,500	25.0×10^6	0- 2,500		
		16.0	2,500- 6,600		
		11.1	6,600- 9,500		
		8.8	9,500-14,500		

<u>Unmineralized Martin</u>

Specimen No.	Failure Stress (psi)	Stiffness (E) (psi)	Stress Range (psi)	Poisson's Ratio	Stress Range (psi)
D-1	10,500	4.8	0- 4,800	.22	0- 2,700
		4.0	4,800- 7,500	.44	2,700- 4,000
		3.0	7,500- 8,900	.50	4,000- 7,100
		2.1	8,900- 9,600	.56	7,100- 8,500
		1.0	9,600-10,500	.76	8,500- 8,900
				.70	8,900-10,500
D-2	13,500	70.0	0- 4,500	.22	0- 1,200
		28.3	4,500- 6,500		
		20.5	6,500- 9,500		
		12.9	9,500-13,500		
D-3	26,600	13.3	5,000- 7,500	.13	0-11,000
		10.0	7,500- 8,800	.22	11,000-15,600
		7.1	8,800-12,800	.32	15,600-19,500
		7.3	12,800-19,000	.46	19,500-22,500
		5.7	19,000-23,000	.60	22,500-24,600
		4.6	23,000-24,900	.72	24,600-25,800
		3.6	24,900-26,600	1.00	25,800-26,600
D-4	16,700	17.5	0- 2,800	.18	0-16,700
		11.4	2,800-12,400		
		7.5	12,400-16,700		
D-5	20,500	15.0	0- 9,300	.26	0-17,100
		12.0	9,300-14,800	.16	17,100-20,500
		10.7	14,800-20,500		
D-6	39,000	23.3	0- 6,000	.11	0-26,800
		16.0	6,000-11,500	.19	26,800-30,500
		12.5	11,500-17,000	.28	30,500-34,700
		10.8	17,000-28,900	.38	34,700-37,000
		9.8	28,900-35,000	.47	37,000-39,000
		10.0	35,000-39,000		

APPENDIX D

SAMPLE COLLECTION AND TEST PROCEDURE
FOR RESIDUAL STRESS RELIEF*

1. The sample is oriented before removal from the drift wall.

2. A plane parallel to the bedding plane and two other planes orthogonal to the bedding plane are cut with a diamond saw. On each plane a surface at least 2 inches in diameter is ground smooth. The locations of these ground areas should not be on or near known fractures wherever possible.

3. The ground areas where the strain gages are to be attached are thoroughly cleaned with a solvent to remove grit and oil.

4. The strain gages are attached to the rock surfaces with epoxy cement in the following manner:

   a. Epoxy is placed on the ground surface where a gage is to be fixed.

   b. The gage is positioned and oriented in the desired manner and then covered with several pieces of Teflon-type tape.

   c. A piece of soft sponge 1/4- to 1/2-inch thick is placed over the Teflon tape.

   d. Masking tape is wrapped around the rock to hold down the sponge, which, in turn, applies equal pressure on the strain gage. The tape holds the strain gage in place and

---

*Procedure is modified from Gentry (1972).

the Teflon tape prevents the sponge from sticking to the gage. The tapes and sponge are removed after epoxy has hardened (approximately 24 hours). BLH three-element, 45° rosette strain gages, Type FABR-50-1256 were used. The gage/grid length of these gages is 0.5 inches and the carrier trim is 1 1/16 inches in diameter.

4. One lead from each of the three elements is soldered to a gold post. The remaining leads are all soldered to the fourth post, thus forming a common ground.

5. A thin protective covering of epoxy is spread over the gage and the trim, especially over the area of the gage. Before the epoxy hardened the four gold posts are placed on the outer edges of the trim. As the epoxy hardened the posts are firmly attached.

6. Each element of every gage is monitored by using a "switch-and-balance unit" connected to a Budd strain indicator. The data measured are strain changes (micro inches per inch) for each element, the time of the reading, and the temperature in degrees Centigrade. Plots are made of change in strain readings versus time for each gage (Fig. 25, in pocket). After deformation due to the saw cuts and surface grinding ceases and the relative changes in strain readings, the conclusion is that the strain readings have essentially stabilized and the gages are indicating contraction and expansion of the rock due to temperature changes. This can take anywhere from 4 to 12 weeks to occur.

7. After the strain readings have stabilized, a plastic disk 1 3/8 inches ID by 1/4 inch thick with approximately a 2-inch OD is

placed around the strain gage and cemented with epoxy. This serves as a collar guide for overcoring.

8. The strain gage is overcovered with a diamond bit to a depth of approximately 2 inches. Rambosek (1964) has shown that relief of stresses in a core is complete when drilling has reached 1 1/2 core diameters from the face of the borehole.

9. After overcoring is completed, the specimen is again monitored. Monitoring continues until the rock specimen has again stabilized. The resultant change in strain readings before and after overcoring represents the measurement of residual strain released as the result of overcoring.

10. The overcored segment is broken free from the block. Again the strain gages are monitored until they stabilize. The resultant change in strain readings before and after release from the block represents the total strain released without crushing the rock.

APPENDIX E

A GUIDE TO THE ESTIMATION
OF IN SITU STRESSES*

It is commonly necessary to make a reasonable estimate of the orientation and magnitude of the in situ stresses without the benefit of stress measurements. The following is presented for estimating the orientation of the three-dimensional principal stresses using the geologic environment. Answer the following questions:

1. What is the rock type?

    Igneous — high horizontal stress probable. (Go to 2.)

    Metamorphic — high horizontal stress probable. (Go to 6.)

    Sedimentary — high horizontal stress possible. (Go to 10.)

2. Is there nearby faulting ($\leq$ 100 ft)

    Yes — σ_{max} is approximately parallel to fault strike.
    (Go to 3.)

    No — (Go to 4.)

3. Normal faulting or reverse and strike-slip faulting?

    Normal — σ_{int} is downdip on the fault.

    σ_{min} is normal to the fault plane. (Go to 18.)

    Reverse — σ_{int} is normal to the fault plane.
      and
    Strike-
    slip — σ_{min} is downdip on the fault plane. (Go to 18.)

---

*This procedure is from Abel (1974a).

163

4. Is one joint set pervasive and predominant?

    Yes — σ_{max} lies in plane of this major joint set.

        σ_{int} lies in plane of this major joint set.

        σ_{min} is normal to plane of this major joint set.
        (Go to 5.)

    No — Principal stresses line up with orthogonal joint sets?

        (Rank joint sets based on average spacing; closer

        spacing means higher rank.)

        σ_{max} is parallel to the line of intersection between the two highest rank joint sets and normal to the lowest rank joint set.

        σ_{min} is normal to highest rank joint set, i.e., the joint set with the closest average spacing

        σ_{int} is orthogonal to σ_{max} and σ_{min}. (Go to 18.)

5. Rank remaining joint sets based on average spacing.

        σ_{max} is in the plane of the highest rank joint set and approximately normal to the lowest rank orthogonal joint set.

        σ_{int} is orthogonal to σ_{max} and σ_{min}. (Go to 18.)

6. Is there a pervasive local foliation orientation?

    Yes — σ_{max} lies in the plane of the foliation. (Go to 7.)

    No —   (Go to 2.)

7. Is there a joint set present in the plane of the foliation?

    Yes — σ_{min} is approximately normal to foliation. (Go to 9.)

    No —   (Go to 8.)

8. Is one joint set pervasive and predominant?

    Yes — σ_{max} lies in plane of this major joint set.

        σ_{int} lies in plane of this major joint set.

σ_{min} is normal to plane of this major joint set. (Go to 9.)

No — Principal stresses line up with orthogonal joint

sets. (Rank joint sets based on average spacing.)

σ_{min} is normal to highest rank joint set, i.e., the joint set with closest average spacing.

σ_{max} is in the plane of the highest rank joint set and approximately normal to the lowest rank orthogonal joint set.

σ_{int} is orthogonal to σ_{max} and σ_{min}. (Go to 18.)

9. Rank remaining joint sets based on average spacing.

σ_{max} is parallel to the line of intersection between the foliation and the predominant joint set.

σ_{int} is orthogonal to σ_{max} and σ_{min}. (Go to 18.)

10. Is the area under study near a fault? (≤ 100 ft)

Yes — σ_{max} lies parallel to the line of intersection between the plane of the fault and the bedding.

σ_{min} is normal to the fault and orthogonal to σ_{max}.

σ_{int} lies in the plane of the fault and orthogonal to σ_{max} and σ_{min}. (Go to 18.)

No — (Go to 11.)

11. Is the bed in which the principal stresses are to be estimated

stiffer than the adjacent beds and less than 10 times as thick,

in feet, as the ratio of the modulus of the bed (E_B) to the aver-

age modulus of the adjacent beds (E_A)?

Yes — σ_{max} and σ_{int} lie in the plane of the bedding.

σ_{min} is normal to the bedding. (Go to 12.)

No — (Go to 13.)

12. Rank crossbedding joints based on average spacing.

> σ_{max} lies parallel to the line of intersection between the bedding and the highest rank crossbedding joint set.

> σ_{int} is orthogonal to σ_{max} and σ_{min}. (Go to 18.)

13. Is the bed in which principal stresses are to be estimated less stiff than the average stiffness of the adjacent beds and less than 10 times as thick, in feet, as the ratio of the average modulus of the adjacent beds (E_A) to the modulus of the bed itself (E_B)?

> Yes — σ_{max} is normal to plane of bedding. (Go to 14.)

> No — (Go to 15.)

14. Rank crossbedding joints based on average spacing.

> σ_{int} lies parallel to line of intersection between bedding and highest rank crossbedding joint set.

> σ_{min} is normal to highest rank crossbedding joint set. (Go to 18.)

15. Bed in which principal stresses are to be estimated is massive (≥ 100 ft).

> Yes — σ_{max} is roughly perpendicular to bedding (Go to 16.)

> No — (Go to 11.)

16. Bedding is flat lying.

> Yes — Rank crossbedding joints based on average spacing.

> > σ_{int} is horizontal to and lies in plane of highest rank crossbedding joint.

> > σ_{min} is horizontal to and normal to highest rank crossbedding joint. (Go to 18.)

> No — (Go to 17.)

17. Are there crossbedding joint sets?

> Yes — Rank crossbedding joint sets based on average spacing
>
>> σ_{int} lies in plane of bedding and in plane of highest rank crossbedding joint set.
>>
>> σ_{min} lies in plane of bedding and normal to highest rank crossbedding joint set. (Go to 18.)
>
> No — σ_{int} is parallel to strike of bedding.
>
>> σ_{min} is perpendicular to strike of bedding.

18. The principal stress orientations you have just estimated are just that, "estimates," subject to change when stress measurements are made.

One method of estimating the magnitude of the three-dimensional principal stresses is to take the orientation results and answer the following:

> σ_{ovb} = overburden stress (γH)

19. What is the rock type?

> Igneous. (Go to 20.)
>
> Metamorphic. (Go to 22.)
>
> Sedimentary. (Go to 24.)

20. Is there nearby faulting? ($\leq$ 100 ft).

> Yes — (Go to 21.)
>
> No — σ_{max} is approximately ($\geq$) 1.5 σ_{ovb}.
>
>> σ_{int} is approximately   1.0 σ_{ovb}.
>>
>> σ_{min} is approximately ($\leq$) 1.0 σ_{ovb}. (Go to 28.)

21. Normal faulting or reverse and strike-slip faulting.

Normal — σ_{max} is approximately ($\leqq$) 2.0 σ_{ovb}.

σ_{int} is approximately   1.0 σ_{ovb}.

σ_{min} is approximately ($\leqq$) 1.0 σ_{ovb}.

Reverse — σ_{max} is approximately ($\geqq$) 2.0 σ_{ovb}.
and
Strike- σ_{int} is approximately   1.5 σ_{ovb}.
slip

σ_{min} is approximately ($\geqq$) 1.0 σ_{ovb}.
(Go to 28.)

22. Is there nearby faulting? ($\leqq$ 100 ft)

Yes — (Go to 23.)

No — σ_{max} is approximately ($\leqq$) 2.0 σ_{ovb}.

σ_{int} is approximately ($\geqq$) 1.0 σ_{ovb}.

σ_{min} is approximately   1.0 σ_{ovb}.
(Go to 28.)

23. Normal faulting or reverse and strike-slip faulting?

Normal — σ_{max} is approximately ($\geqq$) 2.0 σ_{ovb}.

σ_{int} is approximately   1.5 σ_{ovb}.

σ_{min} is approximately ($\geqq$) 1.0 σ_{ovb}.

Reverse — σ_{max} is approximately ($\leqq$) 3.0 σ_{ovb}.
and
Strike- σ_{int} is approximately ($\leqq$) 2.0 σ_{ovb}.
slip

σ_{min} is approximately ($\leqq$) 1.5 σ_{ovb}.
(Go to 28.)

24. Is there nearby faulting? ($\leqq$ 100 ft)

Yes — (Go to 25.)

No — (Go to 26.)

25. Normal faulting or reverse and strike-slip faulting.

   Normal — σ_{max} is approximately ($\geqq$) σ_{ovb}.

   σ_{int} is approximately σ_{ovb}.

   σ_{min} is approximately ($\leqq$) σ_{ovb}.

   Reverse — σ_{max} is approximately ($\geqq$) 1.5 σ_{ovb}.
   and
   Strike- σ_{int} is approximately ($\geqq$) 1.0 σ_{ovb}.
   slip
   σ_{min} is approximately 1.0 σ_{ovb}.
   (Go to 28.)

26. Is the thickness of bed in which principal stresses are to be

   estimated less than 10 times the ratio, in feet, of the higher

   modulus bed(s) to the lower modulus bed(s)?

   Yes — (Go to 27.)

   No — σ_{max} is approximately σ_{ovb}.

   σ_{int} is approximately ($\leqq$) σ_{ovb}.

   σ_{min} is approximately ($\leqq$) σ_{ovb}.
   (Go to 28.)

27. Is the stiffness (modulus) of the bed in which principal stresses

   are to be estimated (E_B) greater than the average stiffness

   (modulus) of the adjacent beds (E_A)?

   Yes — σ_{max} is approximately ($\geqq$) (E_B/E_A) σ_{ovb}.

   σ_{int} is approximately ($\leqq$) (E_B/E_A) σ_{ovb}.

   σ_{min} is approximately σ_{ovb}.

   No — σ_{max} is approximately σ_{ovb}.

   σ_{int} is approximately ($\geqq$) (E_B/E_A) σ_{ovb}.

   σ_{min} is approximately ($\leqq$) (E_B/E_A) σ_{ovb}.
   (Go to 28.)

28. The estimation of the magnitude of the three-dimensional principal in situ stresses is unlikely to produce a truly accurate picture. However, an error between stress estimate and measurement must be quite large before geometric stress concentration locations are greatly altered. Without estimates of stress orientation and magnitude it is impossible to approach the rock stability enigma; applied stress versus in-place strength.

REFERENCES

Abel, J. F., 1974a, A guide to the estimation of in situ stresses: unpublished paper, Golden, Colorado School of mines.

_____ 1974b, Oral communication: Golden, Colorado School of Mines.

Alder, H., Potts, E., and Walker, A., 1951, Research on strata control in the northern coalfield of Great Britain, in Proceedings, Inicher-International Conference at Liege, p. 106-120.

Alder, L., and Sun, M., 1968, Ground control in bedded formations: Research Division, Virginia Polytechnic Institute, Bull. 28, 266 p.

Anderson, E. M., 1951, The dynamics of faulting and dyke formation with applications to Britain, ed. 2: Edinburgh, Oliver and Boyd.

Ashwin, P. P., 1972, Research into the determination of pillar size. Part II. Measurements of stress in two pillars at Lea Hall Colliery: Mining Engineer (London), v. 131, p. 417-427.

Bielenstein, H. V., and Eisbacher, G. H., 1969, Tectonic interpretation of elastic-strain-recovery measurements at Elliot Lake, Ontario: Canadian Dept. of Energy, Mines and Resources, Mines Branch Research Rept. 4210, 64 p.

Bieniawski, Z. T., 1968, The effect of specimen size on compressive strength of coal: Internat. J. Rock Mechanics and Mining Science, v. 5, p. 325-335.

Billings, M. P., 1942, Structural geology: Englewood Cliffs, N.J., Prentice-Hall, Inc.

Braun, E. R., 1969, Geology and ore deposits of the Marble Peak area, Santa Catalina Mountains, Pima County, Arizona: unpublished M.S. thesis, University of Arizona, 79 p.

Call, R. D., 1972, Analysis of geologic structure for open pit slope design: unpublished Ph.D. dissertation, University of Arizona, 204 p.

_____, and Nicholas, D. E., 1974, Method of computing the minimum resistance step path for rock slope design: unpublished report, Tucson, Arizona, 18 p.

171

Coates, D. F., 1970, Rock mechanics principles, revised: Queen's Printer, Ottawa, Mines Branch Monograph 874, 442 p.

_____, and Grant, F., 1966, Stress measurement at Elliot Lake: Canadian Min. Met. Bull., v. 59, no. 649, p. 603-613.

Coates, D. F., and Gyenge, M., 1973, Incremental design in rock mechanics: Ottawa, Queen's Printer, Mines Branch Monograph 880, p. 78.

Cochran, W. G., Mosteller, F., Turkey, J. W., and Jenkins, W. O., 1954, Statistical problems of the Kinsey report on sexual behavior in the human male: Washington, D.C., American Statistical Assoc., 338 p.

Continental Copper, Inc., 1974a, Surface geology map: Oracle, Arizona, unpublished.

_____1974b, Underground geology map: Oracle, Arizona, unpublished.

Coulson, J. H., 1970, The effects of surface roughness on the shear strength of joints in rocks: Omaha, Nebraska, River Division, Corps of Engineers Tech. Rept. MRD2-70, 293 p.

Creasey, S. C., and Theodore, T. G., 1975, Preliminary reconnaissance geologic map of the Bellota Ranch quadrangle: U.S. Geolog. Survey open-file Rept. 75-295.

Deere, D. U., 1968, Geological considerations, in Stagg, K. G., and Zienkiewcz, eds., Rock mechanics in engineering practice: New York, John Wiley & Sons, Inc., p. 1-20.

Denkhaus, H. G., 1962, A critical review of the present state of scientific knowledge related to the strength of coal pillars: South African Inst. Mining Metallurgy J., v. 63, p. 59-75.

Donath, F. A., 1961, Experimental study of shear failure in anisotropic rocks: Geol. Soc. America Bull., v. 72, p. 985-990.

_____1966, A triaxial pressure apparatus for testing of consolidated or unconsolidated materials subject to pore pressure: Testing Techniques for Rock Mechanics, ASTM, STP 402, p. 1-41.

DuBois, R. L., 1959, Geology of the Santa Catalina Mountains, Arizona, in Heindl, L. A., ed., Southern Arizona guidebook II: Tucson, Arizona Geol. Society, p. 107-116.

Evans, I., 1970, Discussion of Z. T. Bienawski's paper, The effect of specimen size on compressive strength of coal: Internat. Jr. Rock Mechanics and Mining Science, v. 7, p. 230.

Evans, W. H., 1941, The strength of undermined strata: Inst. Mining and Metallurgy (London) Trans. Bull., v. 50, p. 475-532.

Fritts, J., 1974a, Geologic techniques and results at the Control mine, Pima County, Arizona: Oracle, Arizona, Continental Copper, Inc., unpublished report.

_____1974b, Oral communication: Oracle, Arizona, Continental Copper, Inc.

Gentry, D. W., 1972, The determination of residual stresses in the vicinity of the 755 breccia pipe at Cananea, Sonora, Mexico: unpublished Ph.D. dissertation, University of Arizona, 106 p.

Handros, G., 1959, The evaluation of Poisson's ratio and the modulus of materials of a low tensile resistance by the Brazilian (indirect tensile) test with particular reference to concrete: Australian J. Applied Science, v. 10, p. 243-268.

Hanson, H. S., 1966, Petrography and structure of the Leatherwood quartz diorite, Santa Catalina Mountains, Pima County, Arizona: unpublished Ph.D. dissertation, University of Arizona, 104 p.

Hardy, H., and Jayaraman, N., 1970, An investigation of methods for the determination of the tensile strength of rock, in Proceed-2nd Congress, Internat. Society of Rock Mechanics, Belgrade: p. 85-92.

Hawkes, I., and Mellor, M., 1970, Uniaxial testing in rock mechnics laboratories: Engineering Geology, v. 4, no. 3, p. 177-285.

_____1971, Measurements of tensile strength by diametral compression of discs and annuli: Engineering Geology, v. 5, no. 3, p. 173-255.

Heim, A., 1878, Untersuchungen über den Mechanismus der Gebirgs-bildung, im Anschluss an die geolische Monographie der Tödi-Windgällen-Gruppe: Basel, Switzerland, B. Schwake.

Hetenyi, M., 1954, Handbook of experimental stress analysis: New York, John Wiley & Sons, Inc.

Holland, C. T., 1973, Pillar design for permanent and semi-permanent support of the overburden in coal mines: Proceedings, 9th Canadian Rock Mechanics Symposium, p. 113-140.

_____, and Gaddy, F. L., 1957, Some aspects of permanent support of overburden on coal beds: Proceedings, West Virginia Coal Mining Institute, p. 43-66.

Jaeger, J. C., 1971, Friction of rocks and stability of rock slopes: Geotechnique, v. 21, no. 2, p. 97-134.

_____, and Cook, N. G. W., 1969, The state of stress underground, Chapter 14 in Fundamentals of rock mechanics: p. 355-362.

John, W. K., 1969, Civil engineering approach to evaluate strength and performability of regularly jointed rock, in Rock mechanics— Theory and practice: 11th Symposium on Rock Mechanics, New York, AIME, p. 69-80.

North of England Safety in Mines Research Committee, 1948-49, Seventh progress report: Inst. Mining Engineers (London) Trans., v. 108, p. 489-510.

Obert, L., and Duvall, W., 1967, Rock mechanics and the design of structures in rock: New York, John Wiley & Sons, Inc., 650 p.

_____, and Merrill, R., 1960, Design of underground openings in competent rock: U.S. Bureau of Mines Bull. 587, 36 p.

Peirce, F. L., 1958, Structure and petrography of part of the Santa Catalina Mounts: unpublished Ph.D. dissertation, University of Arizona, 86 p.

Pincus, H. J., 1951, Statistical methods applied to the study of rock fractures: Geol. Soc. America Bull., v. 62, p. 482-509.

Rambosek, A.J., 1964, The stress field within a core stub in a borehole: U.S. Bureau of Mines Rept. Inv. 6462, 16 p.

Salamon, M. D. G., 1967, A method of designing board and pillar workings: South African Inst. Mining and Metallurgy J., v. 68, no. 2, p. 68-78.

_____, and Munro, A. H., 1967, A study of the strength of coal pillars: South African Inst. Mining and Metallurgy J., v. 68, no. 2, p. 55-67.

Savely, J. P., 1972, Orientation and engineering properties of jointing in the Sierrita pit: unpublished M.S. thesis, University of Arizona, 134 p.

Skinner, W. J., 1956, Compressive strength of the anhydrite mine pillar: Imperial Chemical Industries, Ltd., Billingham Div., 34 p.

Spencer, E. W., 1959, Geologic evoluation of the Beartooth Mountains, Montana and Wyoming. Part 2. Fracture patterns: Geol. Soc. America Bull., v. 70, no. 4, p. 467-508.

Terzaghi, R. D., 1965, Sources of error in joint surveys: Geotechnique, v. 15, no. 3, p. 287-305.

Voight, B., 1967, Interpretation of in situ stress measurements, in Proceedings, 1st Congress, International Society of Rock Mechanics, Lisbon, Portugal: Vol. 3, p. 332-348.

Vouille, G., 1964, Etude monographique de diverse roches: Publication interieure au Laboratoire de Mecanique des Solides de l"Ecole Polytechnique.

Wallace, R. M., 1954, Structures at the northern end of the Santa Catalina Mountains, Arizona: unpublished Ph.D. dissertation, University of Arizona, 44 p.

Wilson, A. H., 1972, Research into the determination of pillar size— Part I. An hypothesis concerning pillar stability: Mining Engineer (London), v. 131, no. 141, p. 409-417.

Wilson, E. D., Moore, R. T., and Cooper, J. R., 1969, Geologic map of Arizona: Arizona Bureau of Mines and United States Geological Survey.
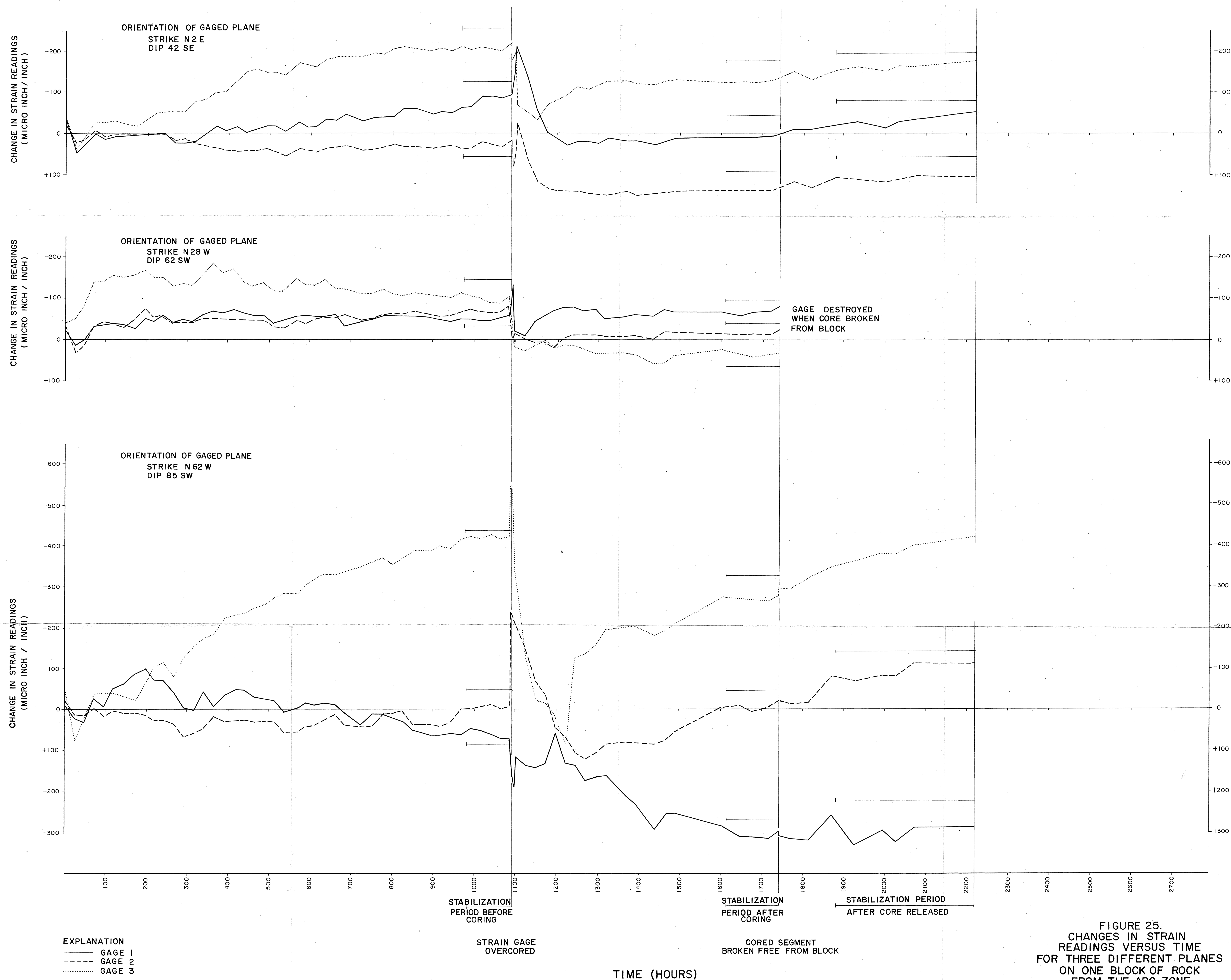
FIGURE 25.
CHANGES IN STRAIN
READINGS VERSUS TIME
FOR THREE DIFFERENT PLANES
ON ONE BLOCK OF ROCK
FROM THE ABC ZONE

D.E. NICHOLAS, G.E. THESIS, 1976